2011

Quantitative and Qualitative Mass Spectrometric Analysis of Anticancer Agents, Drugs of Abuse and Enzyme-Inhibitor Complexes

Keri M. Smith
Cleveland State University

QUANTITATIVE AND QUALITATIVE MASS SPECTROMETRIC ANALYSIS OF ANTICANCER AGENTS, DRUGS OF ABUSE AND ENZYME-INHIBITOR COMPLEXES

KERRI M. SMITH

Bachelor of Science in Chemistry

Cleveland State University

June 2006

submitted in partial fulfillment of requirements for the degree

DOCTOR OF PHILOSOPHY IN CLINICAL AND BIOANALYTICAL CHEMISTRY

at the

CLEVELAND STATE UNIVERSITY

NOVEMBER 2011

This dissertation has been approved
for the Department of CHEMISTRY
and the College of Graduate Studies by

_____
Dissertation Chairperson, Dr. Yan Xu

_____
Department and Date

_____
Dr. Baochuan Guo

_____
Department and Date

_____
Dr. Xue-Long Sun

_____
Department and Date

_____
Dr. John F. Turner

_____
Department and Date

_____
Dr. Yuping Wu

_____
Department and Date

MASS SPECTROMETRIC ANALYSIS OF ANTICANCER AGENTS AND DRUGS OF ABUSE IN BIOMATRICES, AS WELL AS CHARACTERIZATION OF INACTIVATION OF B-LACTAMASE ENZYMES

KERRI M. SMITH

ABSTRACT

Mass spectrometry is a valuable tool in the analysis of many types of compounds. From small molecules to large proteins, mass spectrometry can help to interrogate samples and give insights to the origins of disease as well as calculate an exact concentration. Bioanalytical method development is an integral component in the measurement of such compounds. To facilitate proper analytical investigation, the process of method development, analysis, and interpretation must be understood. This work describes the basis and procedure for bioanalytical method development and its detailed application to preclinical studies of the antineoplastic agent hexamethylene bisacetamide and measurement of illicit drugs of abuse benzylpiperazine and trifluoromethylphenyl piperazine using liquid chromatography tandem mass spectrometry. Additionally, procedures for analyzing protein-drug interactions and their implication in antibiotic resistance are discussed.

TABLE OF CONTENTS

LIST OF TABLES

CHAPTER I

CHAPTER II

CHAPTER III

CHAPTER IV

LIST OF FIGURES

CHAPTER I

CHAPTER II

CHAPTER III

CHAPTER IV

CHAPTER I

INTRODUCTION OF LIQUID CHROMATOGRAPHY MASS SPECTROMETRY FOR BIOANALYTICAL ANALYSIS

1.1 General introduction

The insight of how drugs distribute, transform, and are removed from the biological system is integral in our understanding of how to effectively treat diseases. Analytical interrogation can give information of the toxicity, minimum effective dose, and pharmacokinetics (metabolism and elimination properties) of drugs and chemicals, while furthering drug discovery and development. The challenges regarding analysis include the removal of the drug from the biological matrix, its separation from the matrix components, and finally detection and quantification. Success in each step of the analysis is dependent on parameters including nature of biological Analytical determination of drugs in biological samples may be accomplished using a variety of techniques and instrumentation: Gas

Chromatography [1], Liquid Chromatography [2, 3], and Capillary Electrophoresis [3]. When these separation techniques are coupled to a detector such as mass spectrometry, their power of investigation increases.

1.2. Modern methods for sample analysis

A popular and versatile tool that facilitates analytical measurement is liquid chromatography separation coupled to mass spectrometry detection [4]. This technique has the advantage that it may be partially or fully automated for cost-effective high-throughput and minimal analyst intervention once the methodology is developed [5].

1.2.1. High Performance Liquid Chromatographic separation

High Performance Liquid Chromatography (HPLC) separates compounds based on their differential interactions with a stationary phase (the column). Here, the compound of interest (the analyte) is separated from the other components of the matrix (e.g., blood, serum, urine, etc) (figure 1.1). HPLC systems typically consist of reservoirs for mobile phase, a pumping system, an autosampler for sample introduction to the analytical column for separation, a diverter or switching valve, and finally a detector. Some detectors are listed in table 1.1, but this work will focus on mass spectrometric detection and is described in detail in section 1.2.2.

On injection of the sample, the analyte interacts with the stationary phase and produces a detector response proportional to concentration on elution. The molecules separate and elute in the form of a Gaussian distribution in an ideal situation (figure 1.2). Typically, additional or competing interactions influence the final shape of the peak. These interactions and tactics for their improvement are described.

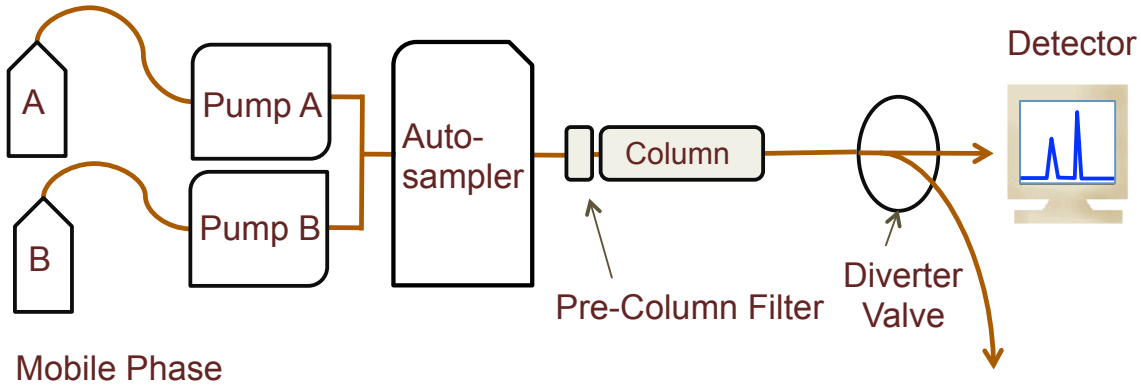

Figure 1.1, Graphic of a typical HPLC instrument setup.

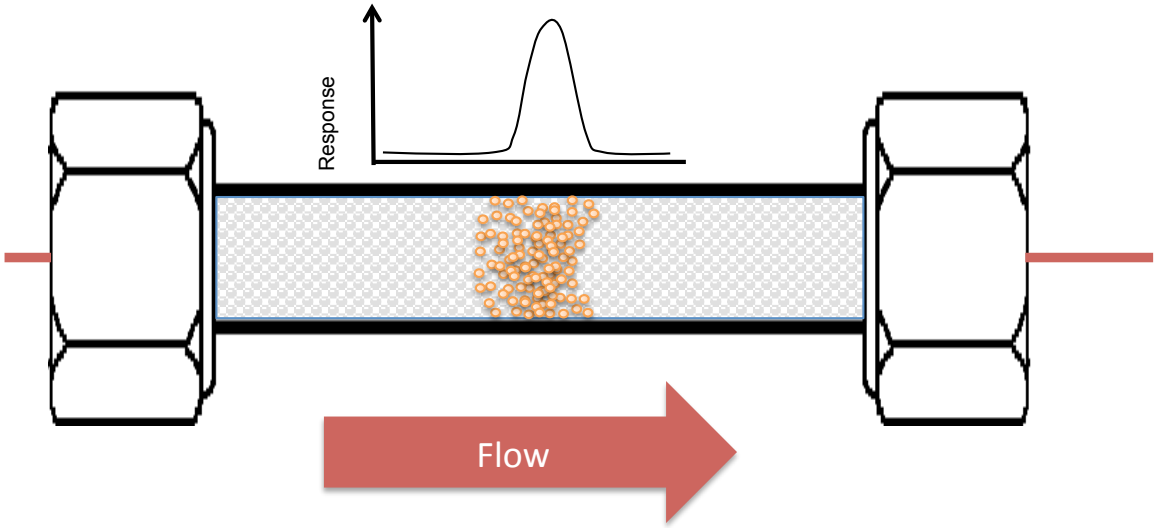

Figure 1.2, Illustration of retentivity and diffusion on HPLC separation

Detector Type	Major Advantage	Major Disadvantage
UV-visible	Sensitive; Nondestructive	Analyte must have a chromophore
Fluorescence	Sensitive and more selective; Nondestructive	Analyte must have a fluorophore
Refractive Index	Wide applicability; Nondestructive	Analyte must have a significant enough difference of refraction from solvent
Evaporative Light Scattering	Wide applicability	Analyte must have lower volatility than solvent; Destructive
Electrochemical	Very sensitive	Analyte must oxidizable or reducable
Mass Spectrometric	Very sensitive with wide applicability	Must use volatile solvent and buffers; Destructive

Table 1.1, Common detectors for HPLC

1.2.1.1. HPLC modes and separation

There are many forms of HPLC separation including size exclusion (SEC), ion exchange (IEX), affinity, normal-phase (NPLC), and the most common form, reversed-phase HPLC (RPLC) [6]. RPLC is characterized by a polar (hydrophilic) mobile phase and a non-polar (hydrophobic) stationary phase, and its description will be the focus of this work. In RPLC, the compound of interest is separated by interaction with the ligand on the stationary phase in different ways. Figure 1.3 shows some general common available stationary phase ligands. Seven of the common interactions that are believed to produce retention and selectivity are depicted in figure 1.4 and described below [2]:

i] Dipole – Dipole interaction – Dipole of analyte interacting with the dipole of the cyano ligand.

ii] Cation Exchange – Silanol groups can be negatively charged ($-SiO^-$) and will interact with a basic analyte [7]. Additionally, charged silanol groups can repulse an ionized acidic analyte (e.g., $R-COO^-$). Both interactions influence peak shape mainly by causing excessive tailing.

iii] Hydrophobic interactions

iv] Steric exclusion – A bulky analyte can not interact with the stationary phase due to chemical structure/shape. This can

influence the separation and selectivity of isomers (e.g., polyaromatic hydrocarbons with same number of phenyl rings, but different structure).

v] π – π interaction – Aromatic rings or other structures having π electrons may interact with a C6-Phenyl column much differently than a C18.

1.2.1.2. Challenges in HPLC separation

A large number of important pharmaceutical and abusable drugs are basic and carry a positive charge at physiological pH [8], including the compounds described in this work. Basic compounds present two specific challenges in efficient chromatographic separation: cation exchange with residual silanols on the column substrate that result in tailing [8] and degradation of the silica substrate under alkaline mobile phase conditions [9]. Technological advances to address these situations lead to end capping the unreacted silanols with a small group to block their ion exchange activity and the development of new hybrid substrates that withstand high pH [10]. Other tactics such as solvent type, pH, and mobile phase modifiers are discussed.

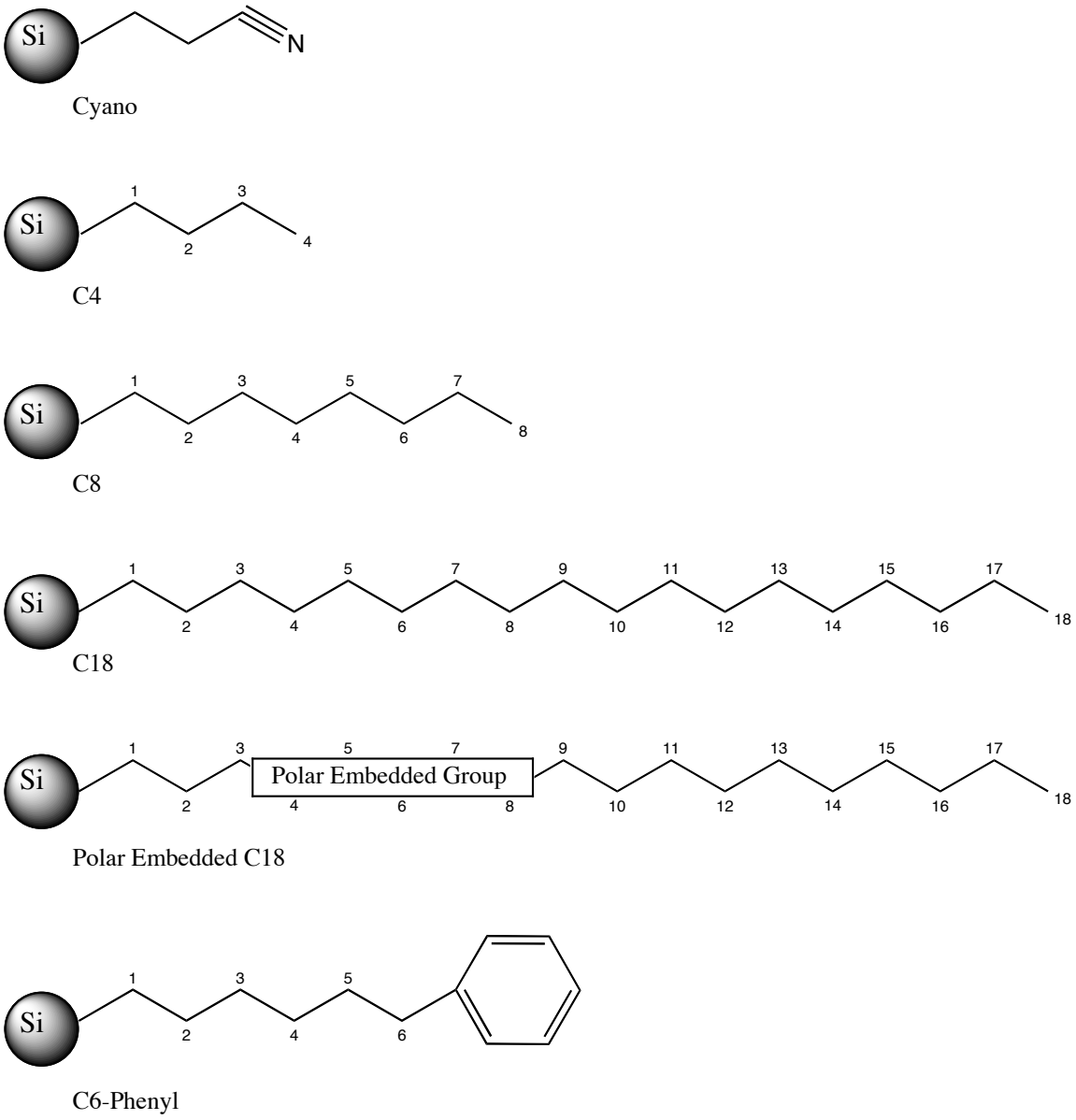

Figure 1.3, Common (simplified) RPLC ligand types

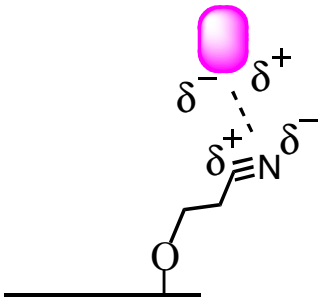

Dipole - Dipole Interactions

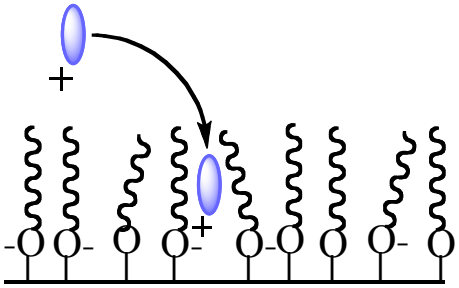

Cation Exchange

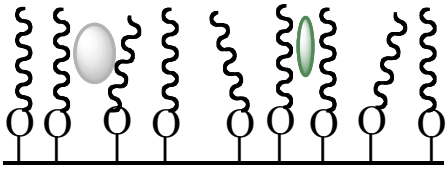

Hydrophobic Interaction

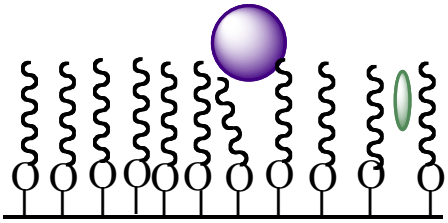

Steric Exclusion

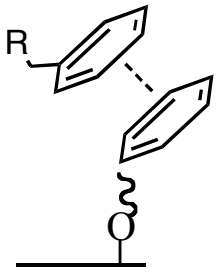

π–π Interaction

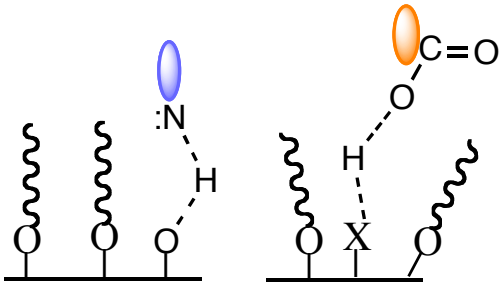

Hydrogen Bonding -
Basic or Acidic Solute

Figure 1.4, RPLC analyte – stationary phase interactions

1.2.1.2.1 Choice of solvent, modifier, and pH

Solvent type can influence the selectivity in RPLC. The two most common solvents used in HPLC are methanol (MeOH) and acetonitrile (ACN). MeOH is polar protic where ACN is polar aprotic. The elution strength of MeOH is weaker than that of ACN, as well, it's absorbance continues to 220 nm in the UV spectrum, where ACN is much lower [11]. Figure 1.5 depicts a nomogram of the relative elution strength of MeOH and ACN referenced against tetrahydrofuran (THF) [12]. Importantly, due to the ability of MeOH to donate and accept hydrogen bonds, selectivity in HPLC separation can change with the two solvents. Figure 1.6 shows an example of change in elution order for the separation of phenol, benzoic acid, and p-toluic acid when ACN is used instead of Methanol (http://www.shimadzu.com/an/hplc/support/lib/lctalk/35/35lab.html).

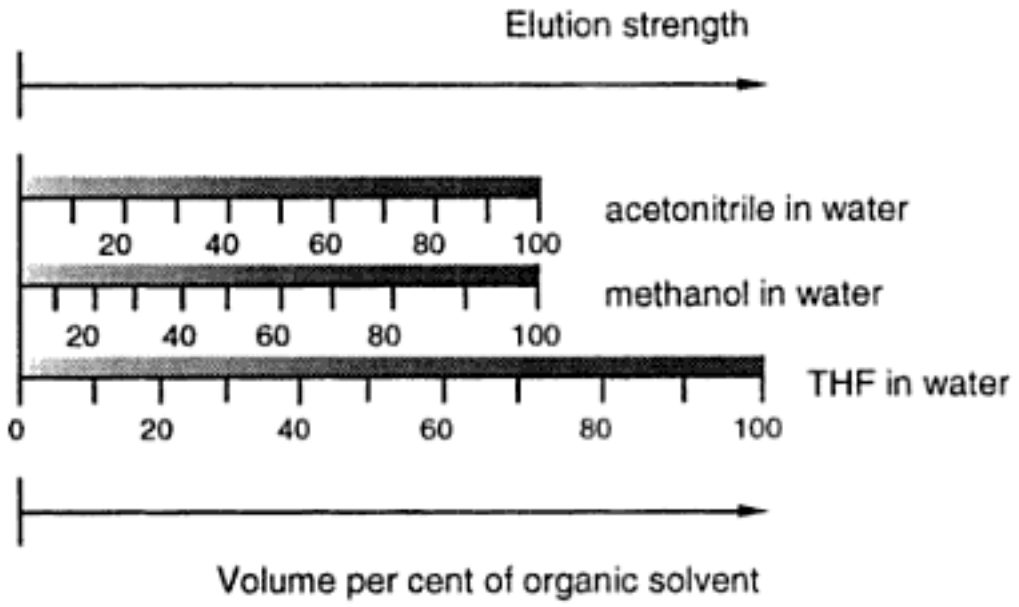

Figure 1.5, Nomogram of the elution strength of acetonitrile and methanol in water compared to tetrahydrofuran.

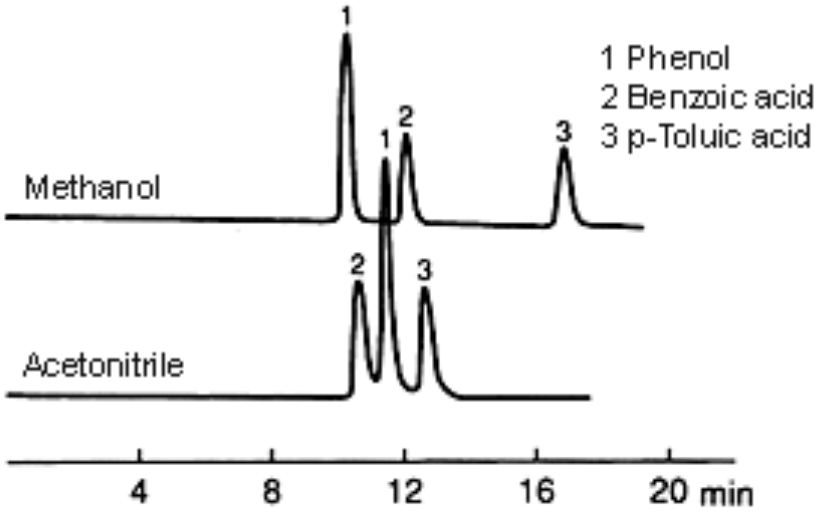

Figure 1.6, Change in elution order when using methanol versus acetonitrile

Mentioned previously, cation exchange is a known interaction and can be problematic in the analysis of basic compounds. Changing the pH below the pKa of $–SiO^-$ to yield –SiOH and reduce the interaction complicates the situation by creating a highly charged analyte that will elute sooner due to reduced interactions with the stationary phase ligand. The addition of mobile phase modifiers to compete with the exchange of the residual silanols can help to improve peak shape [7]. A list of modifiers is in table 1.2.

Finally, changing the pH of the mobile phase can change the retentivity of analytes on the stationary phase. Large changes in selectivity can be acquired by simply changing the pH [13]. To retain compounds longer, one may choose a pH above the pKa for basic analytes and below the pKa for acidic. This will create an uncharged analyte that will have an opportunity to interact with the stationary phase longer. Table 1.3 lists common buffers and their properties.

Modifier	pKa[a]	UV cutoff, nm[b]
Trifluoroacetic acid	0.3	205
Formic acid	3.75	200
Acetic acid	4.76	230
Formate	3.75	200
Acetate	4.76	205
Ammonium hydroxide	9.3	200
Triethylamine	10.8	200

[a] http://pubchem.ncbi.nlm.nih.gov/
[b] http://www.chem.agilent.com/cag/cabu/buffersel.htm

Table 1.2, List of common mobile phase modifiers

Buffer	pKa[a]	pH range	UV cutoff, nm[b]
Formate	3.75	2.8 - 4.8	200
Acetate	4.76	3.8 - 5.8	205
Citrate	3.1	2.1 - 4.1	230
	4.7	3.7 - 5.7	
	5.4	4.4 - 6.4	
Phosphate	2.1	1.1 - 3.1	<200
	7.2	6.2 - 8.2	
	12.3	11.3 - 13.3	
Bicarbonate	7.8	6.8 - 8.8	<200
	10.3	9.3 - 11.3	

[a] http://pubchem.ncbi.nlm.nih.gov/
[b] http://www.chem.agilent.com/cag/cabu/buffersel.htm

Table 1.3, List of common buffers

1.2.2. Mass spectrometric detection

Mass spectrometry can be thought of as a molecular balance. The technique can determine the mass of a compound, and even give information and clues to its molecular makeup by encouraging the fragmentation of compounds in a prescribed manner [14].

Mass spectrometers are made of four basic components and summarized in figure 1.7. The instrument uses an electromagnetic field to discriminate between ions with different mass to charge ratios (m/z). The sample is introduced in liquid form by direct infusion or by HPLC effluent. The solution is evaporated and ions formed in the ion source. Once inside the vacuum, the electromagnetic field of the mass analyzer is tuned to separate the ions based on their m/z, and are sent to the detector for counting and recording by the computer. The abundance of smaller molecules in bioanalysis means that an additional step is needed to increase the specificity. Here, an ion is selected using the electromagnetic field and fragmented. The fragments can then be scanned in a second mass analyzer for a second degree of confidence in analysis [14].

A consideration when using HPLC coupled to mass spectrometry is the choice of solvent and mobile phase modifier or buffer. Since it is

necessary to evaporate and create ions for mass spectrometric analysis, all components must be volatile organic salts and compounds.

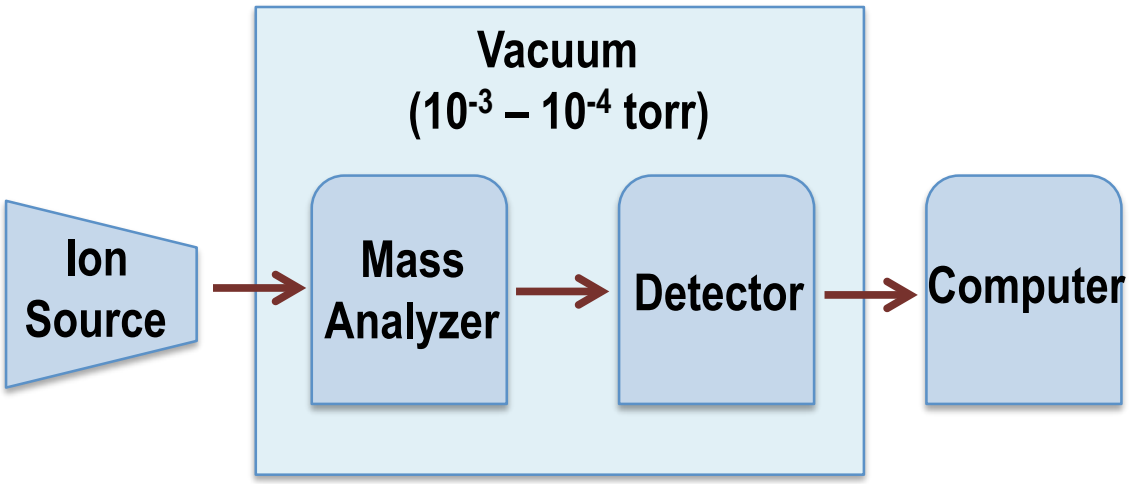

Figure 1.7, Block diagram of a mass spectrometer setup

1.2.2.1. Ionization methods

There are many ionization methods available today [15], but this work will focus on the two most commonly used: electrospray ionization (ESI) and atmospheric pressure chemical ionization (APCI).

ESI

ESI is considered a “soft ionization” technique where the solution passes through a charged capillary and is nebulized producing charged droplets (figure 1.8). On exiting the capillary, the solution forms a Taylor cone [16]. The apex of the Taylor cone is highly charged and pushes a jet of charged droplets that expand to a plume (figure 1.9). As the result of heated drying or desolvation gas, the solvent in the droplets of the plume dries leaving the charged species. The ions then enter the mass analyzer under the influence of vacuum and voltage difference. Once inside, the diffuse ion cloud is focused and then filtered by the quadrupoles.

ESI is useful for producing ions of labile molecules, small polar and some non-polar compounds, all the way to large biomolecules. The technique can produce cation adducts (e.g., H, Na, Li, NH_3, K) (figure 1.10) [17] , solvent adducts (e.g., acetonitrile, methanol, H_2O), and combinations of any/all [18-21]. Sodium (Na) adducts can be especially troublesome as

they tend to create a very strong and stabilizing association with the molecule and can prevent fragmentation. Even so, this and similar adducts can be encouraged to increase the sensitivity of some compounds [22]. A tactic to encourage molecular ions (M+H) for a less complicated spectrum and for compounds where the adduct formation is too stabilizing is to use a buffer containing NH_3: ammonium acetate or ammonium formate. This will encourage the formation of the molecular ion, M + H.

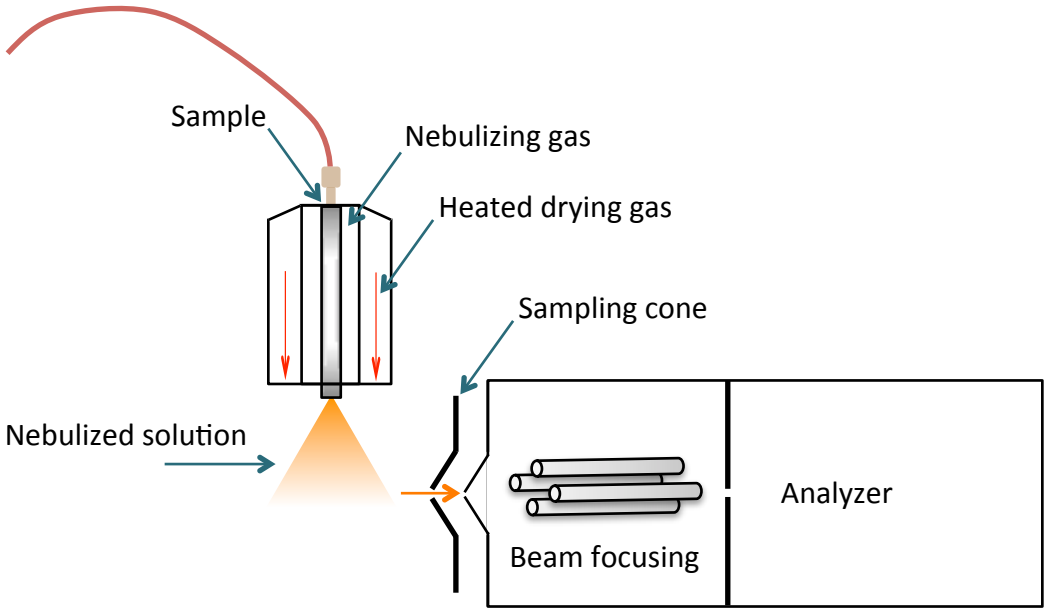

Figure 1.8, Electrospray ionization configuration.

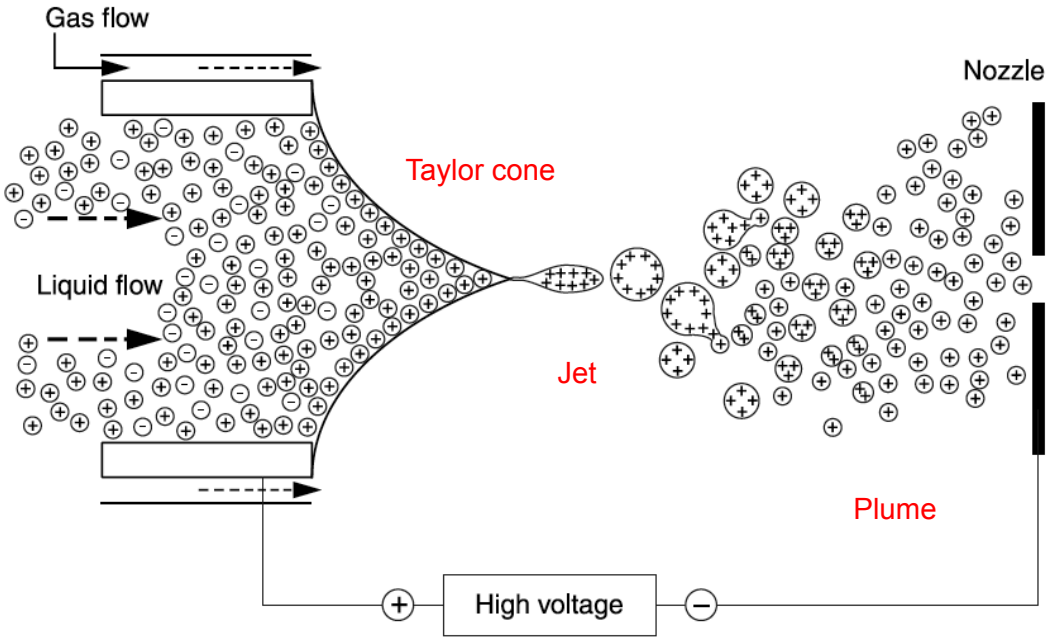

Figure 1.9, Formation of ions in ESI. Adapted from reference: [23].

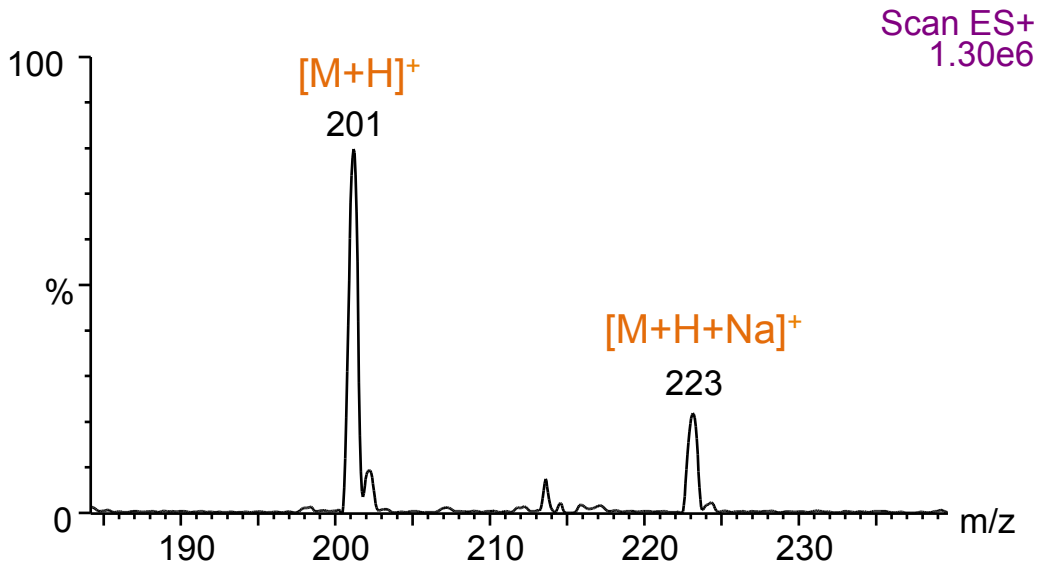

Figure 1.10, Example of sodium (Na) adduct formation in ESI of the compound hexamethylene bisacetamide. Data acquired by the author.

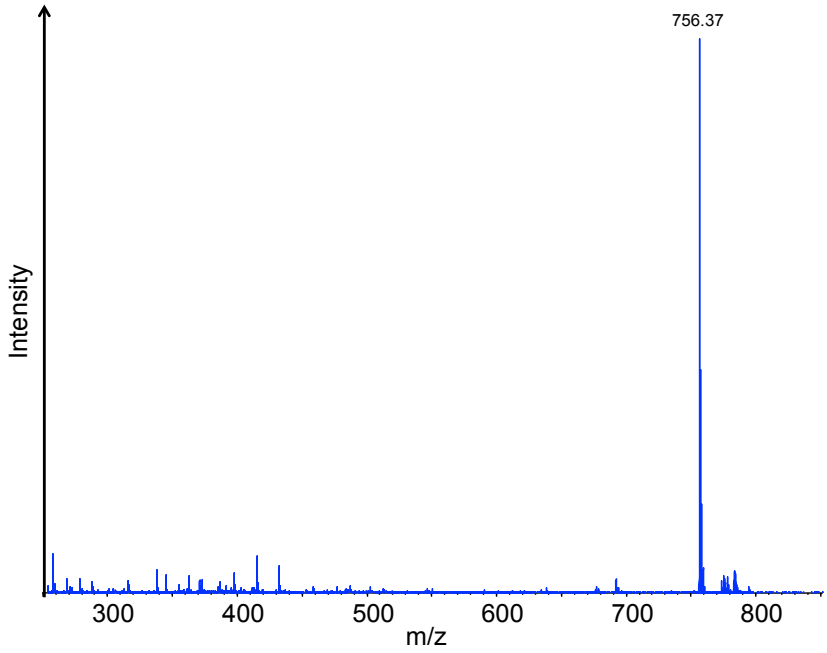

A

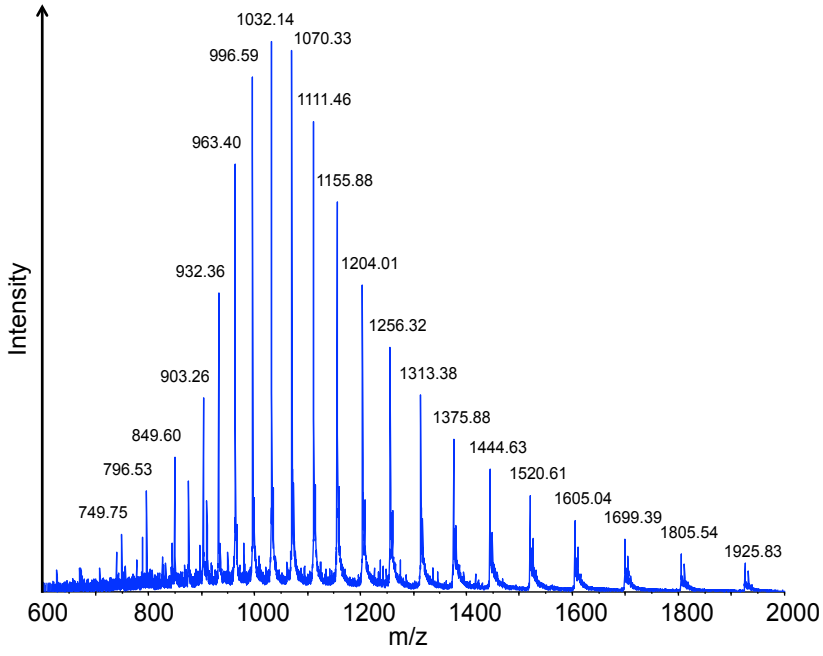

B

Figure 1.11, Positive ESI mass spectrums of (A) a small molecule and (B) a protein. Data acquired by the author.

ESI is able to add or abstract a charge from all the available sites on a compound. This can create multiply charged species, a feature that is very useful for biomolecule mass spectrometric analysis as most quadrupole mass spectrometers are limited in the *m/z* range they can measure. Figure 1.11 shows mass spectrum examples of a small molecule of 756 *m/z* and a large protein with multiple H adducts. Viewing the mass spectrum of the protein as in figure 1.10 B can make it difficult for comparison and analysis. Since there are multiple sites on a protein for protonation, many of those sites do protonate creating a mass spectrum of multiply charged species. Calculating the charge states and the full protein mass is as follows (http://www.astbury.leeds.ac.uk/facil/MStut/mstutorial.htm):

$m/z =$ mass to charge ratio of protein peak in spectrum

$a =$ adduct (use 1.0079 for H)

$MW =$ molecular weight of protein

$n =$ number of charges

$$m/z = \frac{(MW + na)}{n}$$

(1)

If the charge state is unknown, we may solve simultaneous equations to eliminate the MW term. Using the example in figure 1.12 and assuming

adjacent peaks are part of the same charge series and are separated by one charge, we calculate the charges by:

$$Y_{m/z} = \frac{(MW + na)}{n}$$
$$X_{m/z} = \frac{(MW + na)}{n} \quad (2)$$

$$nY_{m/z} - na = (n+1)X_{m/z} - (n+1)a \quad (3)$$

solving for $nY_{m/z}$:

$$nY_{m/z} = nX_{m/z} + X_{m/z} - a \quad (4)$$

therefore:

$$n(Y_{m/z} + X_{m/z}) = X_{m/z} - a \quad (5)$$

solving for n gives us the charge of $Y_{m/z}$:

$$n = \frac{X_{m/z} - a}{X_{m/x} - Y_{m/z}} \quad (6)$$

Using the value for n as determined in equation 6, we can use equation 1 to determine the molecular weight of the protein.

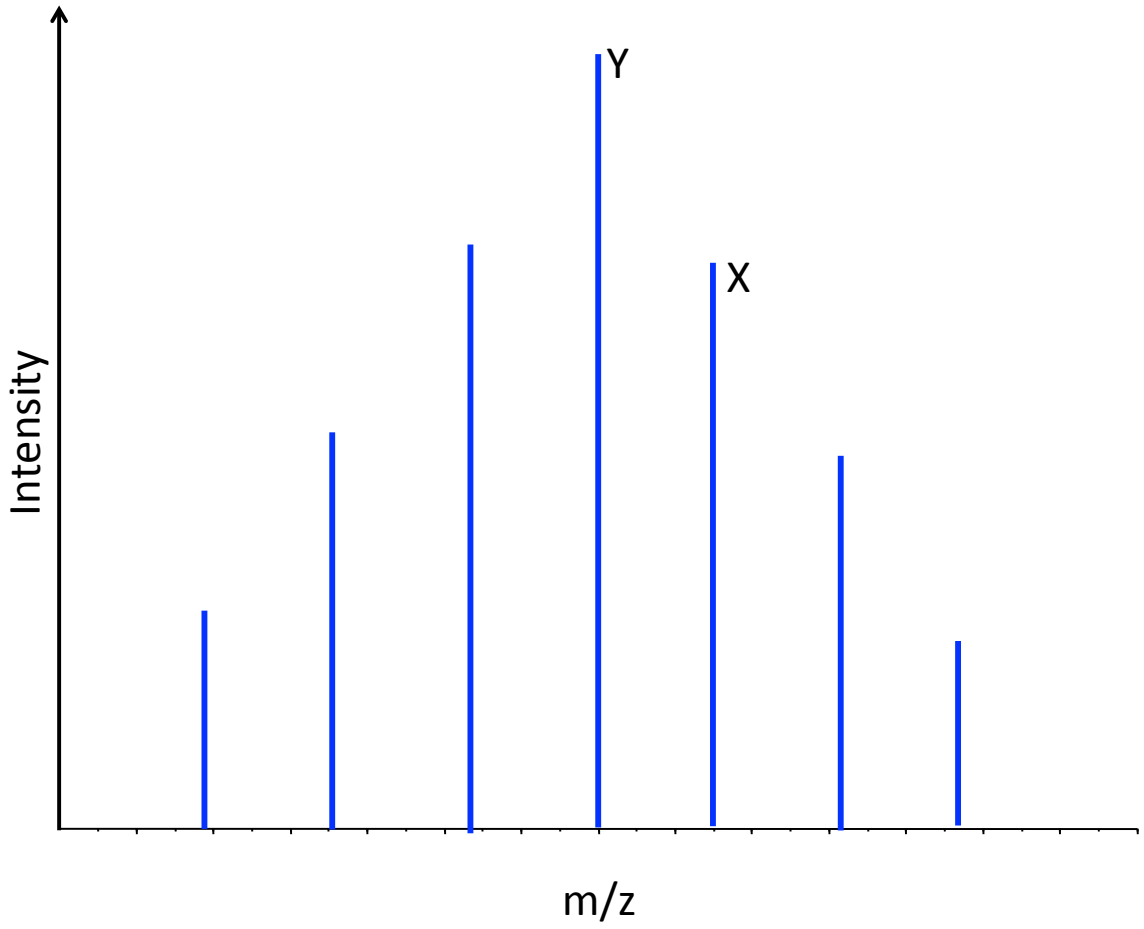

Figure 1.12, Illustration of charge distribution peaks of a protein.

Utilizing the two highest peaks in figure 1.10 B, the calculation is as follows:

$$X_{m/z} = 1070.33$$
$$Y_{m/z} = 1032.14$$

We calculate number of charges (n) of peak Y using equation 6:

$$n = \frac{1070.33 - 1.0079}{1070.33 - 1032.14} = 28$$

Using the number of charges and the m/z of Y, we can calculate the molecular weight of the protein:

$$(1032.12 * 28) - (28 * 1.0079) = 28871.70 \text{ Da}$$

Many mass spectrometric software programs have automatic calculation, called charge deconvolution. Using the Bioanalyst QS v.2.0 (AB Sciex, Foster City, CA), the results of the charge deconvolution, illustrated in figure 1.13, is 28,872.10 Da, an error of 0.4 Da or 0.001%.

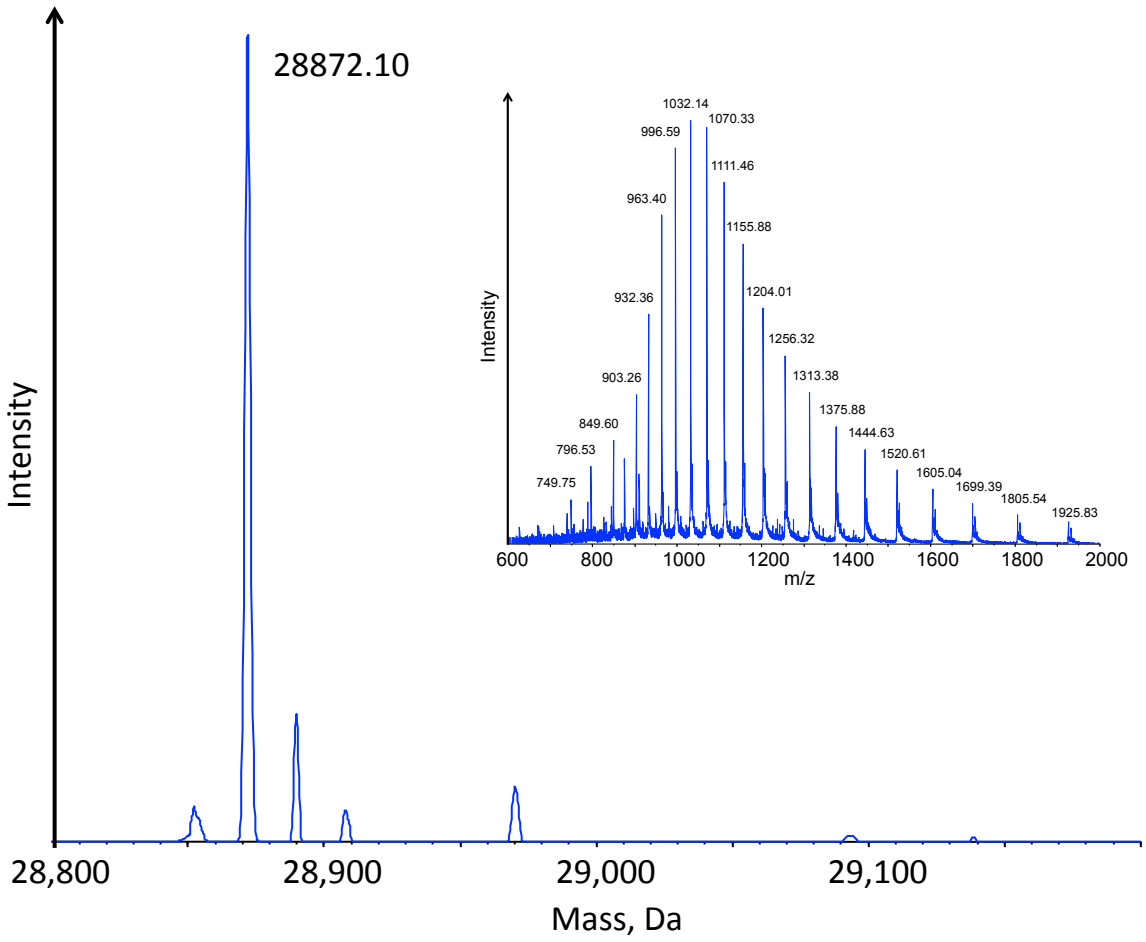

Figure 1.13, Automated mass calculation

APCI

APCI is similar to ESI, but with one prominent difference: ions are created after nebulization of the solution (figure 1.14). A corona current starts at the discharge needle tip, abstracts an electron and ionizes N_2 and O_2 each to $N_2^{\square+}$ and $O_2^{\square+}$. These primary ions collide with the vaporized solvent and form intermediate ions, which then collide with the sample molecules forming sample ions [24]. Figure 1.15 shows an example of 25-hydroxyvitmin D2 using both ESI and APCI ion sources. On ionization in APCI, the 25-hydroxyvitamin D2 loses one molecule of water (-18).

APCI is useful for non-polar to moderately polar compounds of rather lower molecular weight (up to approximately 1500 Da), but it is not amenable to compounds that are charged in solution [24]. Additionally, higher flow rates may be used, allowing for faster analysis times. A major advantage of APCI over ESI is its resilience against matrix effects. In ESI, the solution is charged through a metal capillary, then nebulized and dried before analysis. This presents competition for charges; a feature that APCI can avoid by creating ions in the gaseous phase.

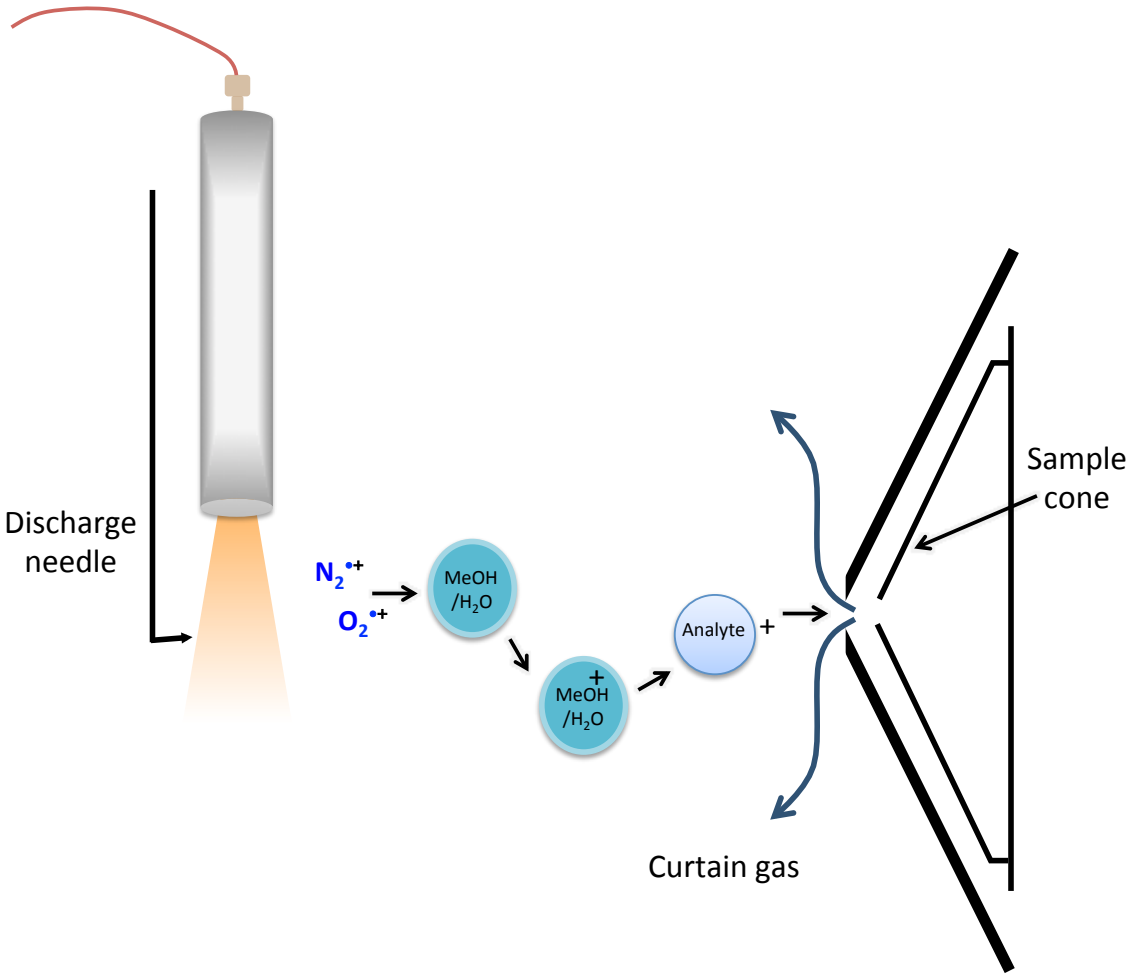

Figure 1.14, Atmospheric pressure chemical ionization.

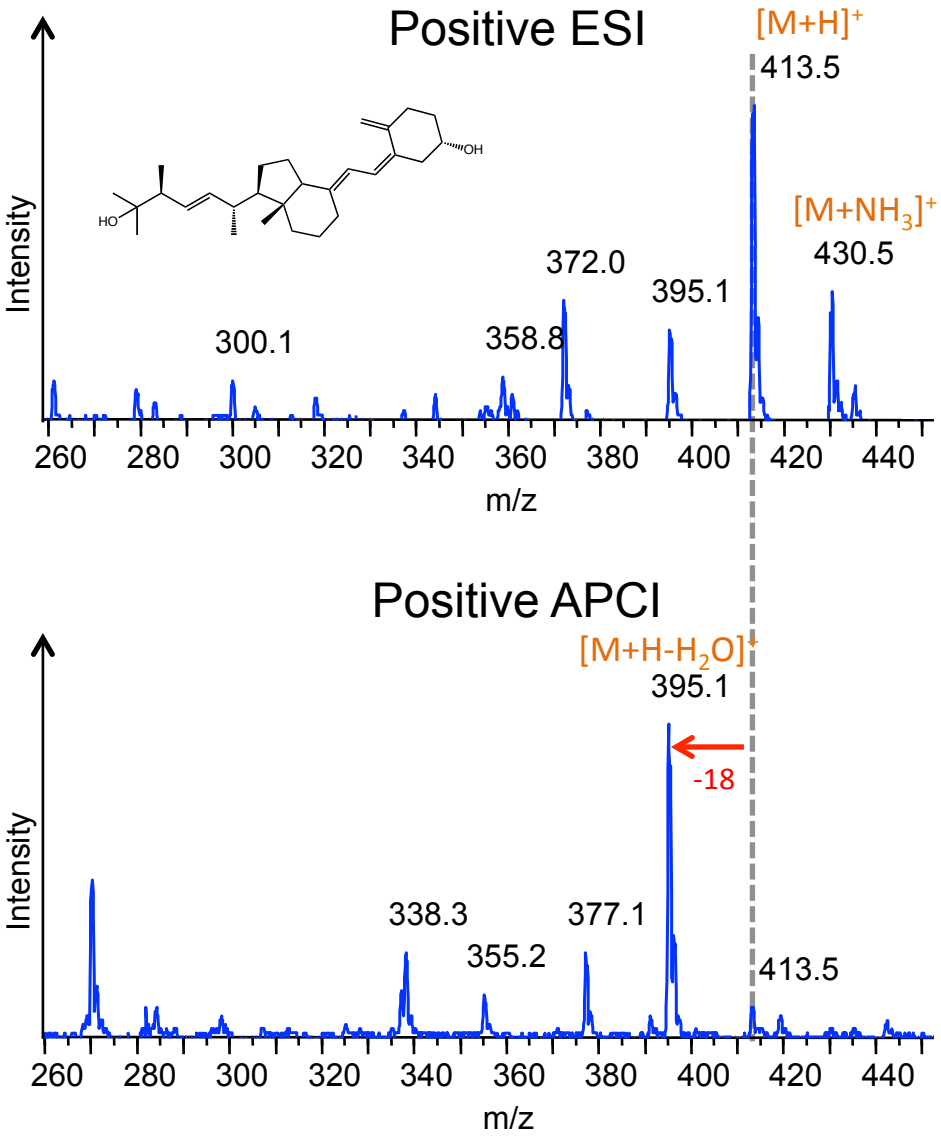
Positive ESI
[M+H]+
413.5
[M+NH3]+
430.5
372.0
395.1
300.1
358.8
Intensity
260 280 300 320 340 360 380 400 420 440
m/z
Positive APCI
[M+H-H2O]+
395.1
-18
338.3
377.1
355.2
413.5
Intensity
260 280 300 320 340 360 380 400 420 440
m/z

Figure 1.15, An example of 25-hydroxyvitamin D2 ionization by ESI and APCI. Data acquired by the author.

1.2.2.2. Mass analyzers

Mass analyzers most commonly used are quadrupole (Q), ion trap (IT) and linear ion trap (LIT), time-of-flight (TOF), and combinations as Q-TOF and Q-LIT. This work will focus on Q, IT/LIT, and TOF analyzers.

Quadrupole

Quadrupole mass analyzers have four poles arranged in a square formation. Opposite pairs are connected electrically and have radiofrequency (RF) and direct current (DC) potentials applied, with the pairs 180 ° out of phase (figure 1.15) forming a quadrupole electromagnetic field based on the laws on motion, equations 7 and 8, where ϕ = potential applied to the rods, U = DC Voltage and (VcosT) = RF Voltage [24]. These oscillating and opposite electric fields create an electric potential (F) along the x-y axis (eq. 9) (see figure 1.15). On introduction of the newly formed ions (by ESI or other source), the phase difference influences the trajectories of the ions through the quadrupoles. The quadrupole voltages are programmed to make stable trajectories for ions with certain m/z ratios. Any ion that falls outside of this stable region will oscillate too largely and strike the rods (for instance, when the values

of either x or y reach r, as in eq. 9 and depicted in figure 1.16). Stable ions will move through the rods to the detector for counting and analysis [25].

$$\phi = U - (V \cos \omega T) \tag{7}$$

$$\phi = -U + (V \cos \omega T) \tag{8}$$

$$F = [(x^2 - y^2) / r^2](U + V \cos \omega T) \tag{9}$$

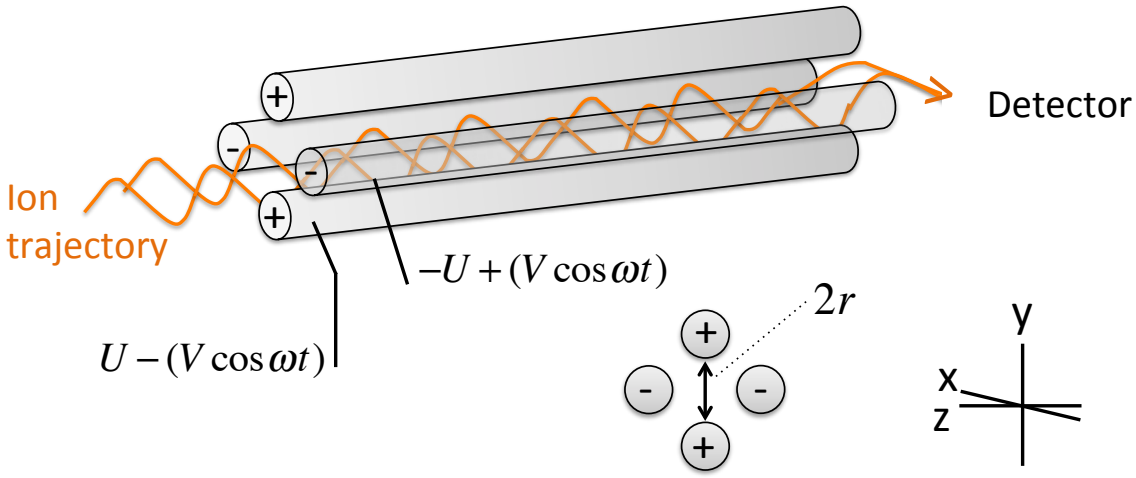

$$F = \text{ electric potential} = [(x^2 - y^2)/r^2](U + V\cos\omega T)$$

Ions move through the quadrupoles in response to an electric potential

Figure 1.16, Graphic representation of the quadrupole arrangement

Ion trap: cubic and linear

Ion trap analyzers works similarly to the quadrupole, but have a 3D geometry (figure 1.17). Ions from the source are introduced to the ion trap and form stable 3D trajectories. Similar to the quadrupole, ions with specific m/z can be selected, but unlike the quadrupole, the ions are trapped and expelled to the detector [26]. A disadvantage to using the ion trap is the formation of the “ion cloud” inside the trap itself. Ions not only respond to the RF oscillations of the ring and endcap electrodes, but they repel each other as well. To overcome this, extra inert gas (N_2, He_2) is added to collide with and offer collisional cooling [24]. On cooling, the ions remain stable and avoid expanding their trajectories to collide with the sides of the trap.

The linear trap is essentially a modified quadrupole with additional lenses at the beginning and end tuned to the same polarity as the analysis (positive for positive ions, and negative for negative ions). The like polarities repel each other thus trapping the ions [24].

The multiplexing of mass analyzers can increase their functionality and sensitivity. Aligning two quadrupoles in sequence with a collision cell in between allows the first quadrupole (Q1) to filter the molecular ion of choice, send it to the collision cell for fragmentation by collision-induced

dissociation (CAD), and finally, all fragments or the most abundant (or unique) fragment ion may be scanned by the second quadrupole (Q2). A common mass spectrometric experimental setup in quantitative analysis has Q1 set to the molecular ion of choice, fragmentation by CAD, and Q3 selection of a fragment ion. This Multiple Reaction Monitoring (MRM, also denoted MS/MS) is very sensitive and highly specific. Other common setups such as Q-IT and Q-LIT offer similar functionality. But just as the ions are able to be trapped, they are able to be fragmented inside the trap. These fragments oscillate inside and can be fragmented again before ejection and analysis. Figure 1.18 depicts the arrangement of two quadrupoles in series with the second quadrupole having the ability to also function as a linear ion trap.

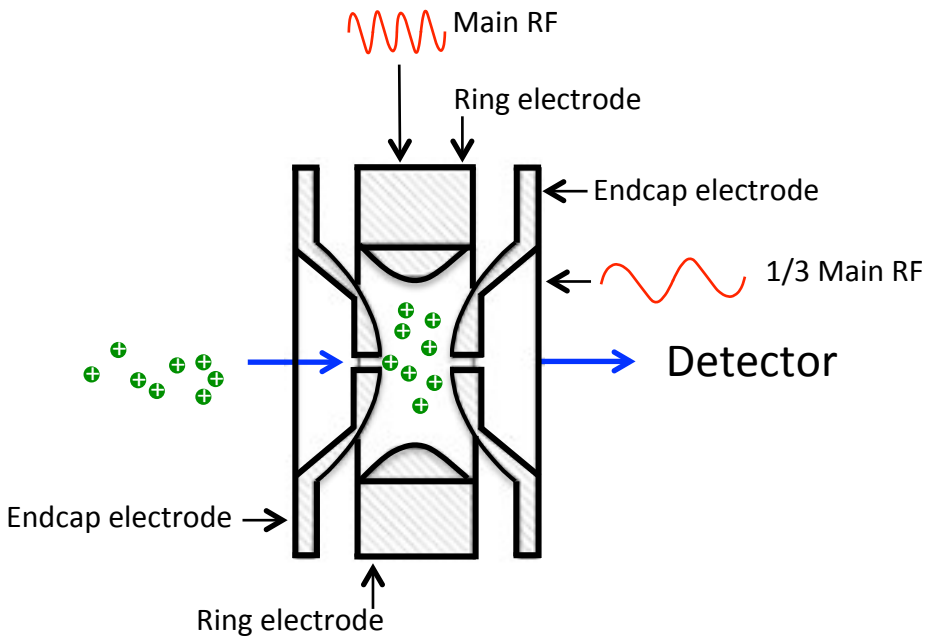

Figure 1.17, Graphic representation of an ion trap analyzer

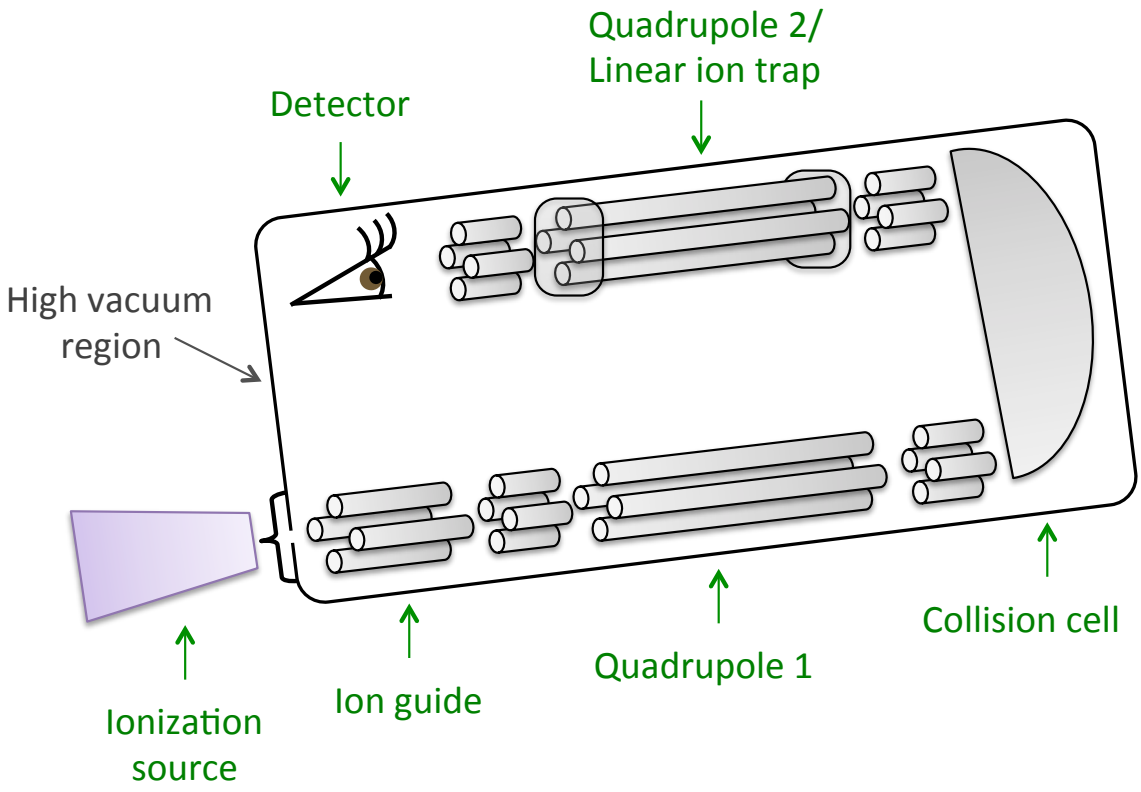

Figure 1.18, Multiplexing of two quadrupoles in series, where the second quadrupole can function as a linear ion trap.

Time of Flight

Time of Flight (TOF) analyzers separate and distinguish ions of differing m/z based on their flight times through a field-free vacuum [15]. Unlike quadrupole mass analyzers where scanning RF and DC voltages guide ions of differing m/z through an electromagnetic region to the detector, TOF analyzers distinguish each m/z present in discrete packets of ions as they arrive at the detector.

It is important for all the ions in each packet to have the same kinetic energy as their m/z is calculated by difference in flight time. Equation 10 is the mathematical definition of kinetic energy of an ion [24, 27]:

$$qE = \frac{1}{2}mv^2 \text{ , where } qE = qV = zeV \tag{10}$$

Where m = mass, v = velocity, q = ze = charge, and E = V = electric potential energy. We know that:

$$\text{velocity}, v = \frac{\text{distance traveled}, L}{\text{time}, t} \tag{11}$$

So rearrangement of equation 10 with incorporation of equation 11 yields,

$$zeE = \frac{1}{2}m\left(\frac{L}{t}\right)^2 \tag{12}$$

and further:

$$m/z = \frac{2eEt^2}{L^2} \quad (13)$$

So we can see that the drift time of an ion in a field free vacuum is related to the m/z of that ion. To achieve equal initial kinetic energies, ions created at the source are guided towards a region where they are directed orthogonally into the flight tube [28]. This orthogonal acceleration introduces kinetic energy of the same amount to each ion, but importantly, this kinetic energy is a different vectoral component and is separate from the initial velocity. Highly resolved m/z can be calculated from the difference in time of the orthogonal acceleration and detector strike. A great benefit to this development is the ability to use continuous flow into the ion source, as liquid chromatography – electrospray ionization. Ions are created continuously at the source and directed towards the flight tube. They can be filtered first by a quadrupole, and then momentarily slowed down (or trapped) in packets before entrance into the accelerator. Figure 1.19 is a schematic of a typical orthogonal-acceleration quadrupole-TOF mass spectrometer.

In typical configurations of the flight tube, ions are accelerated down towards an electrical “mirror,” also called a reflectron [29]. Here the ions drift into an electrical gradient of the same charge and cause repulsion.

Although initial kinetic energy of ions with the same m/z can be somewhat corrected by the use of the orthogonal acceleration, these are often produced at different places in the source. This kinetic energy dispersion [24] reduces resolution because of spread. To overcome this, ions are accelerated into the field-free region to a reflectron and re-directed back towards their original path. Ions with more kinetic energy will penetrate further into the reflectron and emerge to strike the detector the same time as their lower kinetic energy brother m/z.

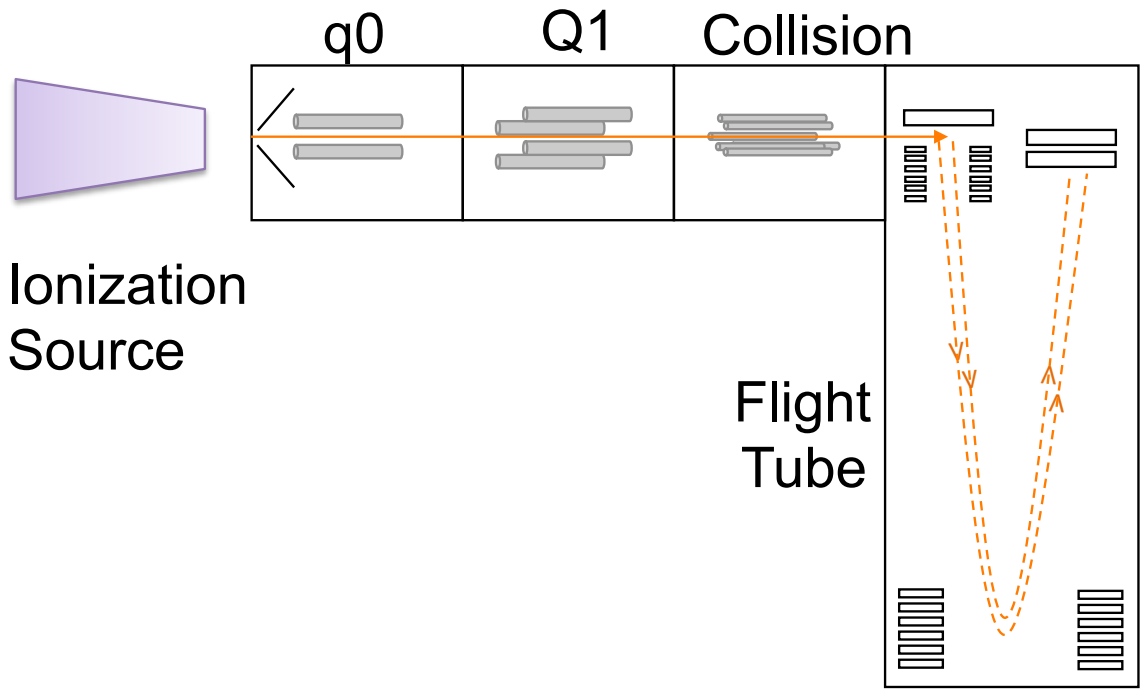

Figure 1.19, Schematic of typical orthogonal acceleration quadrupole-TOF mass spectrometer.

Resolving power, or mass resolution, is the ratio of peak mass to the width at half mass (equation 14).

$$resolution = \frac{m}{\Delta m} \tag{14}$$

Quadrupole instruments are typically ran at unit resolution meaning that at the Full Width at Half Maximum of the peak (FWHM), the Δm = 0.7 Da. This corresponds to a resolution of roughly 1000 at lower masses, and grows as the mass becomes larger. TOF instruments operate at least 10 times quadrupole resolution and are considered to be high mass accuracy instruments [24]. Figure 1.20 demonstrates the resolving power of a quadrupole and TOF mass spectrometer using Benzylpiperazine. Benzylpiperazine is discussed in Chapter III.

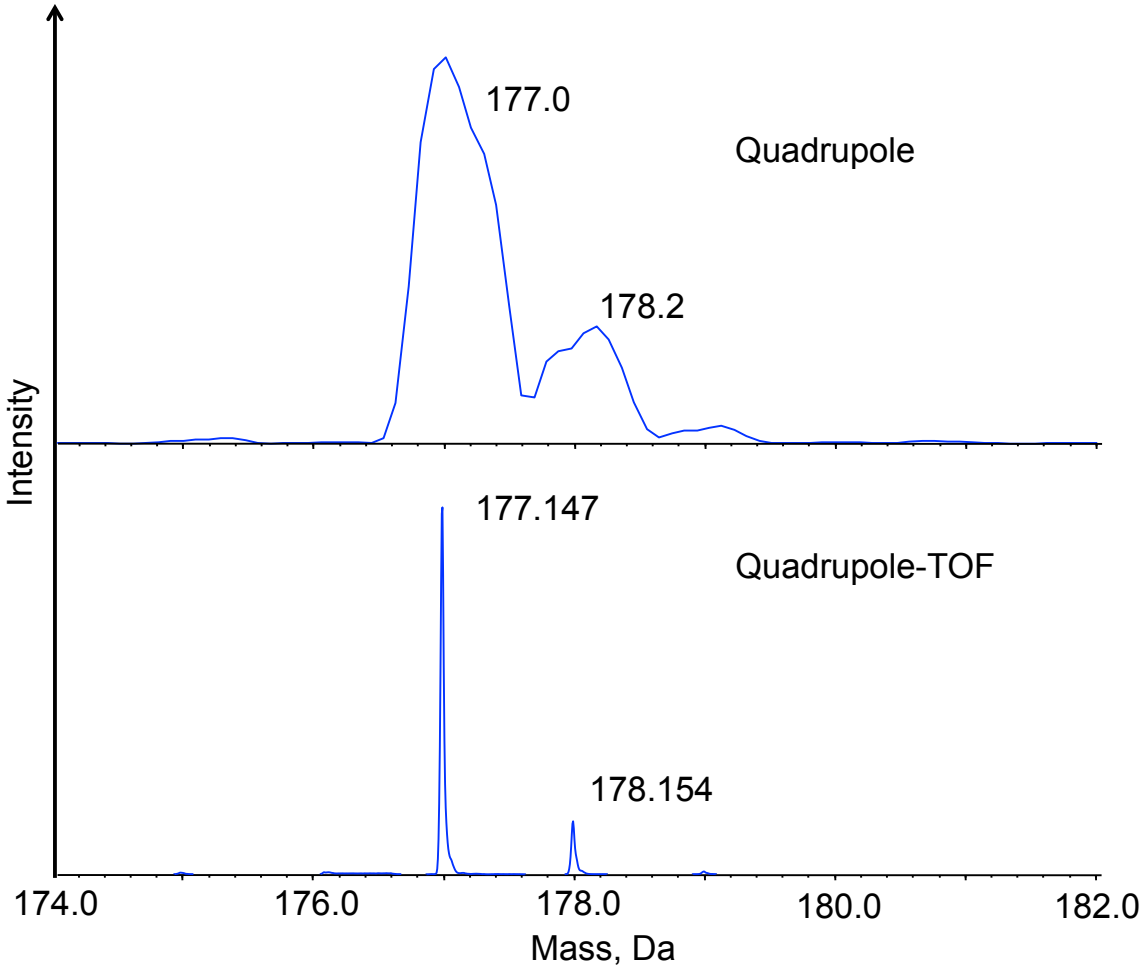

Figure 1.20, Illustration of resolution of a quadrupole vs. quadrupole-TOF mass spectrometer using benzylpiperazine (C11H16N2).

1.2.3. Quantitative bioanalytical HPLC-MS/MS method validation

Utilization of HPLC tandem mass spectrometry (MS/MS, or MRM) requires that the method used to quantify the analyte be sufficiently reproducible and reliable. To ensure reproducibility and reliability, standards of known concentrations are added to the biomatrix intended for the study, extracted, and analyzed using the instrumental setup to determine their concentration – response correlations. A standard curve of calibrators is created to determine the concentration range of the analysis, and three quality control (QC) samples, also of known concentration, spanning the range of the curve are compared. Parameters to be examined include recovery of the analyte from the biomatrix, selectivity of the measured analyte from the matrix, accuracy and precision of the measurement, reproducibility, and stability replicating the study and storage conditions.

The U.S. FDA developed a draft of recommended bioanalytical method validation guidelines in 2001 [30] with a more recent update and summary [31]. The abbreviated guidelines and considerations are listed in figure 1.21 (from reference [28]).

Parameter or Process	Requirement
Selective (matrix interference)	Review noninterference in at least 6 sources of matrix for non-MS assays. For MS assays determine MFs in 6 sources if the nonisotopically labeled IS is used. If isotopically labeled IS is used, demonstrate that IS-normalized MF is close to unity.
Validation batches	Analyze at least 3 batches for accuracy and precision. At least 1 validation batch should be made as large as the largest anticipated sample analysis batch.
QC samples	Concentration of QC samples should be: Low QC: About 3 times the LLOQ Mid QC: Middle of the range (at about the geometric mean of low and high QC concentration) High QC: Near the high end of the range, ~70% to 85% of ULOQ Dilution QC: Suffi cient to cover highest anticipated dilution
QC acceptance criteria	Intra- and inter-batch precision (%CV) and accuracy (%RE) should be: QCs prepared at all concentrations greater than LLOQ ≤15%; QC prepared at LLOQ concentration ≤20%
Calibration standards	Include the following calibration standards with each batch: Minimum of 6 non-zero standards Matrix blank: Matrix sample without internal standard Zero standard: Matrix sample with internal standard
Standard acceptance criteria	Acceptance criteria for calibration standards are: LLOQ standard ≤20% All other standards ≤15% At least 75% of standards should meet above criteria
Matrix blank	Interference in matrix blank should be ≤20% of LLOQ response
Recovery	Extent of recovery of analyte and IS should be consistent, precise, and reproducible. Determine recovery at 3 concentration levels.
Stability	Perform the following stability experiments: Stock solution: Minimum of 6 hours at room temperature Postpreparative (extracted samples/autosampler tray): Longest time from preparation through sample analysis. Assess against fresh standards, except for autosampler reinjection reproducibility. Benchtop: Stability at ambient temperature (or temperature used for processing of samples) to cover the duration of time taken to extract the samples (typically ~4-24 hours). Freeze-thaw: QC samples at minimum of 2 concentrations, 3 cycles, completely thawed, refrozen at least 12 hours between cycles, at anticipated temperature of sample storage. Long-term: Cover longest time from collection to fi nal analysis for any sample in study. Analyze 3 aliquots at low and high concentrations with fresh standard curves and compare against intended (nominal) concentrations. Long-term stability can be completed postvalidation.

*MS indicates mass spectrometry; MF, matrix factor; IS, internal standard; QC, quality control; LLOQ, lower limit of quantitation; ULOQ, upper limit of quantitation; CV, coefficient of variation; and RE, relative error.

Figure 1.21, Typical U.S. FDA bioanalytical method validation requirements (from reference [28]).

1.2.3.1. Biological sample preparation

Biological sample preparation begins first with spiking the analyte in the biological matrix. Analyte spiking is not a trivial matter, as the goal is to replicate the incurred samples (samples from a dosed human or animal) as much as possible. As standard solutions are usually prepared in organic solvent, it is advisable to limit their volume in the biomatrix calibrators and quality controls to less than 5%. Not only does this avoid unnecessary dilution of the biomatrix before extraction and analysis, this low percentage will not cause precipitation of the protein constituents while ensuring reproducible extractions.

There are four common sample preparation methods: solid phase extraction, liquid-liquid extraction, deproteinization, and simple dilution (usually reserved for low protein samples like urine).

1.2.3.1.1. Solid phase extraction

Solid phase extraction (SPE) is a technique to isolate the analyte of interest from the biomatrix that is similar to liquid chromatography. The packing, or sorbents, used are silica and polymeric-based with ligands of C8, C18, IEX (cation exchange and anion exchange), phenyl, and

versatile mixed-mode sorbents like the hydrophobic and hydrophilic mixture, HLB [32].

The general protocol for SPE involves conditioning the sorbant with 100% organic (usually methanol), conditioning with water or buffer, loading the sample (usually diluted with water or buffer), rinsing away the other matrix components, and finally elution. Paramount considerations are pH loading and organic percentage at washing and elution (figure 1.22). These steps are dependent on the analyte chemical properties and the mode of extraction chosen.

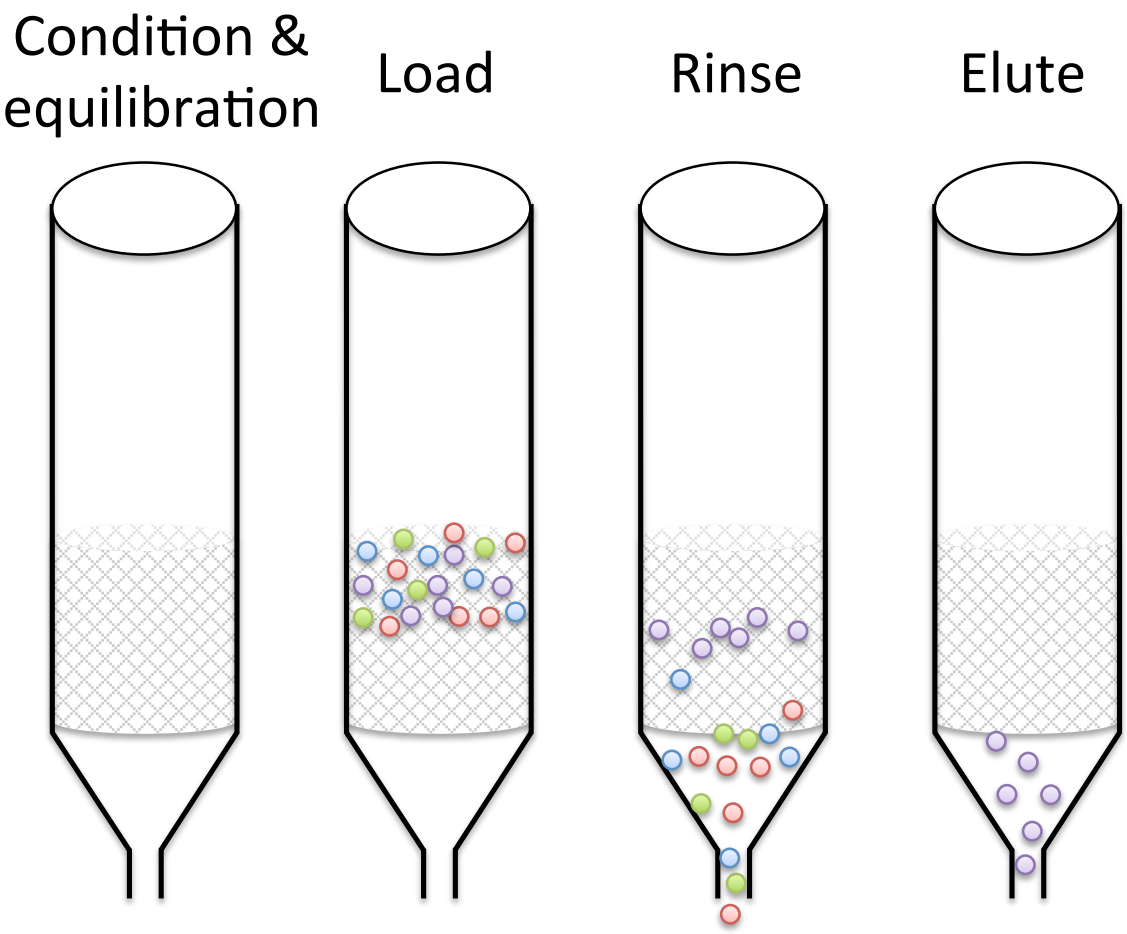

1.22, Illustration of SPE

1.2.3.1.2. Liquid-liquid extraction

Liquid-liquid extraction (LLE) is a fast and useful procedure to separate analytes from matrix based on their differential partitioning into solvents [33]. Solvents that are not miscible with aqueous solution are used, and the analyte partitions into the solvent based on their distribution into the organic versus the aqueous phase.

Table 1.4 lists common solvents and their densities and boiling points. Considering the density of water (and ergo the biomatrix) is 1, any solvent with a density <1 will settle above the matrix and facilitate easy removal. The partition coefficient refers to a ratio of concentration of solubility of analyte between the two phases:

$$K_d = \frac{[A]_{organic}}{[A]_{aqueous}} \quad (15)$$

Most analytes have an order of magnitude higher solubility (K_d) in organic over aqueous. If the analyte is ionized at physiological conditions, pH manipulation may be utilized to form a non-charged species. Still, incomplete extraction is expected as extraction is based on equilibrium. The fraction of analyte that remains in the aqueous phase after one extraction can be calculated by the following equation,

$$\frac{mole_{A_X}}{mole_{A_Y}} = \text{mole fraction}, f = \frac{V_{aqueous}}{V_{aqueous} + K_d V_{organic}} \quad (16)$$

Where V = volume in mL.

As is evident by the above equation, it is often necessary to perform more than one LLE to achieve acceptable extraction recoveries of the analyte from the biomatrix as there is always a small amount of analyte that will be left in the aqueous phase.

Solvent	density, g/mL
Hexne	0.685
Diethyl ether	0.713
Methyl-*tert*-butyl ether	0.740
Methylethyl ketone	0.805
N-butanol	0.810
Ethyl acetate	0.897
Methylene chloride	1.33
Chloroform	1.48

density of water = 1

Table 1.4, Properties of some common solvents for LLE under conditions of standard temperature and pressure.

1.2.3.1.2.1. Salting-out assisted liquid-liquid extraction

LLE is a great extraction method for analytes that are either not charged at physiological pH, or compounds with chemical characteristics that make them amenable to pH manipulation for differential extraction. Very polar compounds may be subjected to a different kind of LLE using solvents that are miscible with the aqueous phase. Adding salts to the aqueous phase before the addition of miscible solvents facilitates phase separation [34]. Appropriate salts include ammonium sulfate, ammonium formate, and ammonium acetate. Adding these salts will facilitate the phase separation of common solvents such as isopropanol and acetonitrile [35].

1.2.3.1.3. Deproteinization

One of the most convenient methods of sample preparation is deproteinization by organic solvents. The addition of sufficient percentage (>50%) of organic solvents such as methanol and acetonitrile influence proteins to associate with each other and effectively fall out of solution [36]. Although this method of sample preparation is fast and inexpensive, one drawback is that higher concentrations of residual salts are left in the extracted portion and can lead to unwanted matrix effects.

1.2.3.2. Matrix effect

An essential evaluation for method development is the consideration and calculation of matrix effects. Matrix effects are defined as the measure of enhancement or suppression of analyte in extracted matrix compared to analyte in solution (equation 17).

$$\text{matrix effect} = \frac{\text{response of analyte in extracted matrix}}{\text{response of analyte in solution}} \quad (17)$$

A calculation of 1 indicates no matrix effects, where <1 indicates suppression and >1, enhancement.

As mentioned in section 1.2.2.1, the ionization technique can have a great effect on matrix effects. Additionally, the extraction method plays an important role in eliminating as many of the interfering components as possible. Other tactics to improve matrix effects include changes in the chromatographic separation and the utilization of internal standard. Internal standards are added to the sample before extraction and used in the quantitative calculations. For example, the matrix effect calculation in the presence of an internal standard is:

$$\text{Matrix Effect} = \frac{\left(\frac{\text{response of analyte in extracted matrix}}{\text{response of internal standard in extracted matrix}}\right)}{\left(\frac{\text{response of analyte in neat solution}}{\text{response of internal standard in neat solution}}\right)} \quad (18)$$

As is evident by equation 18, the division of the response of analyte by the response of the internal standard can help to eliminate errors by extraction and injection. Further, choosing an internal standard the elutes at the same retention time as the analyte ensure that both compounds experience the same matrix enhancement or suppression and hence that deviation can be mathematically eliminated from the quantitation [37].

1.3. Conclusion

Careful consideration in the choice of analytical instrumentation, separation, and extraction method can determine the success of bioanalytical method development. Understanding the chemical properties of the analyte(s) of interest as well as the instrumental and HPLC theory help to ensure that if a roadblock is met, it can be overcome with a new approach.

1.4. References

[1] R.L. Grob, E.F. Barry, Modern Practice of Gas Chromatography, John Wiley & Sons, 2004.

[2] L.R. Snyder, J.J. Kirkland, J.W. Dolan, Introduction to modern liquid chromatography, John Wiley and Sons, 2010.

[3] S.F.Y. Li, Capillary Electrophoresis: Principles, Practice, and Applications. Journal of Chromatography Library, Vol. 52, Elsevier, 1992.

[4] M.S. Lee, E.H. Kerns, Mass Spectrometry Reviews, 18 (1999) 187-279.

[5] R.N.X. Xu, L.M. Fan, M.J. Rieser, T.A. El-Shourbagy, Journal of Pharmaceutical and Biomedical Analysis, 44 (2007) 342-355.

[6] M.W. Dong, Modern HPLC for Practicing Scientists, John Wiley & Sons, INC., Hoboken, NJ, 2006.

[7] J. Nawrocki, Journal of Chromatography A, 779 (1997) 29-71.

[8] D.V. McCalley, Liquid Chromatographic Separations of Basic Compounds, in: E. Grushka, N. Grinberg (Eds.) Advances in Cromatography, Volume 46, CRC Press, 2008.

[9] J.J. Kirkland, M.A. Vanstraten, H.A. Claessens, Journal of Chromatography A, 691 (1995) 3-19.

[10] U.D. Neue, J.E. O'Gara, A. Mendez, Journal of Chromatography A, 1127 (2006) 161-174.

[11] P.C. Sadek, The HPLC Solvent Guide, John Wiley & Sons, 1996.

[12] V. Meyer, Practical High-Performance Liquid Chromatography, John Wiley & Sons, 2004.

[13] U.D. Neue, A. Mendez, Journal of Separation Science, 30 (2007) 949-963.

[14] C.G. Herbert, R.A.W. Johnstone, Mass Spectrometry Basics, CRC Press, 2000.

[15] R. Ekman, J. Silberring, A. Westman-Brinkmalm, A. Kraj, Mass Spectrometry: Instrumentation. Interpretation, and Applications, John Wiley & Sons, 2009.

[16] M.S. Wilm, M. Mann, International Journal of Mass Spectrometry, 136 (1994) 167-180.

[17] X.J. Yang, Y.X. Qu, Q.P. Yuan, P.Y. Wan, Z.X. Du, D.Z. Chen, C. Wong, Analyst, 138 (2013) 659-665.

[18] K. Schug, H.M. McNair, Journal of Separation Science, 25 (2002) 760-766.

[19] R.E. Ardrey, Liquid Chromatography - Mass Spectrometry: An Introduction, John WIley & Sons, 2003.

[20] A. Jones, R. LoBrutto, Y. Kazakevich, Journal of Chromatography A, 964 (2002) 179-187.

[21] J.H. Zhu, R.B. Cole, Journal of the American Society for Mass Spectrometry, 11 (2000) 932-941.

[22] M. Jemal, R.B. Almond, D.S. Teitz, Rapid Communications in Mass Spectrometry, 11 (1997) 1083-1088.

[23] A. Westman-Brinkmalm, G. Brinkmalm, Mass Spectrometry and Hyphenated Techniques in Neuropeptide Research, in: J. Silberring, R. Ekman (Eds.), John Wiley &Sons, 2002.

[24] E. de Hoffmann, V. Stroobant, Mass Spectrometry - Principals and Applications, John Wiley & Sons, 2007.

[25] L. Ding, S. Kumashiro, Rapid Communications in Mass Spectrometry, 20 (2006) 3-8.

[26] S. Sevugarajan, A.G. Menon, International Journal of Mass Spectrometry, 218 (2002) 181-196.

[27] M. Guilhaus, Journal of Mass Spectrometry, 30 (1995) 1519-1532.

[28] M. Guilhaus, D. Selby, V. Mlynski, Mass Spectrometry Reviews, 19 (2000) 65-107.

[29] M. Guilhaus, V. Mlynski, D. Selby, Rapid Communications in Mass Spectrometry, 11 (1997) 951-962.

[30] US Food and Drug Administration. Guidance for Industry: Bioanalytical Method Validation. US Department of Health and Human Services, US FDA, Center for Drug Evaluation and Research, Rockville, MD, USA (2001).

[31] S. Bansal, A. DeStefano, Aaps Journal, 9 (2007) E109-E114.

[32] K.M. Li, L.P. Rivory, S.J. Clarke, Current Pharmaceutical Analysis, 2 (2006) 95-102.

[33] P. Patnaik, Extraction Methods, in: Dean's Analytical Chemistry Handbook, McGraw-Hill, 2004.

[34] G. Grueiro Noche, M.E. Fernandez Laespada, J.L. Perez Pavon, B. Moreno Cordero, S. Muniategui Lorenzo, Journal of Chromatography A, 1218 (2011) 6240-6247.

[35] M. Tabata, M. Kumamoto, J. Nishimoto, Analytical Sciences, 10 (1994) 383-388.

[36] R.G. Harrison, Bioseparations Science and Engineering, Oxford University Press, 2003.

[37] M.P. Taillon, M. Furtado, F. Garofolo, Bioanalysis, 3 (2011) 1201-1215.

CHAPTER II

DETERMINATION OF HEXAMTHYLENE BISACETAMIDE, AN ANTINEOPLASTIC COMPOUND, IN MOUSE AND HUMAN PLASMA AND MOUSE MAMMARY TUMOR BY LC–MS/MS

2.1. Introduction

Hexamethylene bisacetamide (HMBA) is a hybrid bipolar compound first synthesized and characterized as an erythroid differentiator for murine erythroleukemic cells (MELC) in 1976 [1]. Initially inspired by the structures and functions of DMSO and N-methylacetamide, HMBA was used as the model differentiating agent for a class compounds known as acetylated diamines. At a concentration of 5 mM, HMBA caused > 99% of MELC in culture to differentiate without cytotoxicity [1]. Furthermore, experimentation showed that HMBA also induced terminal differentiation in a variety of leukemic cell lines [2, 10]. Based on these findings, HMBA

was studied in several Phase I and Phase II clinical trials for the treatment of myelodysplastic syndrome (MDS), acute myelogenous leukemia (AML), general advanced cancer, and solid tumors [3-9]. Pharmacokinetic studies of HMBA in humans revealed a relatively short half-life of 2.4 – 2.9 hours [24] (figure 2.1). Serious side effects of HMBA, such as thrombocytopenia, limited the dose escalation and prevented sufficient plasma concentrations to be realized for its terminal differentiating potential.

	Human
t½, hour	2.4-2.9
Vd, L/m^2	1.1 – 30.2 (4 – 21%)
Max tolerated (humans) , (g/m^2)/day	33.6
Highest plasma concentration, mM	1.5-2
Clearance (total body), (mL/min)/m^2	61-82
Renal Clearance %	40-45%

Figure 2.1, Pharmacokinetic properties of HMBA in humans.

Recent studies show that HMBA induced the expression of an endogenous protein, hexamethylene bisacetamide inducible protein 1 (HEXIM1), which inhibits cell growth [11, 12]. Increased HEXIM1 expression in breast tumor and breast epithelial cells resulted in a decrease of cell proliferation [12]. Additionally, not only did HEXIM1 inhibit cell proliferation, it interacted with the estrogen-receptor (ER)-gene transcription complex and prevented mammary gland development in vivo [13]. Such properties indicated a possible new role for HMBA in the treatment of breast cancer. It has been proposed that HEXIM1 interferes with kinase action at the coding region of ER-responsive genes preventing the phosphorylation of RNA polymerase II (RNAP II) by the kinase complex, positive transcriptional elongation factor b (P-TEFb) [13, 14]. Phosphorylation of RNAP II by P-TEFb facilitates complete mRNA elongation [15]. The prevention of this phosphorylation commits the cell to the abortive phase of elongation, and halts transcription [16] (figure 2.2).

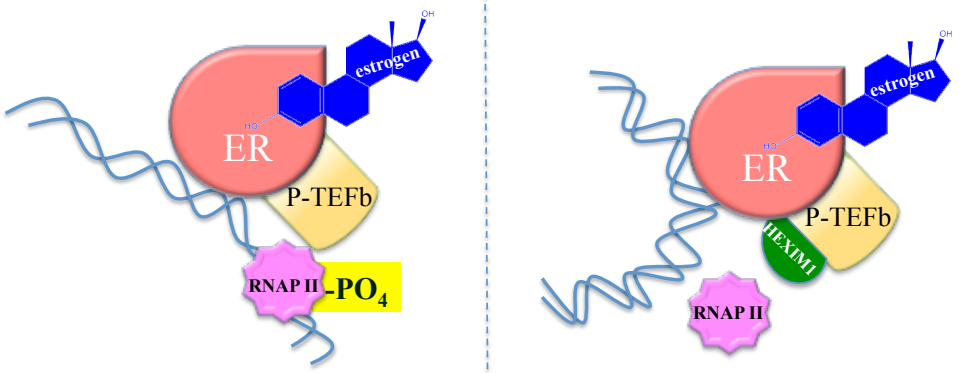

ER binds to Estrogen Response Element (ERE) on certain genes, P-Tefb phosphorylates RNAP II which allows elongation of the message.
Cells grow and divide.

HMBA upregulates HEXIM1 expression, which interferes with ER to ERE as well as P-Tefb action.
Cells can not replicate.

Figure 2.2, Graphic of the antiproliferative action of HEXIM1.

To support studies of HMBA at lower doses as a potential therapeutic agent for breast cancer, a sensitive analytical method is required. Up to date, the published analytical methods for the measurement of HMBA in plasma and urine are LC-UV and GC-N/P based methods, which have lower limits of quantitation (LLOQs) of 1.00 µg/mL and 2.00 µg/mL, respectively [17, 18]. These and other methods have been applied to several high-dose HMBA Phase I and II clinical trials [3-9, 19, 20], but the LLOQs of these methods are not sufficient for the measurement of HMBA in the majority of biological samples for breast cancer study with concentrations less than 1.00 µg/mL. This paper describes, for the first time, the development and validation of an LC-MS/MS method for the quantitative measurement of HMBA in both mouse and human plasma and mouse mammary tumor homogenate with an LLOQ of 0.500 ng/mL and a linear calibration range up to 100 ng/mL. To circumvent the toxic effects of HMBA, directed dosing using the FDA approved polymer poly(lactic-co-glycolic) acid is used. In this work, heptamethylene bisacetamide (7MBA) was used as the internal standard. Both HMBA and 7MBA were recovered from biological matrices by a simple step of deproteinization with acetonitrile. Separation of the analyte and internal standard was achieved on a Waters Atlantis® T3 column using 15% acetonitrile 85% 10 mM ammonium acetate, pH 4.0 as mobile phase. Quantitation was carried out by tandem mass spectrometry operated in the positive

multiple-reaction-monitoring (MRM) mode. Finally, the validated method was applied to the measurement of HMBA concentrations in two preliminary mouse studies.

2.2. Materials and methods

2.2.1 Chemicals and standard solutions

Ammonium acetate and hexamethylene bisacetamide (catalog no. 224235) were from Sigma-Aldrich (St. Louis, MO, USA). HPLC-grade acetonitrile was from Pharmco-AAPER (Louisville, KY, USA). HPLC-grade glacial acetic acid was from J.T. Baker through VWR (West Chester, PA, USA). Sodium chloride, sodium hydrogen phosphate, potassium dihydrogen phosphate, sodium chloride, potassium chloride, 2,2,2-tribromoethanol, and tert-amyl alcohol were from Fisher Scientific (Pittsburgh, PA, USA). Heptamethylene bisacetamide (7MBA) was obtained from the DTP Open Chemical Repository of the US National Cancer Institute (http://dtp.cancer.gov) with assigned code NSC36911. Six pooled blank human plasmas with specific lot numbers (W06509203366, W06509105961, W069509203227, W069509203370, W069509203365, and W069509203234) were from Haemtech, Inc (Essex Junction, Vermont, USA), which were donated by Dr. Michael Kalafatis at Cleveland State University. Six pooled blank mouse plasmas (citrated) with specified lot

numbers (09F21004, 11B21080, 11B21081, 11B21082, 11B21083, and 11B21084) were purchased from Lampire Biological Laboratories (Pipersville, PA, USA). The Type 1 deionized water was obtained from a Barnstead NANOpure® water purification system (Thermo Scientific, Waltham, MA, USA).

The mobile phase for liquid chromatographic separation was prepared by mixing acetonitrile and 10 mM ammonium acetate (pH 4.0) at a ratio of 15:85 (v/v). The standard stock solutions of HMBA and 7MBA were prepared in acetonitrile at a concentration of 1 mg/mL. The standard working solutions of HMBA at concentrations 50.0, 100, 150, 500, 1.00 x 10^3, 3.00 x 10^3, 5.00 x 10^3, 9.00 x 10^3, and 10.0 x 10^3 ng/mL for the plasma studies and at 10.0, 20.0, 100, 200, 1.00 x 10^3, 2.00 x 10^3, 30.0, 600, and 1.80 x 10^3 ng/mL for tissue study were prepared by serial dilutions of the standard stock solution of HMBA with the mobile phase. The internal standard working solution of 100 ng/mL was prepared by two subsequent dilutions (1:100) of the standard stock solution of 7MBA in the mobile phase. The standard stock solutions were kept in amber glass vials and stored at -20°C.

2.2.2. Liquid chromatography tandem mass spectrometry

The liquid chromatography tandem mass spectrometry system was comprised of a AB Sciex QTrap® 5500 mass spectrometer equipped with electrospray ionization (ESI) probe and syringe pump (AB Sciex, Foster City, CA, USA), and a Shimadzu Prominence UFLC system with binary pump and autosampler (Shimadzu, Columbia, MD, USA). The system was connected using PEEK tubing (1/16 in. o.d. x 0.01 in. i.d.). Data was acquired and processed using AB Sciex Analyst software (version 1.5.1).

Analytical separation of HMBA and the IS was performed isocratically at ambient temperature on a Waters Atlantis® T3 (3 µm, 120 Å, 2.1 x 50 mm) column (Waters, Milford, MA, USA) with the mobile phase at the flow rate of 0.150 mL/min. The injection volume of each sample was 5 µL. Prior to initial sample injection, the column was equilibrated with the mobile phase at the above flow rate for a minimum of 15 min.

The AB Sciex QTrap® 5500 mass spectrometer was operated by the positive electrospray ionization (ESI) mode using the following instrument settings: CUR 34; CAD HIGH; IS 4500; TEM 550; GS1 38; GS2 32; DP 70; EP 10; CE 20; CXP 16. These settings were optimized first by direct infusion of 200 ng/mL each HMBA and the IS at 10 µL/min using the integrated syringe pump, then refined by the “Compound Optimization”

feature of the Analyst software using flow injection analysis. HMBA and the IS were quantitated by MRM mode using the following mass transitions: m/z 201.2 → 159.2 for HMBA and m/z 215.2 → 173.2 for 7MBA, with a dwell time of 300 ms for each analyte.

2.2.3. Preparation of plasma calibrators and quality controls

Plasma calibrators and quality controls (QCs) were prepared using the pooled blank human and mouse plasmas and mouse mammary tumor tissue homogenate which contained no detectable HMBA. Tumor tissue was homogenized with 1x PBS to 0.4 mg/mL for approximately 2 minutes on ice using a handheld polytron homogenizer. The homogenizer was rinsed between each sample with fresh methanol followed by 1x PBS. Plasma calibrators were prepared by addition of 10 µL of the mobile phase (for the blank of HMBA) or each standard working solution of HMBA to 990 µL of blank pooled plasma. Tumor homogenate calibrators were prepared by the addition of 5 µL of the mobile phase (for the blank of HMBA) or each standard working solution of HMBA to 95 µL of blank tumor homogenate. These preparations made final concentrations of 0.00, 0.500, 1.00, 5.00, 10.0, 50.0, and 100 ng/mL each in a 1.5-mL microcentrifuge tube (VWR, West Chester, PA, USA). Plasma QCs were prepared by addition of 10 µL of each standard working solution of HMBA to 990 µL of blank pooled plasma where tumor homogenate QCs were

prepared by the addition of 5 µL of each standard working solution to 95 µL blank tumor homogenate to make final concentrations of 1.50, 30.0, and 90.0 ng/mL each in a 1.5-mL microcentrifuge tube. The calibrators and QCs were vortex-mixed for 30 s, and then stored overnight at -20°C before use..

2.2.4. Animal study

The animal study protocol for this work was approved by the Institutional Animal Care and Use Committee at Case Western Reserve University. FVB mice from Jackson Laboratories (Bar Harbor, ME, USA). The mouse model of human breast cancer, FVB - MMTV/HEXIM1/PyMT, was generated by crossing MMTV/HEXIM1 mice [13] with PyMT transgenic mice [unpublished data]. Treatment regimens were started at 4 – 6 weeks of age. For investigation, the mice were anesthetized using Avertin (containing 1.3% tribromoethanol and 0.8% tert-amyl alcohol). HMBA concentrations in plasma and mammary tumor tissue were investigated two ways: by direct injection (10 mg/kg) in saline (0.9% sodium chloride in water) and by injection of 2 mg/kg (to 0.05 cc) of 5 mM HMBA-loaded PLGA each into the left thoracic mammary gland through the nipple. At 0 (pre-dose), 15, 30, 45, 60, 120, 240, 360, and 480 min, the mice were ocularly bled and then sacrificed. Blood samples were collected in sterile 1.5-mL microcentrifuge tubes and centrifuged at 3000 x g for 15 min.

Tumor samples were weighed and homogenized with 1x PBS to 0.4 mg/mL. Mouse plasma and tumor homogenate samples were stored at -20°C until analysis. The developed LC/MS method was used to determine the concentrations of HMBA in mouse plasma over the time course of study.

2.2.5. Sample preparation

Plasma and tumor homogenate calibrators and QCs, as well as mouse plasma and tumor homogenate samples from FVB mice, were prepared as follows: samples were removed from -20°C freezer, and thawed to room temperature; for each plasma sample, 25 µL of plasma together with 5 µL of the IS working solution (100 ng/mL) or the mobile phase (for the blank of IS) were added to 1.5-mL microcentrifuge tube, vortex-mixed for 30 s, and kept at 4°C for 30 min; the sample was then deproteinized with 100 µL of HPLC-grade acetonitrile at a ratio of 3.3 to 1 by vortex-mixing for 30 s; following centrifugation at 24,400 x g for 10 min, the supernatant was pipetted into a 1.5-mL microcentrifuge tube and dried in a Savant DNA120 SpeedVac® concentrator (Thermo Scientific, Asheville, NC, USA) at 43°C for 30 min; finally, the resultant residual was reconstituted in 25 µL of the mobile phase for the subsequent LC-MS/MS analysis.

2.2.6. Stability studies

The stability of HMBA in human and mouse plasma before and after sample preparation, and through freeze-and-thaw cycles were investigated at low, medium, and high QC concentrations. These studies included QC samples kept on bench top at 22°C for 0, 4, 8, and 24 h before sample preparation and analyses, QC samples kept in autosampler at 4°C for 0, 4, 8, and 24 h after sample preparation and before LC-MS/MS analyses, and QC samples undergone three freeze-and-thaw cycles where the samples were frozen at −20°C for at least 24 h and thawed at room temperature unassisted 3 times.

2.3. Results

2.3.1. LC–MS/MS

Due to its chemical structure, HMBA has a propensity to interact with the particle substrate of the bonded phase resulting in a tailing peak. Therefore, columns with endcapping (e.g., Waters XBridge™ C8, Waters XTerra® C8, and Waters Atlantis® T3) were considered for analytical separation. Among the columns tested, Waters Atlantis® T3 (2.1 x 50 mm, 3 µm) displayed not only excellent retention times and reproducibility for

the analytes, but also symmetrical peak shapes without adding additional modifiers to the mobile phase. Therefore, it was chosen for this work.

Full-scan infusion analysis revealed $[M+Na]^+$ as the predominant precursor ion in the aqueous solutions of both HMBA and the IS (mass spectra not shown). The addition of an ammonium salt was effective to suppress the formation of $[M+Na]^+$ and produce $[M+H]^+$ as the major precursor ions. After investigation with each ammonium acetate and ammonium formate, it was determined that the former resulted in greater detection signal; therefore, ammonium acetate was added to the mobile phase in the subsequent studies. Precursor ions $[HMBA+H]^+$ at m/z 201.2 and $[IS+H]^+$ at m/z 215.2 produced major product ions at m/z 159.2 and m/z 173.2 by breaking the amide bond (Figure 2.3). Therefore, the mass transitions of m/z 201.2 → 159.2 for HMBA and m/z 215.2 → 173.2 for the IS were used for the quantitation of HMBA by tandem mass spectrometry with MRM mode.

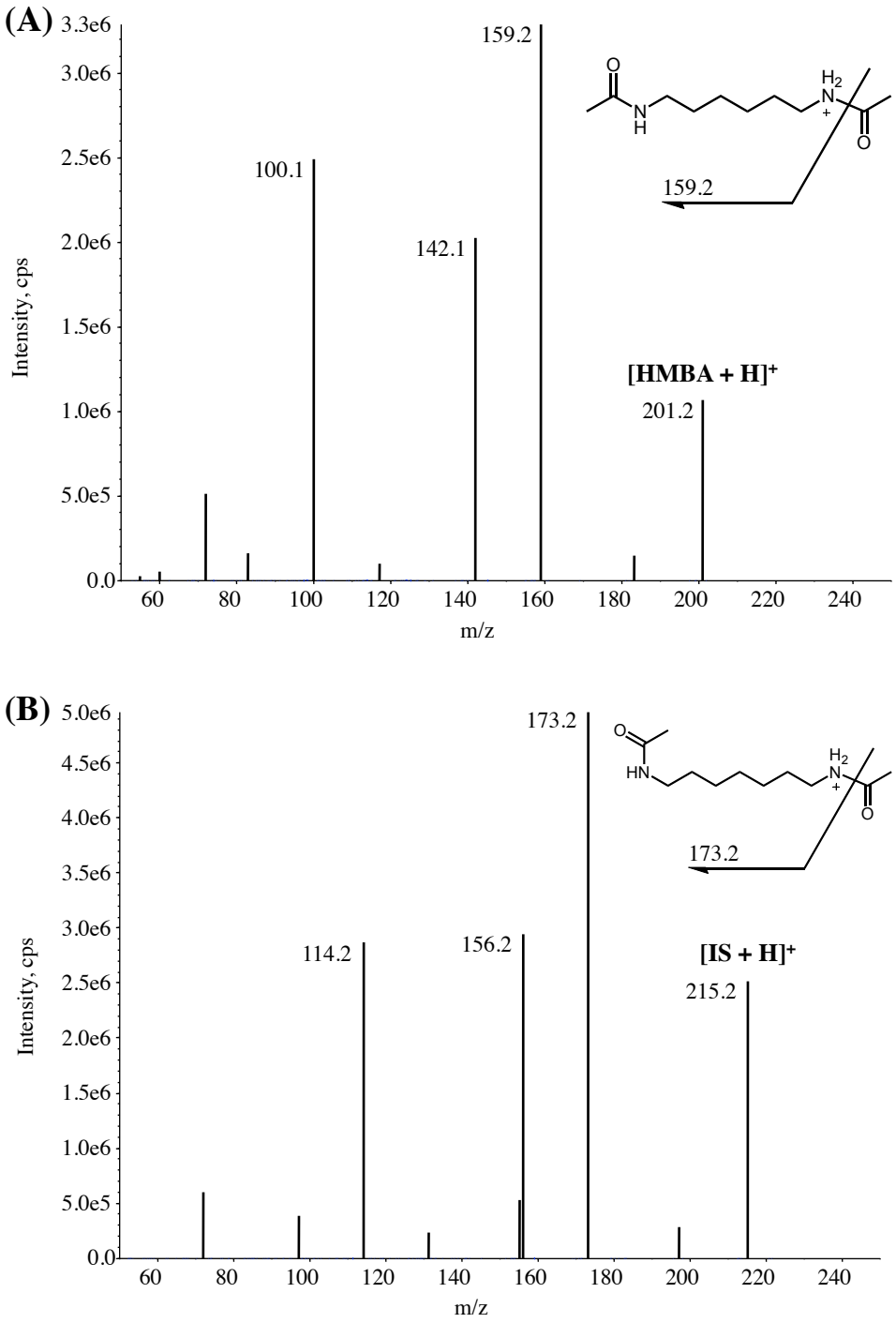

Figure 2.3, Product ion spectra and structures of (A) HMBA and (B) 7MBA, the internal standard (IS).

2.3.2. Matrix interference and specificity

The use of Waters Atlantis® T3 (2.1 x 50 mm) as analytical column for separation and 35% methanol and 5 mM ammonium acetate (pH 6.8) as mobile phase was first evaluated. While achieving excellent retention and separation for HMBA and the IS, interferences were encountered in both plasma matrices, more severely in mouse plasma (chromatograms not shown). This unidentified endogenous compound co-eluted and produced a common product ion of m/z 159.2 with HMBA in the tandem mass spectrometer.

Since choosing a different product ion for quantitation of HMBA reduced the sensitivity of detection significantly, other approaches to minimize the interference were examined: (i) various sample preparation methods, such as (a) protein precipitation using various volume ratio of plasma to organic solvent(s) [i.e., plasma to acetonitrile ratio of 1:2, 1:3, 1:4, and 1:5 with and without 0.1% formic acid or 0.1% ammonium hydroxide modifiers; plasma to acetonitrile/methanol (75/25) ratio of 1:5, as well as plasma to acetonitrile/ethanol (75/25) ratio of 1:5], (b) liquid-liquid extraction with saturated ammonium sulfate and 15/85 isopropanol/ethyl acetate [21], and (c) denaturation of plasma proteins by heating the sample at 100°C for 5 min prior to centrifugation; (ii) separation by different types of column [e.g.,

Waters XBridge™ C8 (2.1 x 50 mm, 3 µm, 120 Å) and Waters XTerra® C8 (2.1 x 50 mm, 3 µm, 120 Å)]; and (iii) changing mobile phase composition and/or pH.

All sample preparation methods tested yielded similar results except liquid-liquid extraction with saturated ammonium sulfate and 15/85 isopropanol/ethyl acetate, which worsened the interference. Among the columns examined, the Waters Atlantis® T3 (2.1 x 50 mm) column displayed the best chromatographic performance. The most satisfactory results were obtained by changing the mobile phase organic composition and pH (i.e., 15% acetonitrile, 85% 10 mM ammonium acetate at pH 4.0) for both human and mouse plasma.

Finally, the optimal separation of HMBA and the IS was achieved on a Waters Atlantis® T3 (2.1 x 50 mm) column at 2.2 and 3.7 minutes by a mobile phase containing 15% acetonitrile, 85% 10 mM ammonium acetate at pH 4.0 using 3.3 volumes of acetonitrile for deproteinization. Under these conditions, the previously co-eluted interference was completely resolved from human plasma (Figures 2.4A and 2.4B). Even though the interfering compound in mouse plasma and tissue homogenate was not completely removed (Figure 2.4C and 2.4E, top traces), it had been reduced to a minimum that was insignificant for the analysis. The peak area of the interference in mouse plasma was about 8% and homogenate

was 14% of the LLOQ for HMBA by the LC-MS/MS method (Figure 2.4C-F), an acceptable level by the industry [22]. The specificity of the LC-MS/MS method was further demonstrated by measuring HMBA at the LLOQ (0.500 ng/mL) of the method from six lots of human plasma samples and six lots of mouse plasma samples (see Section 2.3.3.2.)

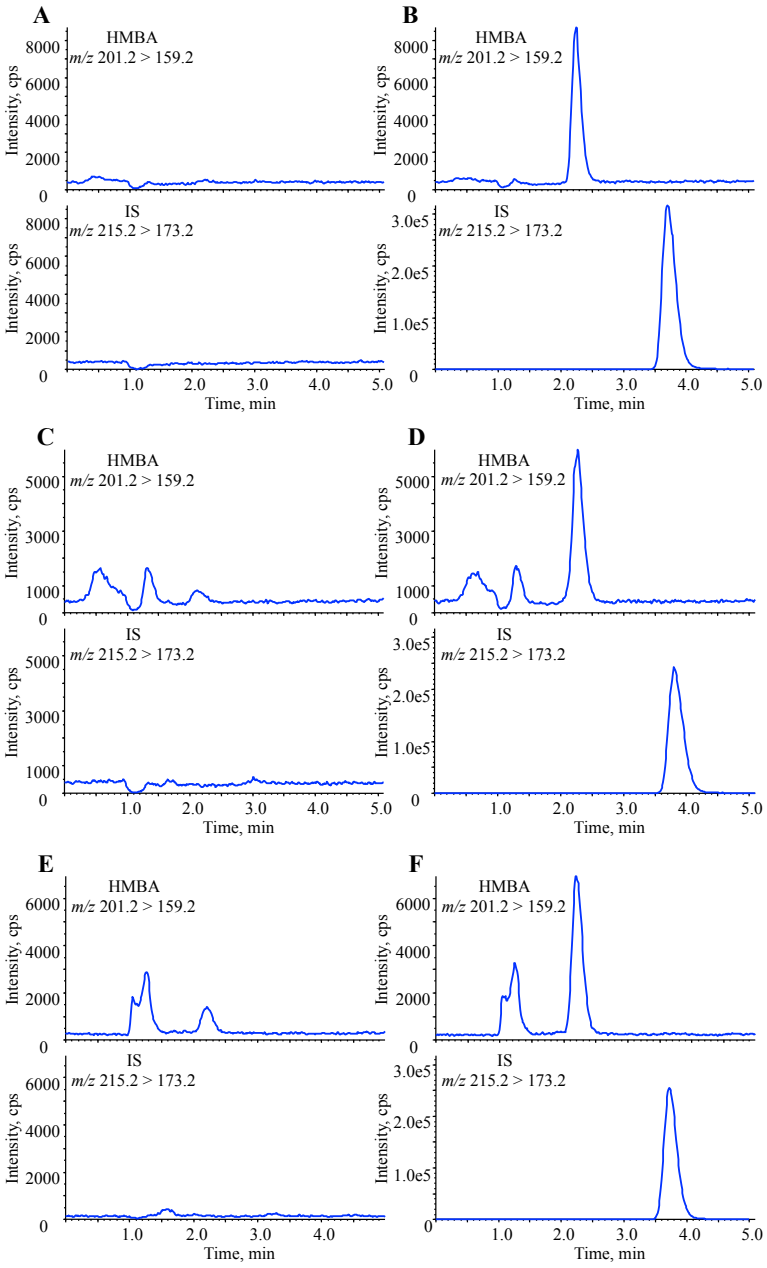

Figure 2.4, Representative MRM chromatograms of human plasma: (A) double blank and (B) 0.500 ng/mL HMBA (LLOQ), 20 ng/mL IS, mouse plasma: (C) double blank and (D) 0.500 ng/mL HMBA, 20 ng/mL IS, and tumor homogenate: (E) double blank and (F) 0.500 ng/mL HMBA, 20 ng/mL IS.

2.3.3. Method validation

The method was fully validated following the guidelines brought forth by the FDA's Bioanalytical Method Validation Guidance for Industry [22, 23] for both plasmas, and fit-for-purpose for tumor homogenate.

2.3.3.1. Recovery and matrix factor

Recovery was calculated by comparing the mean-peak-area ratios of HMBA to the IS of corresponding QC samples prepared by spiking the analytes to matrix before and after deproteinization. Matrix factor was calculated by comparing the mean-peak-area ratios of HMBA to the IS in the QC samples prepared by spiking the analytes after deproteinization to those prepared in the mobile phase. For these studies, triplicate measurements were performed for all low, medium, and high QC concentrations.

Table 2.1 shows that the recoveries of HMBA were consistent and between 96% and 98% in human plasma, 97% and 102% in mouse plasma, and 100% and 108% in tumor homogenate over the three concentrations examined. Deproteinization by 3.3 volumes of acetonitrile was sufficient to recover HMBA from the matrices.

Matrix factor is a measure of sample matrix effect (either suppression or enhancement) on analytical signal of HMBA. In this work, matrix factor for the matrices ranged 0.93 - 1.02 (Table 2.1), which indicated that the matrix effect was in the magnitude of -7% to 2% (< ±15%). Hence, the matrix suppression or enhancement of the analytical signals was not significant and could be neglected without further correction.

	Nominal [HMBA] (ng/mL)	A_{HMBA}/A_{IS} extracted ± SD	A_{HMBA}/A_{IS} spike after extraction ± SD	A_{HMBA}/A_{IS} in mobile phase ± SD	Recovery[a] ± SD (%)	MF[b] ± SD
Human	1.50	0.053 ± 0.001	0.055 ± 0.001	0.054 ± 0.001	96 ± 1	1.02 ± 0.03
	30.0	1.04 ± 0.003	1.05 ± 0.01	1.05 ± 0.01	99 ± 1	1.00 ± 0.01
	90.0	2.92 ± 0.01	3.01 ± 0.02	2.95 ± 0.02	98 ± 0.2	1.02 ± 0.01
Mouse	1.50	0.050 ± 0.001	0.049 ± 0.001	0.051 ± 0.002	102 ± 1	0.96 ± 0.03
	30.0	0.94 ± 0.002	0.97 ± 0.04	0.96 ± 0.01	97 ± 4	1.01 ± 0.01
	90.0	2.66 ± 0.004	2.68 ± 0.02	2.70 ± 0.03	99 ± 1	0.99 ± 0.01
Tumor Homogenate	1.50	0.056 ± 0.001	0.056 ± 0.002	0.058 ± 0.001	100 ± 2	0.97 ± 0.05
	30.0	0.96 ± 0.003	0.92 ± 0.02	0.98 ± 0.02	104 ± 1	0.94 ± 0.04
	90.0	2.81 ± 0.01	2.61 ± 0.06	2.82 ± 0.03	108 ± 3	0.93 ± 0.04

n = 3

[a] Recovery = [(mean area ratio of HMBA to IS extracted) /(mean area ratio of HMBA to IS spike

[b] Matrix Factor (MF) = [(mean area ratio of HMBA to IS spike after extraction) / (mean area ratio of HMBA to IS in mobile phase)]

Table 2.1, Recovery and matrix factor of HMBA in human and mouse plasmas and mouse tumor homogenate.

2.3.3.2. Calibration curve and lower limit of calibration

The linear calibration ranges of 0.500-100 ng/mL were established for HMBA in both human and mouse plasma and tumor homogenate with internal standard using six non-zero calibrators, a single-blank (IS only), and a double-blank. The calibration equations derived from seven individual calibration curves on three different days with 1/x weighting were y = 0.0287(±0.0046) x + 0.084(±0.0043), r^2 = 1.00 for human plasma, y = 0.0294(±0.0030) x + 0.0118(±0.0057), r^2 = 0.999 for mouse plasma, and y = 0.0272(±0.0045) x + 0.008(±0.004), r^2 = 0.999 for tumor homogenate. The accuracy and precision of each individual calibrator are summarized in Table 2.2, were ≤ ±3% and ≤ 6% in both human and mouse plasma.

The LLOQ of the method was defined by the lowest calibrator (0.500 ng/mL) of the calibration curve, which was confirmed by measuring HMBA from six lots of human plasma samples and six lots of mouse plasma samples. The precision and accuracy of each lot of plasma at LLOQ were calculated based on five separate samples with one injection per sample. The data are summarized in Table 2.3. The accuracy and the precision of the method at the LLOQ were ≤ ±8% and ≤ 3% in human plasma, ≤±6% and ≤9% in mouse plasma, and ≤ ±8% and ≤ 4% in tumor homogenate, respectively.

Nominal [HMBA] (ng/mL)	Accuracy (%E)[a]			Precision (%CV)[b]		
	Human Plasma	Mouse Plasma	Tissue Homogenate	Human Plasma	Mouse Plasma	Tissue Homogenate
0.500	1	1	-8	3	6	4
1.00	-1	3	2	2	2	1
5.00	-0.5	-3	1	3	2	2
10.0	2	-2	5	4	5	1
50.0	-3	2	1	2	3	2
100.	1	-0.6	-1	2	1	1

n = 7, over three different days

[a] %E = {(measured [HMBA] - nominal [HMBA]) / nominal [HMBA]} x100%

[b] %CV = (standard deviation / mean value) x100%

Table 2.2, Accuracy and precision of plasma and tumor homogenate calibrators

		Lot A	Lot B	Lot C	Lot D	Lot E	Lot F
	Nominal [HMBA] (ng/mL)	0.5	0.5	0.5	0.5	0.5	0.5
Human (n = 5)	Mean	0.525	0.502	0.491	0.463	0.461	0.472
	Standard Dev.	0.01	0.004	0.014	0.002	0.004	0.006
	Accuracy (%E)	5	0.3	-2	-7	-8	-6
	Precision (%CV)	2	1	3	0.5	1	1
Mouse (n = 5)	Mean	0.528	0.486	0.498	0.489	0.475	0.497
	Standard Dev.	0.013	0.043	0.031	0.035	0.01	0.028
	Accuracy (%E)	6	-3	-0.3	-2	-5	-1
	Precision (%CV)	3	9	6	7	2	6

Each datum point calculated by five parallel measurements from five identical QCs

Table 2.3, HMBA at LLOQ in six different lots of human and mouse plasma.

2.3.3.3. Precision, accuracy, and dilution studies

Inter-assay precision and accuracy were assessed by five parallel injections from five identical QC samples at each concentration over three separate days of analysis. Intra-assay precision and accuracy were assessed by five parallel injections from five identical QC samples at each concentration. Accuracy was expressed as percent relative error (%E), and precision was determined as percent standard deviation or coefficient of variation (%CV). As shown in Table 2.4, the intra- and inter assay accuracy and precision were ≤ ± 9% and ≤ 10% for both human and mouse plasmas.

Since the upper limits of the linear calibrations curve were 100 ng/mL, sample concentrations beyond these concentrations were subject to dilution studies. In this work, dilution effect was assessed by 1:100 dilution of plasma QCs at the concentrations of 150, 3.00 x 10^3, and 9.00 x 10^3 ng/mL by the pooled blank plasma, with the data summarized in Table 5. As shown in the table, the dilution study had an accuracy of ≤ ±10% and precision of ≤ 3% over the concentration range studied. These results indicated that dilution of plasma samples which had concentrations beyond the upper limit of the calibration curve would not produce significant error in the measurement of actual HMBA concentrations.

		Intra-run			Inter-run		
	Nominal [HMBA] (ng/mL)	Measured [HMBA] [a] ± SD (ng/mL)	Accuracy (%E)	Precision (%CV)	Measured [HMBA] [b] ± SD (ng/mL)	Accuracy (%E)	Precision (%CV)
Human	1.50	1.59 ± 0.03	6	2	1.46 ± 0.14	-3	10
	30.0	31.2 ± 0.6	4	2	29.5 ± 1.6	-2	6
	90.0	87 ± 3	-3	3	82 ± 4	-9	5
Mouse	1.50	1.60 ± 0.02	7	1	1.44 ± 0.14	-4	10
	30.0	31.6 ± 0.8	5	2	32.1 ± 1.1	7	3
	90.0	94 ± 1	4	1	94 ± 4	4	4
Tumor Homogenate	1.50	1.52 ± 0.04	1	4			
	30.0	30.0 ± 0.8	0	3			
	90.0	88 ± 2	-2	3			

[a] Each datum point calculated by five parallel measurements from five identical QCs.
[b] Each datum point calculated by five parallel measurements from five identical QCs of three dif

Table 2.4, Summary of intra- and inter- accuracy and precision in human and mouse plasmas and tumor homogenate.

	Initial [HMBA] (ng/mL)	Dilution Factor	Nominal [HMBA] (ng/mL)	Measured [HMBA] ± SD (ng/mL)	Accuracy (%E)	Precision (%CV)	Actual [HMBA] (ng/mL)
Human (n = 3)	150	100	1.50	1.51 ± 0.05	1	3	151
	3.00×10^3	100	30.0	29.2 ± 0.2	-3	1	2.92×10^3
	9.00×10^3	100	90.0	92.9 ± 1.0	3	1	9.29×10^3
Mouse (n = 3)	150	100	1.50	1.52 ± 0.04	1	3	152
	3.00×10^3	100	30.0	31.9 ± 0.8	6	2	3.19×10^3
	9.00×10^3	100	90.0	98.9 ± 1.6	10	2	9.89×10^3

Table 2.5, Summary of dilution studies in human and mouse plasmas.

2.3.3.4. Stability

The stability of HMBA was determined by comparing the mean-peak-area ratios of HMBA to the IS in the QC samples to those of freshly prepared QCs, expressed in terms of recovery. As shown in Table 6, the recoveries of QC samples were 98-106%, 97-107%, and 91-103% for the bench top, the autosampler, and the freeze-and-thaw studies, respectively. These studies indicated that there was no significant deviation in the quantitation of HMBA under the experimental conditions.

			4 h	8 h	24 h	3 Freeze-thaw cycles
		Nominal [HMBA] (ng/mL)	Recovery ± SD (%)	Recovery ± SD (%)	Recovery ± SD (%)	Recovery ± SD (%)
Bench-top stability (before deproteinization)	Human	1.50	101 ± 5	100 ± 5	101 ± 7	91 ± 1
		30.0	106± 4	104 ± 4	105 ± 2	100 ± 2
		90.0	105 ± 3	104 ± 1	104 ± 1	103 ± 1
	Mouse	1.50	102 ± 1	102 ± 2	103 ± 2	103 ± 2
		30.0	99 ± 1	98 ± 2	99 ± 1	97 ± 0.4
		90.0	100 ± 4	102 ± 4	101 ± 3	101 ± 4
Autosampler stability (after deproteinization)	Human	1.50	102 ± 2	100 ± 4	107 ± 4	
		30.0	102 ± 2	100 ± 3	101 ± 3	
		90.0	104 ± 0.1	103 ± 2	103 ± 0.3	
	Mouse	1.50	100 ± 3	101 ± 1	98 ± 1	
		30.0	100 ± 1	103 ± 1	97 ± 1	
		90.0	101 ± 5	103 ± 2	97 ± 3	

n = 3

Table 2.6, Summary of stability of HMBA in human and mouse plasmas.

2.3.4. Application to animal study

The validated LC–MS/MS method was applied to the measurement of HMBA in FVB mice. Due to the dose-limiting effects of HMBA (thrombocytopenia) and the need for millimole concentrations to elicit an effect, HMBA-loaded PLGA particles were developed. In this work, mouse plasma samples collected by the procedure described in the Section 2.2.4 together with eight calibrators (i.e., one single-blank, one double-blank and six nonzero) and a set of QCs at low-, mid- and high-concentrations (i.e., 1.50, 30.0, 90.0 ng/mL) were thawed at room temperature. These samples were prepared by the procedures described in the Section 2.2.5, and analyzed by the validated method. The samples of concentrations beyond the upper limit of calibration curve (i.e., 100 ng/mL) were re-run by 1:100 dilution using the pooled blank mouse plasma together with the dilution QC at the concentration of 9.00×10^3 ng/mL. Figure 2.5 shows the HMBA concentration-time profile in FVB mice after a nipple injection of 10 mg/kg. Each datum point was based on duplicate measurement of a blood sample from a FVB mouse. To evaluate the release of HMBA from PLGA, mice were injected with 2 mg/kg of 5 mM HMBA-PLGA and treated the same as the saline model. The results of the analysis are depicted in figure 2.6. Additional data from two- and ten- days post injection reveal measurable amounts of HMBA in both tumor and plasma (table 2.7)

Although a higher dose of HMBA was used in these preliminary studies, the concentration-time profile of HMBA demonstrated not only the applicability of the method in its intended sample matrix, but also its feasibility for a wide concentration range of HMBA in plasma (from sub ng/mL to high µg/mL).

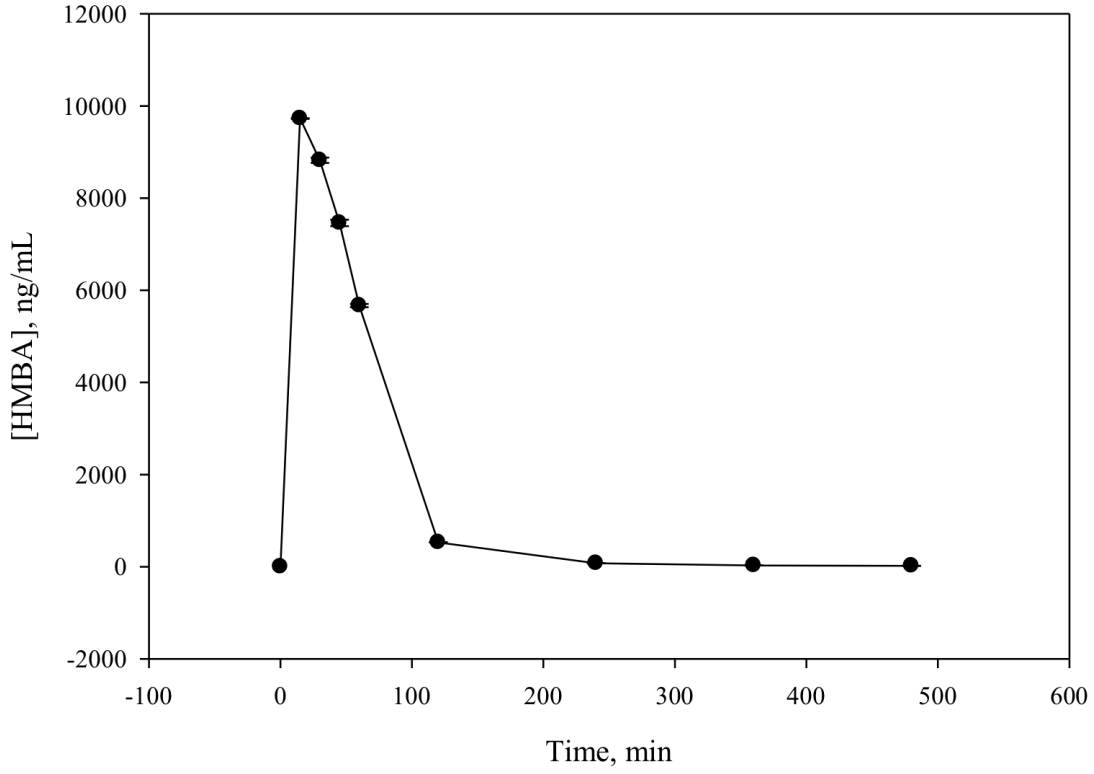

Figure 2.5, Mean concentrations of HMBA in mouse plasma over time.

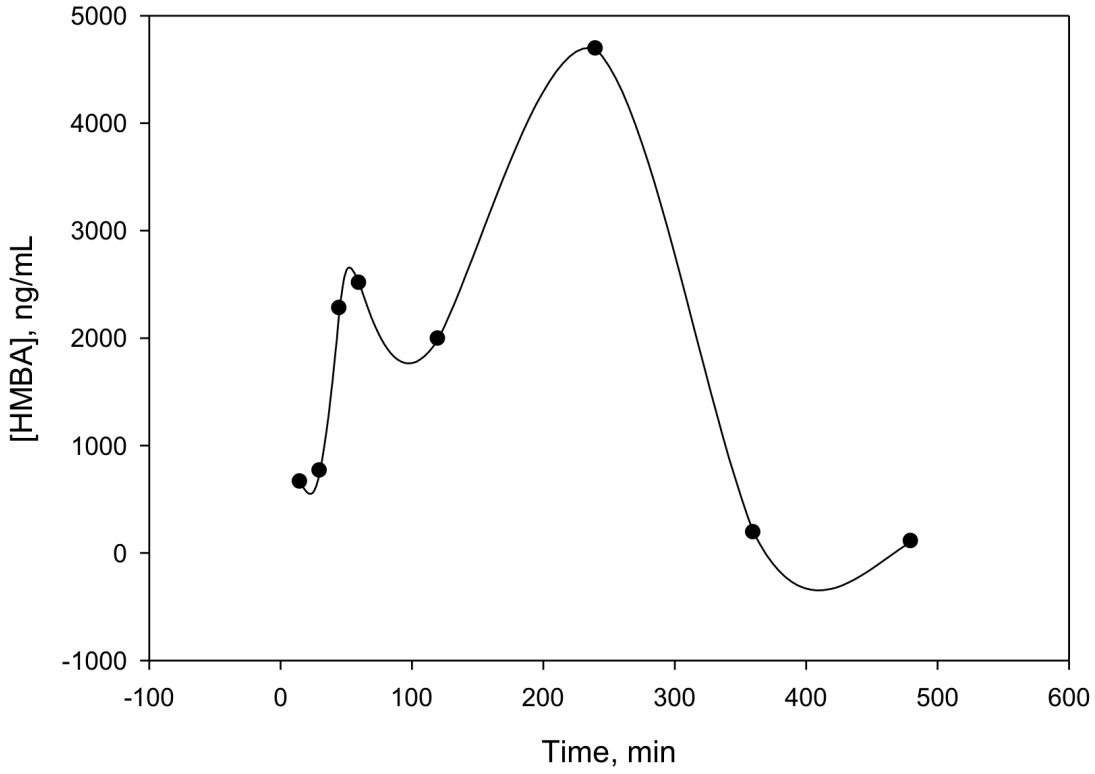

Figure 2.6, Mean concentrations of HMBA release from PLGA in mouse plasma over time.

	Timepoint (day)	Measured [HMBA] [a] ± SD (ng/mL)
Plasma	2.00	20.1 ± 0.4
	10.0	16.0 ± 0.4
Tumor Homogenate	2.00	5.34 ± 0.06
	10.0	5.97 ± 0.11

n = 3

Table 2.7, Concentration of HMBA after injection in PLGA at two and 10 days.

2.4. Conclusion

This work detailed the development and validation of a LC-MS/MS method for the quantitation of HMBA in human and mouse plasma and mouse tumor tissue. The method used a simple deproteinization step for sample preparation, and a reversed-phase chromatographic column for analyte separation. It has a linear calibration range of 0.500-100 ng/mL and stability for routine analysis. The method was successfully applied to the measurement of HMBA in mouse plasma samples, as well as mouse tumor tissue. It may be useful for the toxicokinetic study of HMBA in mice as well as pharmacokinetic study in humans.

2.5. References

[1] R.C. Reuben, R.L. Wife, R. Breslow, R.A. Rifkind, P.A. Marks, Proc. Natl. Acad. Sci., 73 (1976) 862-866.

[2] P.A. Marks, V.M. Richon, H. Kiyokawa, R.A. Rifkind, Proc. Natl. Acad. Sci., 91 (1994) 10251-10254.

[3] E.K. Rowinsky, D.S. Ettinger, L.B. Grochow, R.B. Brundrett, A.E. Cates, R.C. Donehower, J. Clin. Oncol., 4 (1986) 1835-1844.

[4] M.J. Egorin, E.G. Zuhowski, A.S. Cohen, L.A. Geelhaar. P.S. Callery, D.A. Van Echo, A. Forrest, Cancer Res., 47 (1987) 6142-6146.

[5] E.K. Rowinsky, D.S. Ettinger, W.P. McGuire, D.A. Noe, L.B. Grochow, R.C. Donehower, Cancer Res., 47 (1987) 5788-5795.

[6] C.W. Young, M.P. Fanucchi, T. Declan Walsh, L. Baltzer, S. Yaldaei, Y.W. Stevens, C. Gordon, W. Tong, R.A. Rifkind, P.A. Marks, Cancer Res., 48 (1988) 7304-7309.

[7] E.K. Rowinsky, R.C. Donehower, J.L. Spivak, P.J. Burke, C.A. Griffin, R.J. Jones, J. Natl. Cancer Inst., 82 (1990) 1926-1931.

[8] M.J. Egorin, L.M. Sigman, D.A. Van Echo, A. Forrest, M.Y. Whitacre, J. Aisner, Cancer Res., 47 (1987) 617-623.

[9] M. Andreeff, R. Stone, J. Michaeli, C.W. Young, W.P. Tong, H. Sogoloff, T. Ervin, D. Kufe, R.A. Rifkind, P.A. Marks, Blood, 80 (1992) 2604-2609.

[10] V. Cecchinato, E. Erba, A. Basile, B. Scarpati, C. Fazi, B. Brando, P. Comi, R. Chiaramonte, Leuk. Res., 32 (2008) 791-797.

[11] K.N. M Kusuhara, K Kimura, N Maass, T Manabe, S Ishikawa, M Aikawa, K Miyazaki, K Yamaguchi, Biomed Res., 20 (1999) 273-279.

[12] B.M. Wittmann, N. Wang, M.M. Montano, Cancer Res., 63 (2003) 5151-5158.

[13] N. Ogba, L.J. Chaplin, Y.Q. Doughman, K. Fujinaga, M.M. Montano, Cancer Res., 68 (2008) 7015-7024.

[14] B.M. Wittmann, K. Fujinaga, H. Deng, N. Ogba, M.M. Montano, Oncogene, 24 (2005) 5576-5588.

[15] R.J. Sims, R. Belotserkovskaya, D. Reinberg, Genes Dev., 18 (2004) 2437-2468.

[16] N.H. He, A.C. Pezda, Q. Zhou, Mol. Cell. Biol., 26 (2006) 7068-7076.

[17] Y. Li, S. Jiang, L. Chen, Chromatographia, 34 (1992) 63-66.

[18] T.D. Walsh, M.P. Fanucchi, J. Chromatogr., B: Anal. Technol. Biomed. Life Sci., 414 (1987) 510-513.

[19] P.S. Callery, M.J. Egorin, L.A. Geelhaar, M.S. Nayar, Cancer Res., 46 (1986) 4900-4903.

[20] C.L. Litterst, J.S. Roth, J.A. Kelley, Invest. New Drugs, 3 (1985) 263-272.

[21] H. Jiang, J. Jiang, P. Hu, Y. Hu, J. Chromatogr., B: Anal. Technol. Biomed. Life Sci., 769 (2002) 169-176.

[22] S. Bansal, A. DeStefano, The AAPS J., 9 (2007) E109-E114.

[23] Http://www.fda.gov/downloads/Drugs/GuidanceComplianceRegulatoryInformation/Guidances/ucm070107.pdf) (accessed on June 1st, 2011)

[24] F.T. Ward, J.A. Kelley, J.S. Roth, F.A. Lombardo, R.B. Weiss, B. Leylandjones, H.G. Chun, Cancer Res., 51 (1991) 1803-1810.

CHAPTER III

DEVELOPMENT OF A RAPID LIQUID CHROMATOGRAPHY TANDEM MASS SPECTROMETRY METHOD FOR THE ANALYTICAL DETERMINATION OF ILLICIT DRUGS BZP AND TFMPP IN HUMAN BLOOD, URINE, BILE, AND VITREOUS HUMOR

3.1 Introduction

Benzylpiperazine (BZP) and 1-3-trifluoromethylphenylpiperazine (TFMPP) are synthetic designer drugs with psychoactive properties (figure 3.1 A and B, respectively). BZP is a dopamine, serotonin, and noradrenalin agonist [1] and can also inhibit their reuptake [2]. TFMPP is a nonselective serotonin agonist [1]. Having structural similarity to amphetamine and methamphetamine (figure 3.2), early studies confirmed that the two drugs had similar physiological effects [3]. Additionally, former amphetamine addicts could not tell the difference upon their

administration [4]. Nowadays, BZP and TFMPP are commonly abused together as they have physiological effects similar to the illegal drug 3,4-methylenedioxymethamphetamine (MDMA or ecstasy).

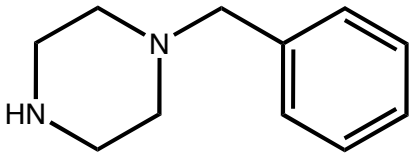

A

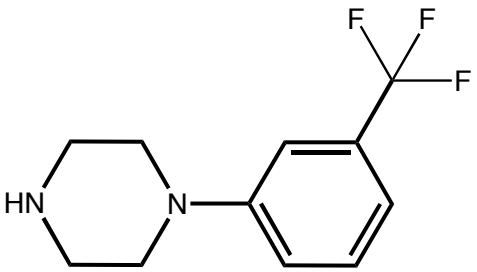

B

Figure 3.1, Structures of (A) Benzylpiperazine and (B) 1-3-trifluoromethylphenylpiperazine.

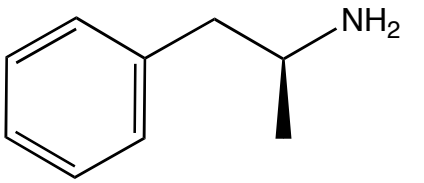

Amphetamine

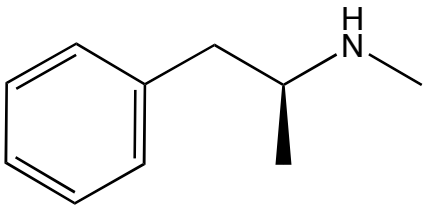

Methamphetamine

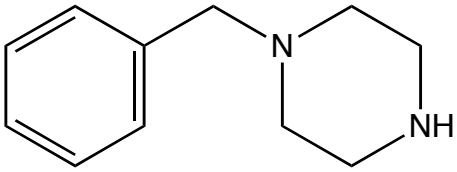

Benzylpiperazine

Figure 3.2, Structural similarity of amphetamine, methamphetamine, and Benzylpiperazine.

3.1.1. History

In 1979, Hoechst-Roussel Pharmaceuticals, Inc. developed a new antidepressant, Befuraline (figure 3.3A), that showed promising effects in the treatment of depression in humans despite stimulatory side effects [5-7]. Similarly, Trelibet (also known as Piberaline) (figure 3.3B) was introduced by Hungarian pharmaceutical company, Egis Pharmaceutical Works, in 1986 and enjoyed success until it was noted that amphetamine-like side effects brought questions of its safety [8, 9]. It was determined that the effects of Trelibet (and presumably Befuraline) were predominantly due to its metabolite, benzylpiperazine [10]. Benzylpiperazine had been shown to have similar effects as amphetamine in two previous studies [3, 4], therefore further study as an antidepressant was considered a risk. The antidepressants were soon therapeutically abandoned.

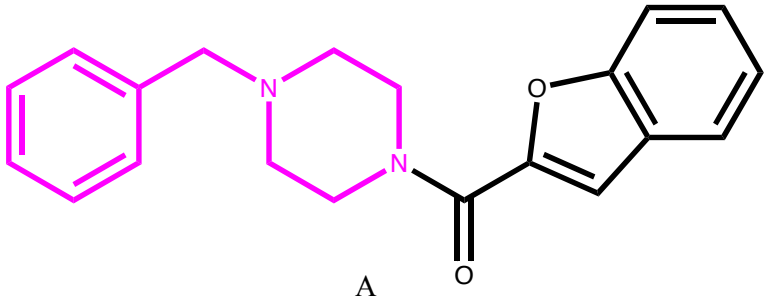

A

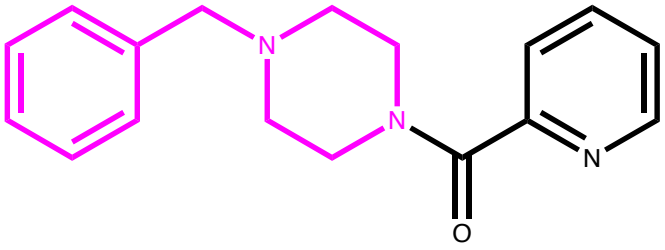

B

Figure 3.3, Representative structures of BZP precursors A. Befuraline and B. Trelibet.

3.1.2. Safety and legal status

There are no reported fatalities due to either BZP or TFMPP alone, but BZP is reported to have a low seizure threshold. More importantly, the co-administration of BZP and MDMA has resulted in sudden death most likely due to the drugs' additive toxicities [11, 12]. The potential for drug mixing is great as they are both sold in similar-looking forms (see figure 3.4 for pictures taken by the U.S. DEA).

As of October 2011, BZP is illegal in the USA and most countries worldwide with the exception of Canada. TFMPP was initially given emergency Schedule 1 status in the USA, but was subsequently removed and is no longer regulated. BZP may still be ordered online, but import laws restrict its delivery to countries where it is illegal. To circumvent the illegality of some abused drugs, individuals search the literature for insights into new compounds with desirable side effects that aren't yet illegal [13, 14] . This practice creates the potential for an ever-changing arsenal of recreational drugs and reinforces the need for dynamic extraction, separation, and detection methods.

A

B

Figure 3.4, Pills seized by the U.S. DEA and testing positive for (A) MDMA or (B) BZP and TFMPP (http://www.justice.gov/dea/).

3.1.3. Current LC-MS methods

There are 4 LC/MS and 3 LC-MS/MS published methods for the screening [15, 16] or quantitation [17-21] of BZP and TFMPP in human plasma, serum, blood, and urine, with Nordgren and Beck [15] achieving the lowest confirmation detection limit of 0.9 ng/mL and Antia et al [17] the lowest limit of quantitation of 5 ng/mL. The methods use an array of sample extraction techniques from solid phase extraction [15, 16, 20], liquid-liquid extraction [19, 21] salting-out assisted liquid-liquid extraction [17], to simple dilution of urine [18]. Since the current work involves the quantitation of BZP and TFMPP in both ante- and post-mortem human blood, urine, bile, and vitreous humor matrices, a new extraction and LC-MS/MS method for the two additional biomatrices is essential.

3.2. Materials and methods

3.2.1 Chemicals

BZP (1-Benzylpiperazine, Quik-Chek™ Drug Standard, 1 mg/mL in methanol, catalog no. 015813) was from Grace (Deerfield, IL, USA). TFMPP (1-3-Trifluoromethylphenylpiperazine hydrochloride 99%, catalog no. T8948), internal standard 2-MBZP (1-(2-Methylbenzyl)piperazine 97%,

catalog no. 644226), HPLC-grade Ammonium acetate, and ammonium hydroxide (28-30 wt %) were from Sigma-Aldrich (St. Louis, MO, USA). HPLC-grade acetonitrile (ACN) was from Pharmco-AAPER (Louisville, KY, USA). HPLC-grade glacial acetic acid was from J.T. Baker (Phillipsburg, NJ, USA). HPLC-grade Omnisolv methanol (MeOH) was from EMD Chemicals (West Chester, PA, USA). Pooled, drug-free hemolyzed ante- and post-mortem human blood was from University Hospitals, Cleveland, OH. Pooled, drug-free human urine was from healthy volunteers. Type 1 deionized water was obtained from a Barnstead NANOpure® water purification system (Thermo Scientific, Waltham, MA, USA).

3.2.2. HPLC-MS/MS

The liquid chromatography tandem mass spectrometry system consisted of a Shimadzu Prominence UFLC system with degasser, binary pump, and autosampler (Shimadzu, Columbia, MD, USA) coupled to an AB Sciex QTrap® 5500 mass spectrometer equipped with electrospray ionization (ESI) probe and integrated syringe pump (AB Sciex, Foster City, CA, USA). The HPLC was connected to the mass spectrometer using PEEK tubing (1/16 in. o.d. x 0.005 in. i.d.). Data was acquired and processed using Analyst™ Software (version 1.5.1).

Analytical measurement of BZP, TFMPP, and 2-MBZP was achieved by isocratic separation on a Waters XBridge™ C6-Phenyl (3.5 µm, 130 Å, 2.1 x 50 mm) column (Waters, Milford, MA, USA) with a flow rate of 200 µL/min. The mobile phase used for separation was 45% 10mM ammonium acetate pH 5.75, 55% MeOH with an injection volume of 5 µL for each sample. The AB Sciex QTrap® 5500 mass spectrometer was operated in positive ESI mode using the following instrument settings: CUR 40; CAD HIGH; IS 5000; TEM 500; GS1 40; GS2 35; DP 100; EP 12; CE 29 (BZP, 2-MBZP), 33 (TFMPP); CXP 8 (BZP, 2-MBZP), 16 (TFMPP) and a dwell time of 100 ms.

3.2.3. Standard solution, calibrators, dilution, and quality control sample preparation

The standard stock solutions of TFMPP and internal standard (IS) were prepared to match the purchased BZP: in MeOH at 1 mg/mL. The standard working solutions of the BZP and TFMPP mixture at concentrations 50.0, 100, 150, 500, 1.00×10^3, 1.50×10^3, 5.00×10^3, 1.00×10^4, 1.50×10^4, 2.50×10^4, and 5.00×10^4 ng/mL were prepared by serial dilution of the standard stock solutions with 50% ACN. The IS working solution was prepared by serial dilution of the standard stock solution of 2-MBZP to a final concentration of 500 ng/mL in 100% ACN.

The standard and working stock solutions were kept in amber glass vials and stored at -20°C.

Calibration and quality control (QC) samples were prepared by spiking 990 µL of biological matrix with 10 µL of standard working solution to final concentrations of 0.500, 1.00, 5.00, 10.0, 50.0, 100, 250, and 500 ng/mL for calibration standards and 1.50, 15.0, and 150 ng/mL for QC samples.

Dilution study standards were prepared by spiking 990 µL of biological matrix with 5 µL of each 1 mg/mL stock solution to make 5.00 x 10^3 ng/mL or 10 µL 1.00 x 10^5 ng/mL standard working solution to make 500 ng/mL. Biological matrix calibration, QC, and dilution standards were stored in 1.5-mL microcentrifuge tubes (VWR, West Chester, PA, USA) at -20°C until use.

3.2.4. Sample preparation

To 100 µL of thawed biomatrix, 10 µL of IS (500 ng/mL) is added followed immediately by 390 µL of ACN (1:4 v/v biomatrix to ACN). The samples are vortex mixed for 60 s and then centrifuged for 10 min at 24400 x g. A 100 µL aliquot of the supernatant is diluted with 100 µL water (blood samples) or 100 µL 10 mM ammonium acetate, pH 5.75 (urine samples) (1:1 v/v) in a 1.5-mL microcentrifuge tube. The diluted samples are vortex

mixed briefly and then transferred to limited volume polypropylene vials (National Scientific, Rockwood, TN, USA) for analysis.

3.2.5. Dilution and concentration studies

Dilution-after-extraction was performed by diluting the above extracted samples up to 1000 times in 50% ACN containing IS at 5 ng/mL. Concentration studies of blood samples was performed by first adding 10 µL of IS (50 ng/mL) to 100 µL of thawed matrix. 390 µL of ACN is then added and the samples vortex mixed for 60 s followed by centrifugation for 10 min at 24400 x g. 80% of the supernatant is transferred to a 1.5-mL microcentrifuge tube and dried under 11 psi of nitrogen in a TurboVap II Evaporator (Zymark, Hopkinton, MA, USA) at 25°C for 40 min. The residual is reconstituted in 160 µL of 50% ACN for analysis.

3.2.6. Validation parameters

3.2.6.1. Recovery and matrix factor

Recoveries were calculated by comparison of the area ratios of analyte to internal standard spiked before and after plasma deproteinization. Matrix factor was calculated by comparison of the area ratios of analyte to internal standard of samples in mobile phase and spiked after plasma

extraction. Both analyses were performed by triplicate injections at low, medium, and high calibrator concentrations.

3.2.6.2. Precision and accuracy

Intra-assay precision and accuracy was assessed by single injections of five separate samples at each calibrator concentration. Inter-assay precision and accuracy was assessed by single injections of five separate samples at each calibrator concentration on three different days. Accuracy was determined by back-calculation of the analyte to internal standard area ratios of the analyte detected to analyte spiked into blank plasma from the calibration curve. Dilution studies up to 1000 times were assessed by serial dilution of a 5000 ng/mL extracted sample. The dilution study samples were injected 3 times, and the precision and accuracy evaluated. The results were considered satisfactory if accuracy was ≥85% and precision was ±15.

3.2.6.3. Stability

The stability of BZP and TFMPP in human blood and urine was determined in the matrix (pre-deproteinization), autosampler (post-deproteinization), and through three freeze-thaw cycles at low, medium, and high QC concentrations. Matrix stability was investigated by incubating the QC samples on the bench top at 22°C for 0, 4, 8 and 24 hours. The internal standard was added and the samples were extracted as above. Autosampler stability was investigated by analyzing extracted concentrations in the autosampler (4°C) for 0, 4, 8 and 24 hours. Freeze-thaw stability was determined after three unassisted thaw and re-freeze cycles. All stability measurements were determined by comparing the sample analyte-to-internal standard area ratios to freshly prepared QC calibrators.

3.2.7. Method application

The validated analytical method was used to confirm the presence and amount of BZP and/or TFMPP in 7 ante- and post- mortem cases from the Cuyahoga County Coroner's Office. These cases presented to the Coroner for various reasons: accidental or intentional death, or drug testing cases for police investigations. Each sample initially tested positive for Amphetamines Enzyme Multiplied Immunoassay Technique

(EMIT) using a Viva-Jr® Drug Testing System (Sylva Dade Behring – Siemens, Deerfield, IL, USA) and subsequently confirmed negative for amphetamines by GC/MS. It is known that BZP and TFMPP have some cross-reactivity with the Amphetamine EMIT assay [18], so after the negative amphetamine GC/MS test, BZP and TFMPP were suspected. All blood samples were extracted from the femoral artery, except case #6, which was sampled directly from the heart.

3.3. Results and discussion

3.3.1. Optimization of MS/MS parameters

The mass spectrometer settings were optimized by direct infusion of each analyte using the “Compound Optimization” feature of Analyst software at a concentration of 10 ng/mL in ACN/water (50/50, v/v) at a rate of 10 µL/min. 190 µL/min of the mobile phase was joined by T-connection at the ESI source to make up the flow rate difference. The major parent ions of 177.1, 231.1, and 191.1 m/z representative of $[BZP+H]^+$, $[TFMPP+H]^+$, and the $[IS+H]^+$ produced product ions of 91.0, 188.0, and 105.0 m/z respectively (figure 3.5 A-F). These mass transitions were used for analyte quantification in MRM mode.

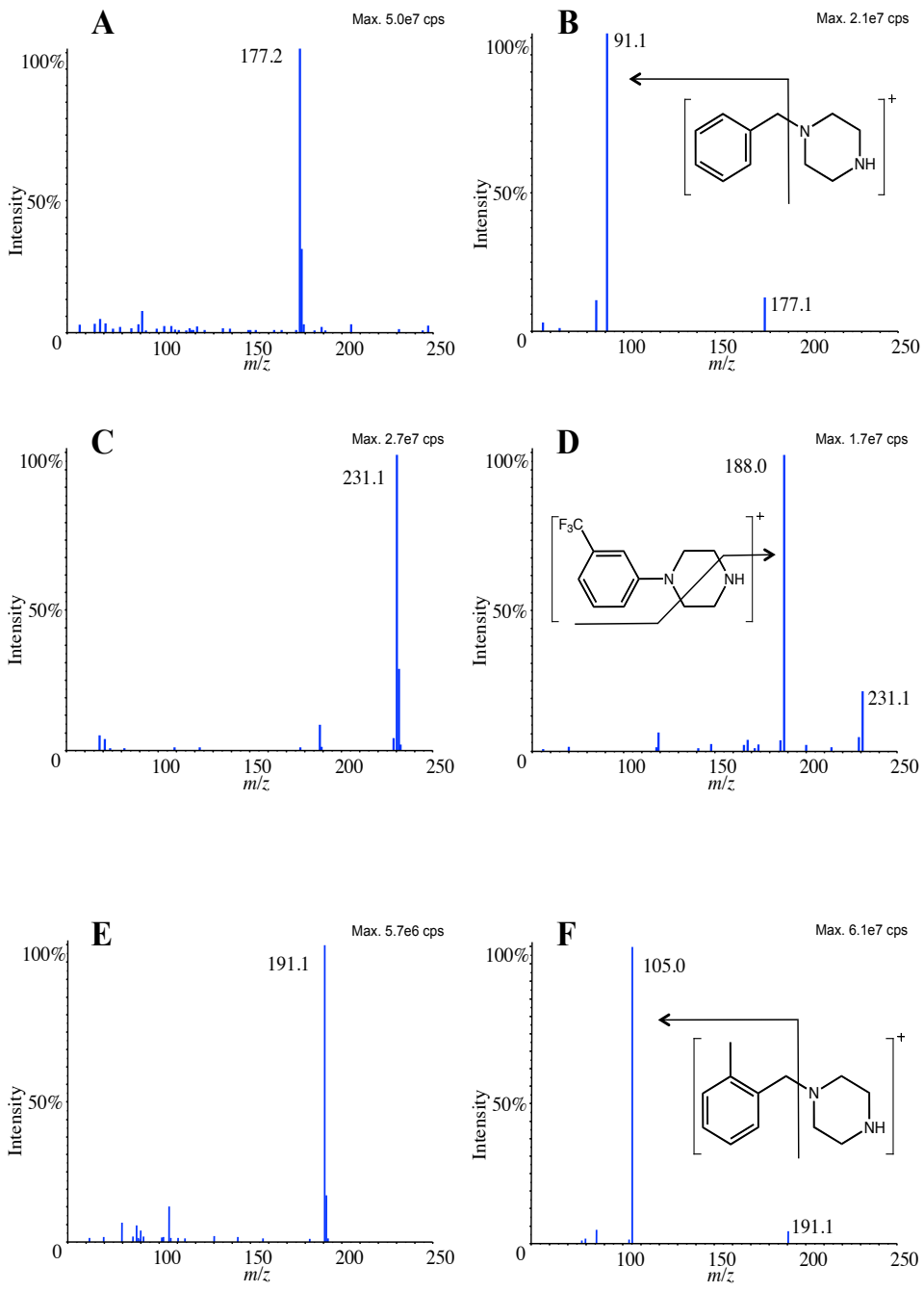

Figure 3.5, Representative structures, full scan and fragmentation spectra of (A,B) BZP, (C,D) TFMPP, and (E,F) the internal standard, 2-MBZP.

3.3.2. Chromatographic separation and carryover

BZP and TFMPP are basic compounds with calculated pKa of 8.79 and 9.59 and LogP of 1.35 and 2.43 respectively (data from ACD/Labs software v8.14). Even though each analyte contains a phenyl moiety, the basic character of BZP especially presents difficulty for the chromatographic separation. While a lower pH aids in more efficient ionization translating to better sensitivity in the mass spectrometer, the charged state significantly reduces the retention of the analytes on traditional reversed phase columns such as C4, C8, and C18. To overcome this, a Waters XBridge™ C6-Phenyl (3.5 µm, 2.1 x 50 mm) column was employed to take advantage of the phenyl moiety of BZP and TFMPP and increase retention of the analytes by hydrophobic interaction.

Optimal separation of BZP and TFMPP was achieved using a mobile phase consisting of 45% 10 mM ammonium acetate (pH 5.75) 55% methanol (v/v) resulting in retention times of 1.7, 2.4, and 2.9 min for BZP, the IS, and TFMPP respectively (figure 3.6). The lower limit of quantitation (LLOQ) was 0.500 ng/mL, while the upper limit of quantification (ULOQ) was 250 ng/mL for BZP and 500 ng/mL for TFMPP.

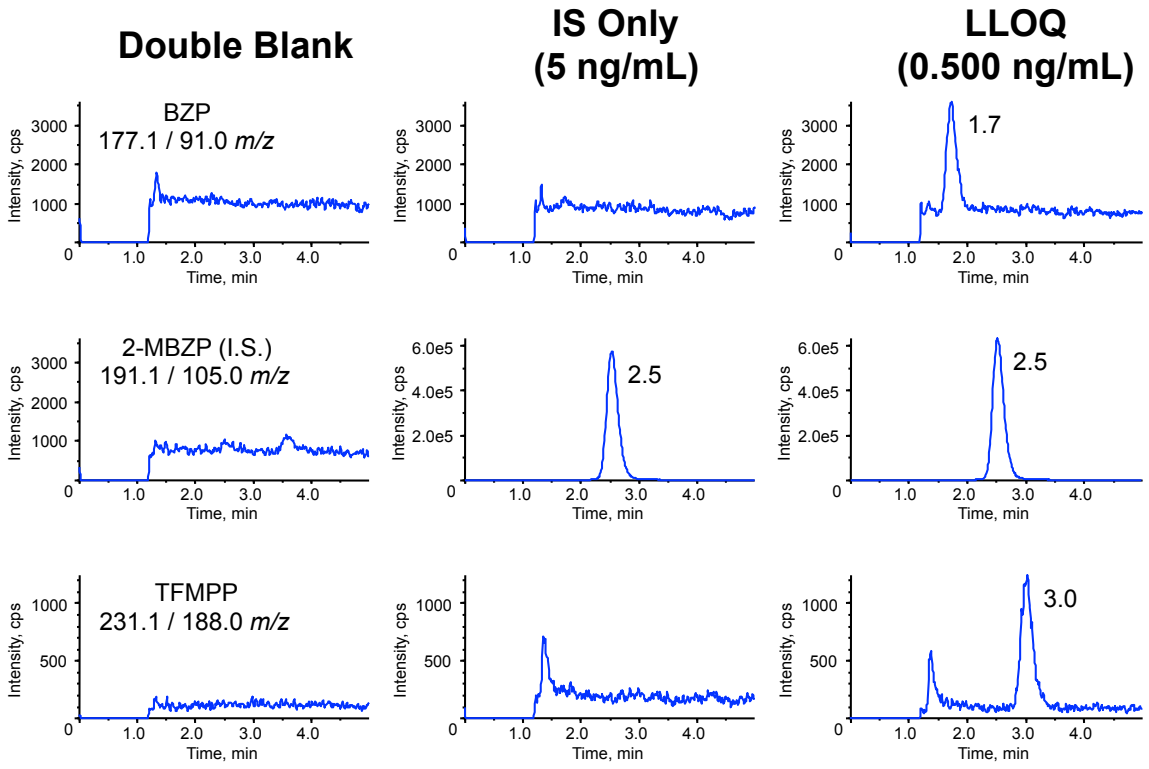

Figure 3.6, Representative MRM chromatograms of BZP (0.500 ng/mL), 2-MBZP (5 ng/mL), and TFMPP (0.500 ng/mL) in human hemolyzed blood.

During the initial efforts to develop the HPLC separation method, it was discovered that there was carryover of the analytes that was associated with the autosampler needle. This carryover was unpredictable, occurred at concentrations within the calibration range, and was not controlled by typical or exotic needle washing solutions (e.g., 50/50 MeOH or ACN/water, 50/50/0.1 MeOH or ACN/water/formic acid, 100 mM perchloric acid solution with MeOH or ACN [22]). It was determined that 50/50/0.1 methanol/water/ammonium hydroxide as the needle wash solution was sufficient to control the carryover. Mobile phase blank injection after of 10 µg/mL in 50% acetonitrile shows no carryover for BZP, and an insignificant amount for TFMPP (figure 3.7).

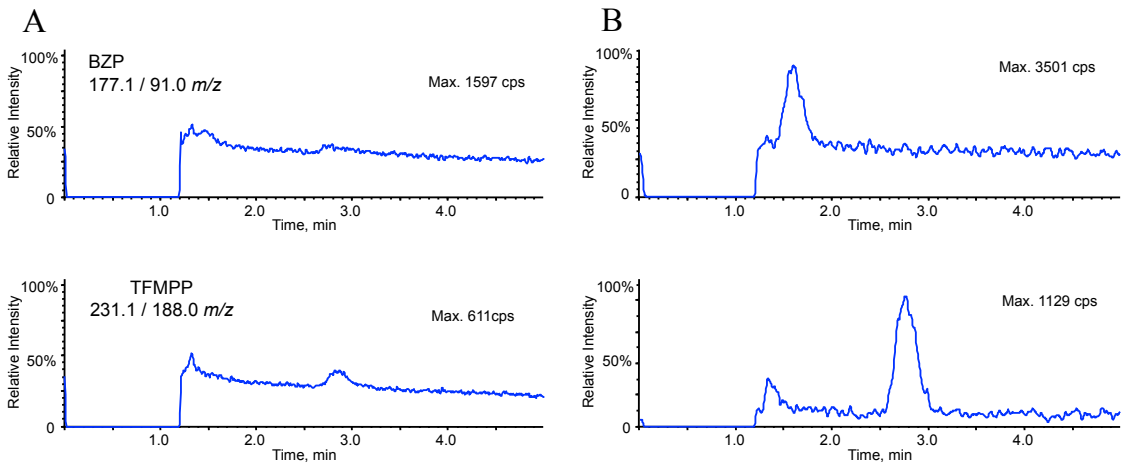

Figure 3.7, Carryover control: (A) injection of mobile phase blank after 10 µg/mL in 50% acetonitrile and (B) LLOQ chromatogram of the method.

3.3.3. Method validation results

The method has been validated according to the parameters listed in 3.2.6 in hemolyzed blood and urine. Bile and vitreous humor were diluted 10 times in hemolyzed and their recovery, matrix factor, and dilution integrity established.

3.3.3.1. Calibration curves

The linearity of the method for BZP was 0.500 – 250 ng/mL where TFMPP was 0.500 – 500 ng/mL. The curves were established by three injections each of seven non-zero standards (0.500, 1.00, 5.00, 10.0, 50.0, 100, and 250 ng/mL for BZP and 0.500, 1.00, 5.00, 10.0, 50.0, 100, and 500 ng/mL for TFMPP) on three different days and submitted to linear regression with 1/x weighting. The results of this analysis are represented in table 3.1.

Matrix	Equation for BZP	r^2
Hemolyzed Blood	y=0.0139(±0.0019)x + -0.0016(±0.0012)	0.9994
Urine	y=0.0148(±0.0005)x + 0.0006(±0.0005)	0.9998
	Equation for TFMPP	r^2
Hemolyzed Blood	y=0.0045(±0.0022)x + -0.0004(±0.0012)	0.9994
Urine	y=0.0065(±0.0005)x + 0.0004(±0.0004)	0.9997

n = 9

Equation in the form y=mx + b

Table 3.1, Calibration equations in hemolyzed blood and urine over three separate days.

3.3.3.2. Recovery and matrix effects

The sample extraction method used in this work is a variation of the "dilute and shoot" technique [23]. Here, 4x ACN was used to deproteinize the biomatrix and after centrifugation, the supernatant is diluted with equal volume of 10 mM ammonium acetate, pH 5.75 to a final overall dilution of 10x. This "crash and shoot" technique serves dual purpose: to extend the linear range of the method without compromising sensitivity and to effectively dilute out any potential ion suppressing or enhancing components.

Recovery and matrix factor was determined in hemolyzed blood, urine, bile, and vitreous humor at 1.50, 15.0, and 150 ng/mL, representing the calibration range. Bile and vitreous humor samples were prepared as 15.0, 150, and 1.50 x 10^3 and diluted 10x in hemolyzed blood to facilitate matrix matching for the study. As summarized in table 3.2, recovery ranged from 87% to 108% for BZP and 94% to 109% for TFMPP over the concentration range in all the matrices. Matrix factor, a measure of ionization suppression or enhancement, ranged from 0.90 to 1.03 for BZP and from 0.91 to 10.8 for TFMPP. These results suggest that the "crash and shoot" sample preparation method was successful and sufficient to extract the analytes and to minimize excessive matrix effects.

	Analyte	Nominal Concentration (ng/mL)	Recovery ± SD (%)	MF[a] ± SD	Analyte	Nominal Concentration (ng/mL)	Recovery ± SD (%)	MF[a] ± SD
Urine	BZP	1.50	100 ± 3	1.0 ± 0.01	TFMPP	1.50	100 ± 3	1.08 ± 0.04
		15.0	103 ± 3	0.91 ± 0.02		15.0	100 ± 0.3	1.07 ± 0.01
		150.	99 ± 2	0.92 ± 0.02		150.	99 ± 2	1.03 ± 0.01
Hemolyzed Blood	BZP	1.50	98 ± 1	0.96 ± 0.01	TFMPP	1.50	101 ± 1	1.02 ± 0.03
		15.0	87 ± 1	1.03 ± 0.01		15.0	100 ± 1	1.04 ± 0.02
		150.	87 ± 2	0.97 ± 0.01		150.	94 ± 1	0.98 ± 0.01
Bile	BZP	1.50	104 ± 2	0.94 ± 0.05	TFMPP	1.50	108 ± 9	0.94 ± 0.04
		15.0	104 ± 2	0.97 ± 0.01		15.0	109 ± 1	1.05 ± 0.03
		150.	97 ± 4	0.97 ± 0.03		150.	109 ± 2	1.01 ± 0.05
Vitreous Humor	BZP	1.50	108 ± 10	0.92 ± 0.06	TFMPP	1.50	106 ± 3	0.94 ± 0.02
		15.0	97 ± 1	0.90 ± 0.02		15.0	107 ± 2	0.91 ± 0.02
		150.	101 ± 1	0.91 ± 0.02		150.	109 ± 2	0.92 ± 0.01

Each datum point calculated from triplicate measurements.

[a] Matrix Factor (MF) = [(mean area ratios in spiked extract) / (mean area ratios in mobile phase)]

Table 3.2, Summary of recovery and matrix factor in the biomatrices.

3.3.3.3. Accuracy, precision, dilution, and concentration integrity

The accuracy and precision of the method is established to ensure the analytical method can be relied on to quantify BZP and TFMPP in unknown samples. Here, accuracy and precision were determined on three separate days to ensure method robustness. A summary of the intra- (within) and inter- (between) day results is presented in tables 3.3 and 3.4. As listed, the method had accuracy 90% - 105% and precision ≤8% over the concentration range for both of the matrices.

		Intra-			Inter-		
Hemolyzed Blood	Nominal Concentration (ng/mL)	Mean Analyte Concentration[a] ± SD (ng/mL)	Accuracy (%)	Precision (%CV)	Mean Analyte Concentration[b] ± SD (ng/mL)	Accuracy (%)	Precision (%CV)
BZP	0.500	0.49 ± 0.02	99	3			
	1.50	1.46 ± 0.03	97	2	1.48 ± 0.03	99	2
	15.0	14.2 ± 1	95	7	14.1 ± 0.8	97	5
	150.	145 ± 5	97	3	141 ± 7	94	5
TFMPP	0.500	0.45 ± 0.02	90	3			
	1.50	1.50 ± 0.01	100	7	1.53 ± 0.04	102	2
	15.0	14.7 ± 07	98	5	14.5 ± 1	97	8
	150.	147 ± 10	98	7	151 ± 9	101	6

[a] Each datum point calculated by one injection each of five separate samples.

[b] Each datum point calculated by one injection each of five separate samples on three different days.

Accuracy % = (measured/nominal) × 100%.

%CV = (standard deviation/mean) × 100%

Table 3.3, Summary of accuracy and precision in hemolyzed human blood.

		Intra-			Inter-		
Urine	Nominal Concentration (ng/mL)	Mean Analyte Concentration[a] ± SD (ng/mL)	Accuracy (%)	Precision (%CV)	Mean Analyte Concentration[b] ± SD (ng/mL)	Accuracy (%)	Precision (%CV)
BZP	0.500	0.524 ± 0.039	105	7			
	1.50	1.45 ± 0.04	99	3	1.50 ± 0.04	100	3
	15.0	14.8 ± 0.2	99	1	15.4 ± 0.8	102	4
	150.	141 ± 2	94	2	152 ± 10	101	7
TFMPP	0.500	0.492 ± 0.042	98	8			
	1.50	1.34 ± 0.03	90	2	1.48 ± 0.11	98	8
	15.0	13.6 ± 0.1	91	1	14.7 ± 1	99	7
	150.	140 ± 1	93	1	152 ± 11	101	7

[a] Each datum point calculated by one injection each of five separate samples.

[b] Each datum point calculated by one injection each of five separate samples on three different days.

Accuracy % = (measured/nominal) × 100%.

%CV = (standard deviation/mean) × 100%

Table 3.4, Summary of accuracy and precision in human urine.

Since drugs of abuse are often taken in large doses, it was important to establish the dilution ability of the method. To save sample processing time, dilution after extraction was investigated by diluting the QC or unknown with a solution of 5 ng/mL 2-MBZP in 50% ACN. Sample concentration studies were also investigated, as this procedure might be useful for badly decomposed samples. Here, the samples were extracted as described in section 3.2.4, but instead of diluting the sample in water, the sample is dried under a gentle stream of nitrogen at 25 °C and reconstituted in 2 times the volume of 50% ACN for analysis. As summarized in table 3.5 dilution after extraction up to 1000 times and concentration up to 10 times yielded good results where accuracy ranged from 89% to 101% and precision was always ≤5% for both analytes over the four matrices. These results suggest that samples whose concentration lies above or below the calibration range may be either re-extracted and concentrated, or diluted directly from the autosampler with confidence.

	Analyte	Initial Concentration (ng/mL)	Dilution Factor	Concentration Factor	Nominal Concentration (ng/mL)	Measured Concentration (ng/mL)	Accuracy (%)	Precision (%CV)
Urine	BZP	5000	1000		5	4.90 ± 0.03	98	3
	TFMPP	5000	1000		5	4.45 ± 0.04	89	1
Hemolyzed Blood	BZP	0.5		10	5	4.49 ± 0.03	90	1
		5000	1000		5	4.48 ± 0.06	90	1
	TFMPP	0.5		10	5	4.43 ± 0.1	89	2
		5000	1000		5	4.57 ± 0.2	92	5
Bile	BZP	500	100		5	5.07 ± 0.1	101	2
	TFMPP	500	100		5	4.93 ± 0.2	99	4
Vitreous Humor	BZP	500	100		5	5.01 ± 0.03	101	1
	TFMPP	500	100		5	4.66 ± 0.02	93	1

Each datum point calculated from triplicate measurements.

Table 3.5, Summary of dilution and concentration studies in the biomatrices.

3.3.3.4. Stability

QC samples were analyzed after being subjected to conditions that would approximate potential handling conditions. Stability of the analytes up to 24 hours in the matrix (before extraction) and in the autosampler (after extraction) as well as after three consecutive freeze and thaw cycles were performed. The results are listed in table 3.6 and demonstrate sufficient stability for the analytes under standard working conditions.

			Hemolyzed Blood	Urine
		Nominal Concentration (ng/mL)	Recovery ± SD (%)	
Matrix Stability at room temperature for 24 hours	BZP	1.50	98 ± 3	99 ± 3
		15.0	105 ± 6	97 ± 2
		150.	94 ± 4	94 ± 1
	TFMPP	1.50	93 ± 1	95 ± 4
		15.0	93 ± 4	93 ± 1
		150.	103 ± 9	90 ± 2
Autosampler Stability at 4°C for 24 hours	BZP	1.50	103 ± 4	97 ± 3
		15.0	102 ± 1	98 ± 1
		150.	102 ± 1	98 ± 2
	TFMPP	1.50	95 ± 4	97 ± 3
		15.0	95 ± 4	104 ± 1
		150.	95 ± 2	104 ± 2
3 Freeze-thaw cycles	BZP	1.50	95 ± 2	97 ± 2
		15.0	97 ± 2	102 ± 2
		150.	96 ± 1	101 ± 1
	TFMPP	1.50	91 ± 2	98 ± 4
		15.0	93 ± 1	105 ± 2
		150.	95 ± 1	102 ± 4

Each datum point calculated from triplicate measurements.

Table 3.6, Summary of stability in hemolyzed blood and urine.

3.3.4. Application to ante-and post-mortem samples

The method was applied to confirm the presence and amount of BZP and TFMPP in 7 cases presented to the Cuyahoga County Coroner's Office. These samples tested positive for Amphetamines by EMIT assay. Following GC/MS analysis, it was found that the substance showing positive in the immunoassay was not in fact amphetamine. Analysis with the developed LC-MS/MS method in this work confirmed that the substances were BZP and/or TFMPP. The results of the antemortem samples are listed in table 3.7, and postmortem in table 3.8.

Case	Matrix	BZP (ng/mL)	TFMPP (ng/mL)	Other Drugs Present	Circumstance
2	Blood	47.0 ± 0.4	0.059 ± 0.002		
	Urine	$6.27 \times 10^4 \pm 1.30 \times 10^3$	464 ± 44	THC-COOH, Oxazepam, Temazepam	Drug-Facilitated Sexual Assault
3	Urine	$3.61 \times 10^4 \pm 808$	$1.03 \times 10^3 \pm 23$	Cocaine, THC-COOH, GHB	Drug-Facilitated Sexual Assault
7	Urine	$1.23 \times 10^4 \pm 58$	$1.13 \times 10^3 \pm 21$	Ethanol, MDMA, MDA, THC-COOH, Methamphetamine	Drug-Facilitated Sexual Assault

Table 3.7, Results of analysis in ante-mortem samples.

Case	Matrix	BZP (ng/mL)	TFMPP (ng/mL)	Other Drugs Present	Circumstance
1	Vitreous Humor	113 ± 1	BLOQ	Ethanol	Gunshot Wound
4	Blood	778 ± 38	10.2 ± 0	THC-COOH	Gunshot Wound
	Urine	$5.51 \times 10^4 \pm 1.41 \times 10^3$	$2.50 \times 10^3 \pm 57$		
	Bile	$1.84 \times 10^3 \pm 17$	398 ± 11		
5	Blood	$1.07 \times 10^3 \pm 26$	34.7 ± 0.6	Ethanol	
	Urine	$3.68 \times 10^4 \pm 1.20 \times 10^3$	$1.77 \times 10^3 \pm 99$	Ethanol, THC-COOH, Dextromethorphan	Struck by Car
6	Blood	761 ± 4	85.1 ± 1.3	Cocaine, Morphine, Oxycodone, Diazepam, Temazepam, MDMA	
	Urine	$8.02 \times 10^3 \pm 76$	788 ± 17	Cocaine, Methamphetamine, Oxycodone, MDMA, MDA	Acute Intoxication by Cocaine
	Bile	$1.57 \times 10^4 \pm 153$	$5.59 \times 10^3 \pm 101$		
	Vitreous Humor	599 ± 20	44.7 ± 3.2		

Table 3.8, Results of analysis in post-mortem samples.

3.4. Conclusion

This work describes a sensitive and robust LC-MS/MS method for the analytical determination of the drugs of abuse BZP and TFMPP in human hemolyzed blood, urine, bile, and vitreous humor. The method is linear from 0.500 ng/mL to 250 ng/mL for BZP and 500 ng/mL for TFMPP and can accommodate concentration to 10 times and dilution to 1000 times. The dilution of samples may be performed after extraction for ease and speed of analysis. Validation parameters performed include recovery, matrix factor, intra- and inter-day accuracy and precision, and stability under common analysis conditions. The column used for analysis is a Waters XBridge™ C6-Phenyl column and shows enhanced retention for the highly polar analytes. This column ensures versatility of the method and may be amended to include other piperazine derivatives in the future. The sensitive nature of the method lends itself to many applications where sensitivity is desired, including fluid spotting on paper and highly decomposed samples.

3.5. References

[1] M.H. Baumann, R.D. Clark, A.G. Budzynski, J.S. Partilla, B.E. Blough, R.B. Rothman, Neuropsychopharmacology, 30 (2005) 550-560.

[2] S. Elliott, Drug Testing and Analysis, 3 (2011) 430-438.

[3] C. Bye, Munrofau.Ad, A.W. Peck, P.A. Young, European Journal of Clinical Pharmacology, 6 (1973) 163-169.

[4] H. Campbell, W. Cline, M. Evans, J. Lloyd, A.W. Peck, European Journal of Clinical Pharmacology, 6 (1973) 170-176.

[5] I.J.E. Boksay, K. Popendiker, R.O. Weber, A. Soder, Arzneimittel-Forschung/Drug Research, 29-1 (1979) 193-204.

[6] L. Conti, D. Toschi, P. Mazzella, F. Ibba, D. Pirolo, G. Mariani, U. Puntoni, M. Marchetti, Current Therapeutic Research, 44 (1988) 434-447.

[7] M. Gastpar, G. Gastpar, U. Gilsdorf, Pharmacophychiatry, 18 (1985) 351-355.

[8] K. Magyar, M.I.K. Fekete, K. Tekes, T.L. Torok, European Journal of Pharmacology, 130 (1986) 219-227.

[9] B. Malomvolgyi, L. Tothfalusi, K. Tekes, K. Magyar, Acta Physiologica Hungarica, 78 (1991) 201-209.

[10] K. Magyar, Polish Journal of Pharmacology and Pharmacy, 39 (1987) 107-112.

[11] P. Gee, T. Jerram, D. Bowie, Clinical Toxicology, 48 (2010) 230-233.

[12] C. Balmelli, H. Kupferschmidt, K. Rentsch, M. Schneemann, Deutsche Medizinische Wochenschrift, 126 (2001) 809-811.

[13] J. Whalen, in, In Quest for 'Legal High,' Chemists Outfox Law, The Wall Street Journal. October 30, 2010. Accessed online November 2nd, 2010.

[14] L. Wang, Chemical & Engineering News, 88 (2010) 43.

[15] H.K. Nordgren, O. Beck, Therapeutic Drug Monitoring, 26 (2004) 90-97.

[16] A. Wohlfarth, W. Weinmann, S. Dresen, Analytical and Bioanalytical Chemistry, 396 (2010) 2403-2414.

[17] U. Antia, M.D. Tingle, B.R. Russell, Journal of Forensic Sciences, 55 (2010) 1311-1318.

[18] C. Bell, C. George, A.T. Kicmana, A. Traynorb, Drug Testing and Analysis, 3 (2011) 496-504.

[19] S. Elliott, C. Smith, Journal of Analytical Toxicology, 32 (2008) 172-177.

[20] H. Tsutsumi, M. Katagi, A. Miki, N. Shima, T. Kamata, M. Nishikawa, K. Nakajima, H. Tsuchihashi, Journal of Chromatography B-Analytical Technologies in the Biomedical and Life Sciences, 819 (2005) 315-322.

[21] S.P. Vorce, J.M. Holler, B. Levine, M.R. Past, Journal of Analytical Toxicology, 32 (2008) 444-450.

[22] W. Hedgepath, S. Steinike, M. Aiello, R. Ellis, A. Schreiber, D. Caraiman, T. Sakuma, High Sensitivity MS Determination of Carryover in a New Autosampler Design. Application Note. Available at:

http://www.ssi.shimadzu.com/products/literature/hplc/Shimadzu-ABI_Carryover_PC2006.pdf. Accessed October 25th, 2011.

[23] D.L. McCauley-Myers, T.H. Eichhold, R.E. Bailey, D.J. Dobrozsi, K.J. Best, J.W. Hayes, S.H. Hoke, Journal of Pharmaceutical and Biomedical Analysis, 23 (2000) 825-835.

CHAPTER IV

INSIGHTS INTO THE INACTIVATION OF β-LACTAMASE ENZYMES FOR ANTIBIOTIC RESISTANCE BY MASS SPECTROMETRY

4.1 Introduction

Bacterial cell walls are made up of peptidoglycan polymers of N-acetyl-muramic acid (NAM) and N-acetylglucosamine (NAG) (figure 4.1) assembled together by transpeptidases called penicillin binding proteins (PBP) [1]. Penicillin-type (β-lactam) antibiotics bind to and are then catalyzed by the PBP's in the crosslinking of NAG-NAM peptidoglycan as they are similar in structure to D-alanine-D-alanine in the tetra-peptide side chain [2] (figure 4.2). The incorporation of penicillin-type antibiotics results in a compromised cell wall and eventually death. Bacteria have developed a mechanism to circumvent the action of β-lactam antibiotics, such as penicillin, by the development of β-lactamase enzymes. β-Lactamase enzymes hydrolyze the

lactam ring effectively rendering these compounds useless to inhibit PBP cell wall synthesis (see figure).

Over 850 β-lactamase enzymes have been identified to date [3]. Ever-changing bacteria are quickly outsmarting the current arsenal of antibiotics. To help improve the action of antibiotics, β-lactamase inhibitors have been developed. This work describes the inactivation of three β-lactamase enzymes as studied by the use of mass spectrometry. The works thus far described in this thesis have focused on quantitation of small molecules by liquid chromatography – tandem mass spectrometry. This final chapter will demonstrate an additional functionality of mass spectrometry, specifically the use of quadrupole time-of-flight to measure and characterize β-lactamase proteins and their interactions with small molecules. Characterizations of these interactions and correlation to available kinetic data will be presented.

4.1.1 Bacterial Resistance

Bacteria reproduce quickly, and this reproduction allows for fast incorporation of mutations that could prove to be advantageous to their survival. Mutations occur readily in β-lactamase enzymes [4] as well as PBPs [5] causing decreased efficacy of lactam antibiotics. Both mechanisms are detrimental to lactam antibiotics, but this work will focus on β-lactamase enzyme mutations. Tactics to increase the efficacy of lactam antibiotics

include the co-administration of β-lactamase inhibitors. The inhibitors bind to the active site of the β-lactamase more favorably and tightly than the antibiotic (substrate) and therefore allow the antibiotic time to work and weaken the cell structure. Commercially, there are four FDA-approved inhibitor/antibiotic combinations in the USA, table, 4.1 and figure 4.3 [3].

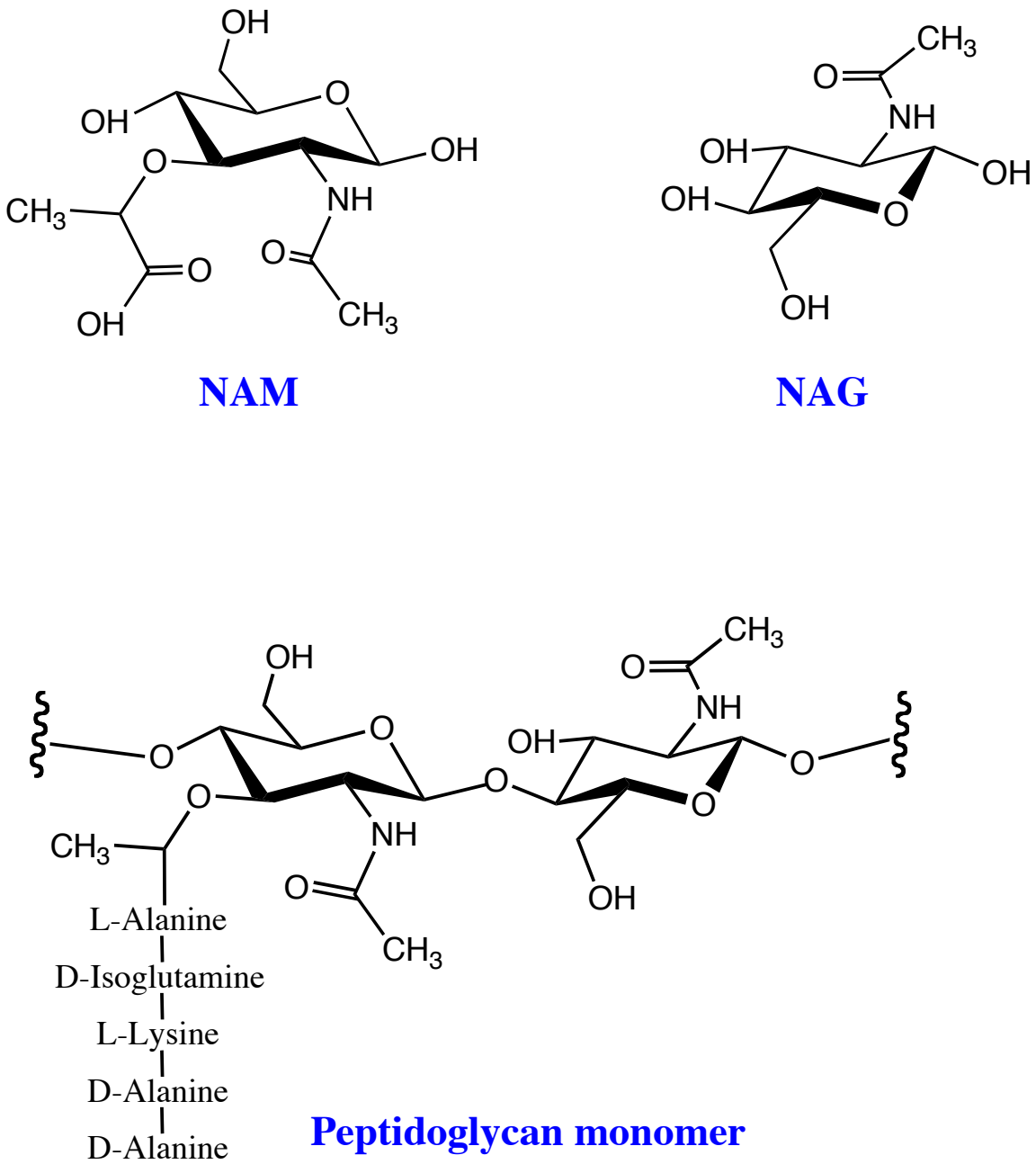

Figure 4.1, Structures of NAM and NAG as well as a peptidoglycan monomer.

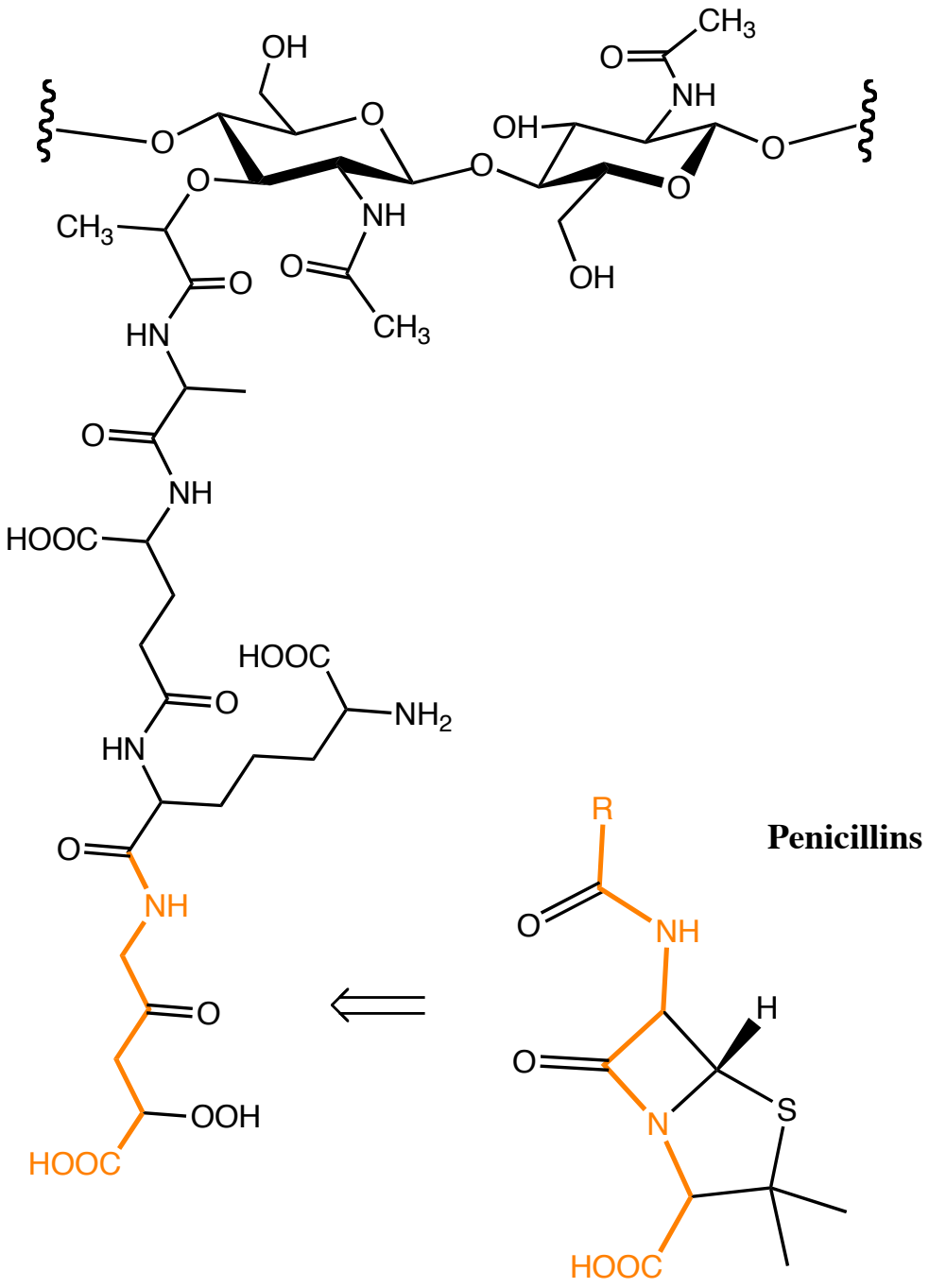

Figure 4.2, Penicillin incorporation into the peptidoglycan crosslinker

Trade Names of antibiotic-inhibitor combinations	β-Lactam antibiotic	β-Lactam Inhibitor
Augmentin	Amoxicillin	Clavulanate
Timentin®	Ticarcillin	Clavulanate
Unasyn®	Ampicillin	Sulbactam
Zosyn®	Piperacillin	Tazobactam

Table 4.1, Commercially available inhibitor/antibiotic combinations

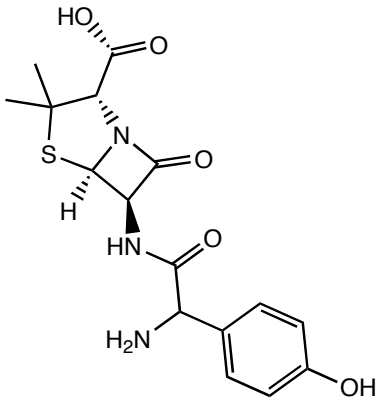

Amoxicillin

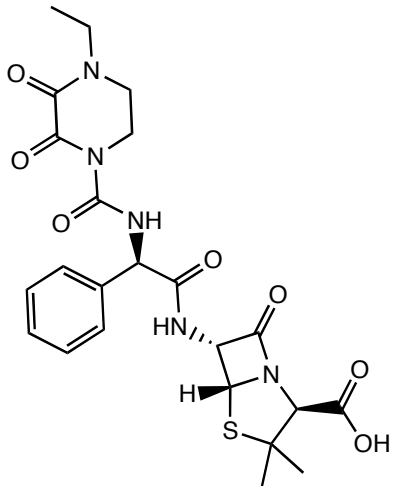

Piperacillin

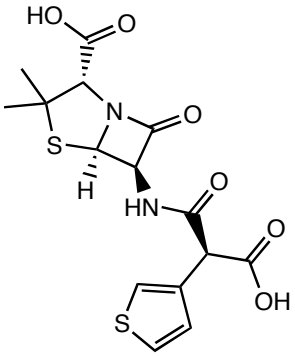

Ticarcillin

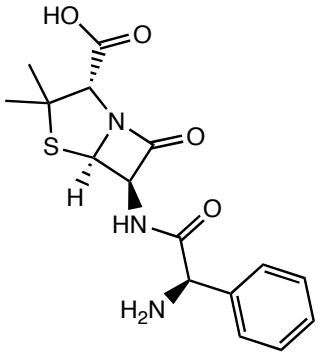

Ampicillin

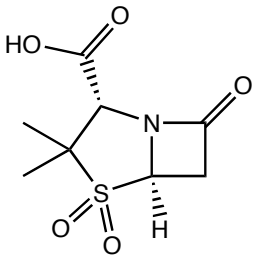

Sulbactam

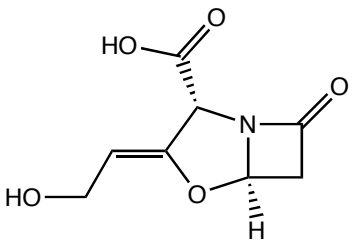

Clavulanate

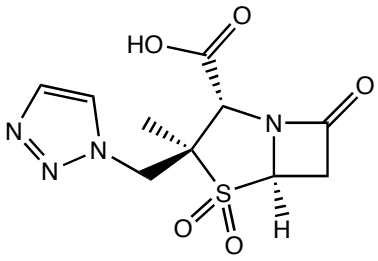

Tazobactam

Figure 4.3, Structures of commercially available lactam antibiotics and inhibitor combinations

4.1.2 β-Lactamase Classes

There are four classes of β-lactamase enzymes categorized by sequence homology. Each class has differences in substrate activity where structural and/or amino acid residue location influence their inactivation. Classes A, C, and D β-lactamases have a catalytic serine in their active sites where Class B β-lactamases utilize Zn^{2+} [3]. There are only three inhibitors available for clinical administration, but many others in different phases of research. Figure 4.4 shows the basic core structure of four different classes of inhibitors [6].

Class A β-lactamases are the most common in occurrence and appear in both gram-positive and gram-negative bacteria; they include TEM and SHV enzymes and are susceptible to clavulanate, tazobactam, and to a lesser extent, sulbactam [4]. An additional sub-category, the extended spectrum β-lactamases, ESBL, includes the methicillin-resistant *S. aureas*, MRSA [7]. Others include the Class A carbapenemase KPC [8], Class C cephalosporinase FOX [9], and Class D oxacillinase OXA [10]. An emerging threat is the recently discovered Class B metallo-β-lactamase, NDM [11]. NDM-1 has proven to have a broad resistance profile and shown the ability to apparently move to more than one species of bacteria [11]. This work will focus on inactivation of both Class A β-lactamase and carbapenemase enzymes.

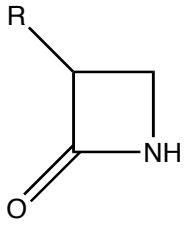

Monobactam

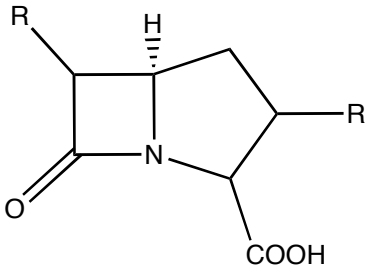

Carbapenem

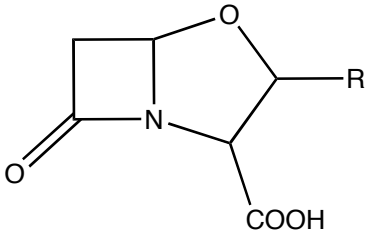

Clavam

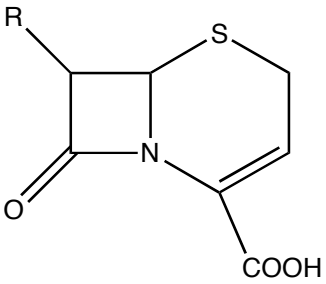

Cephem

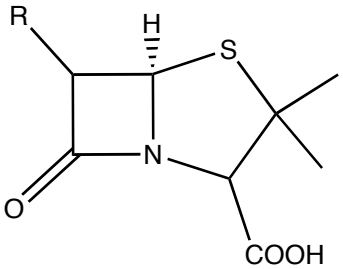

Penicillin

Figure 4.4, Core structures of some inhibitor types

4.1.3 β-Lactam Hydrolysis

The Class A β-lactamase enzymes first acylate and then hydrolyze antibiotics and to a slower extent, the inhibitors. The reaction can be represented by the simplified scheme S1.

$$E + S \underset{k\,\text{off}}{\overset{k\,\text{on}}{\rightleftharpoons}} E{:}S \xrightarrow{k_2\,(\text{acylation})} E\text{-}S \xrightarrow[H_2O]{k_3\,(\text{deacylation})} E + P \qquad \text{(S1)}$$

The enzyme, E, transiently binds to the substrate, S, and forms a complex. The enzyme then acylates the substrate in the active site, and on deacylation, the substrate is released as a product. The rates of each step can be calculated by k_{on}, k_{off}, k_2, and k_3. k_{on} is the association constant, and k_{off} is the dissociation constant. k_2 is the rate of acylation where k_3 is the rate of deacylation. We can calculate the kinetics by the utilization of the work of Michaelis and Menten [12].

The above scheme is a very simplified example of acylation and deacylation. In reality, the enzyme goes through a number of intermediate steps before deacylation and releasing the product and is represented in scheme S2 [3, 13].

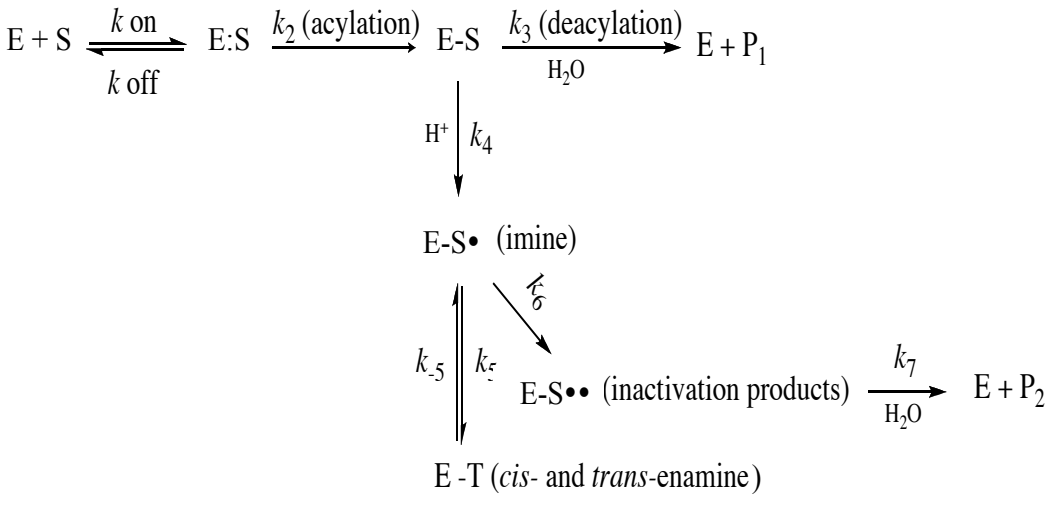

(S2)

This updated scheme reveals transient E-S* imine, E-S** with additional reaction products, E-T enamine tautomer, as well as regenerated enzyme and product, E+P_1 and E+P_2 [3]. Portions of the reaction scheme can be measured by such techniques as UV spectroscopy and mass spectrometry (figure 4.5). Figure 4.6 depicts an accepted inactivation scheme for Class A β-lactamase enzymes where two serines at positions 70 and 130 work with H_2O to acylate and hydrolyze the substrate [14].

The Michaelis constant, K_m, a measure of enzyme:substrate affinity where a smaller number corresponds to high affinity, can be calculated as:

$$K_m = \frac{k_3\left((k_{off} + k_2)/k_{on}\right)}{\left(k_2 + k_3\right)} \qquad 1$$

The turnover number, k_{cat}/k_{inact}, a measure of the number of molecules of inhibitor hydrolyzed by the enzyme before irreversible inactivation, can be calculated as:

$$\text{Turnover number} = k_{cat} / k_{inact} = k_3 / k_4 \qquad 2$$

Calculating kinetics is done by measuring the residual activity or competitive binding of the β-lactamase enzyme by the chromogenic substrate, nitrocefin [15]. Active enzyme will hydrolyze nitrocefin and the absorbance at 482 nm is measured.

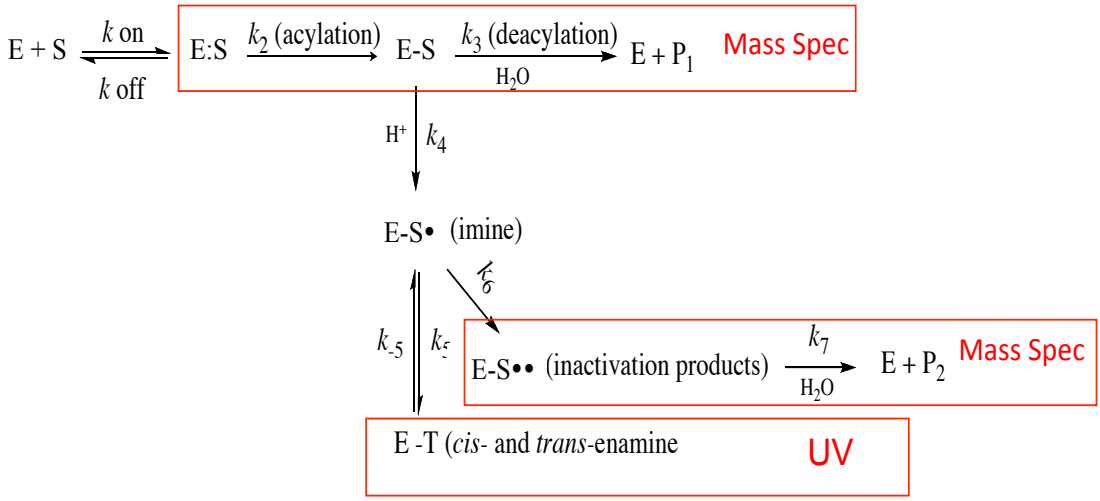

Figure 4.5, Measurement of β-lactamase enzyme inactivation

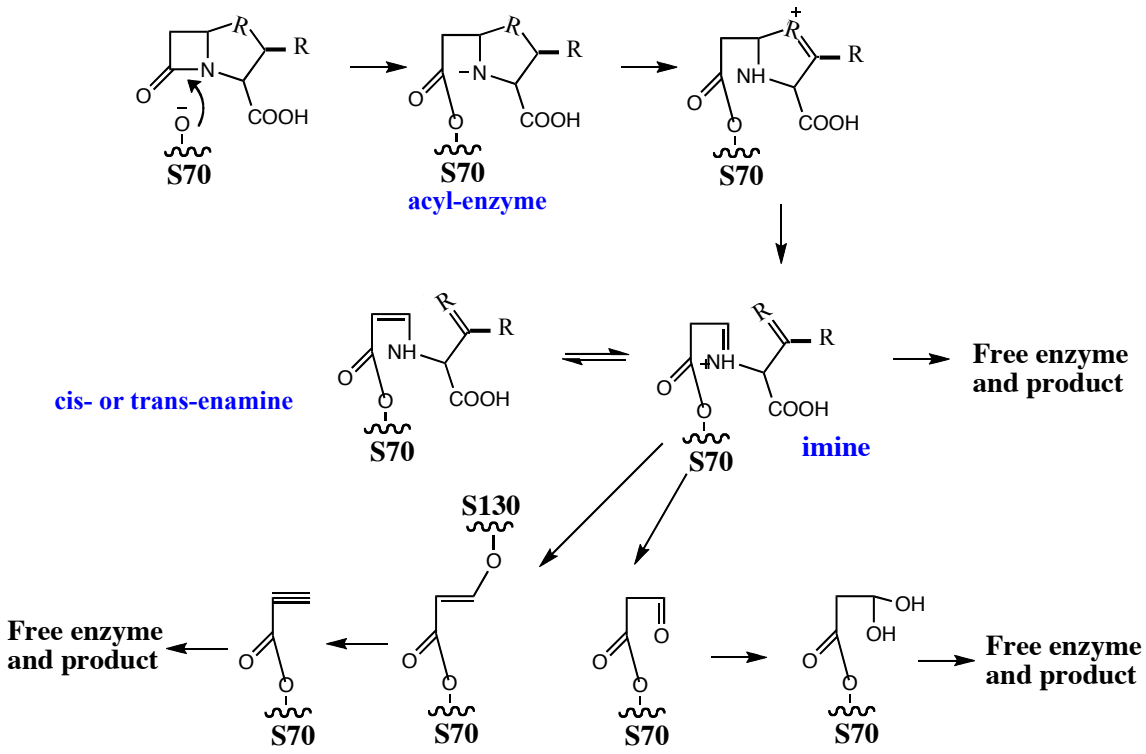

Figure 4.6, Class A β-lactamase enzyme inactivation scheme

4.2 Materials and Methods

4.2.1 Preparation of enzymes for analysis

The β-lactamase enzymes used in this study are the Class A serine β-lactamase SHV-1 and the Class A carbapenemase KPC-2. Mutagenesis of KPC-2 was performed by site-directed mutagenesis. The β-lactamase were expressed in *Escherichia coli* strain DH108 or similar and described previously, [13, 14, 16]. All lysed and fractionated supernatants were subjected to preparative isoelectric focusing followed by ion exchange liquid chromatography according to the previously published methods [13, 17, 18].

4.2.2 Antibiotic Susceptibility and Kinetics

Minimum Inhibitory Concentrations (MIC) to resolve antibiotic susceptibility on *E. coli* DHB10B expressing bla_{KPC-2} was determined by agar broth dilution method described previously [18, 19]. Residual activity was determined at 22 °C in an Agilent 8453 Diode Array Spectrophotometer (Santa Clara, CA) using nitrocefin (BD Biosciences) and the extinction coefficient, $\boldsymbol{\varepsilon}$ = 17,400 $_M^{-1}cm^{-1}$ at 482 nm. K_M and turnover number were calculated using modified versions of equations 1 and 2 in section 4.1.3. For complete details of the concentrations and parameters used, refer to references [17] and [19] for SHV-1, and references [13] and [18] for KPC-2 and KPC-2 R220K.

4.2.3 Inactivation of β-lactamase enzymes

Purified β-lactamase enzymes at concentrations of 10 μM in PBS for KPC-2 or 0.45 μM in 10 mM diethanolamine for SHV-1 were incubated with either sulbactam or clavulanate at 22 °C then the reaction stopped at specific timepoints by the addition of 0.1% trifluoroacetic acid. The proteins were then desalted using C_{18} ZipTips (Millipore, Bedford MA, USA) according to the protocol recommended by the manufacturer. The protein was eluted from the ZipTips by 50 μL of acetonitrile/H_2O/formic acid (50:49:1) for analysis.

4.2.4 Electrospray Ionization Mass Spectrometry (ESI-MS)

The infusion analysis was carried out on an AB Sciex (Foster City, CA, USA) QSTAR®-Elite quadrupole-orthogonal acceleration time-of-flight (Q-TOF) mass spectrometer equipped with a TurboIonSpray™ Source and an integrated syringe pump. Mass calibration was performed in the positive mode with Renin solution using the recommended instrument protocol. The protein eluate was then infused into the mass spectrometer at a flow rate of 5 μL/min. Mass spectra were acquired using Analyst QS v2.0 software with 80-150 MCA cycles and an accumulation time of 1.5 s from 600 – 2800 amu. Temperatures and gases were as follows: GS1 = 20, GS2 = 5, CUR = 15, IS = 5500, and TEM = 300. The mass spectra were deconvoluted by

BioAnalyst™2.0 software using the Bayesian protein reconstruction algorithm.

4.3 Results and Discussion

4.3.1 Antibiotic susceptibility and kinetic analysis of sulbactam and clavulanate on SHV-2, KPC-2 and mutants

Previously, our lab investigated the MICs of bacteria expressing bla_{SHV-1} to ampicillin and piperacillin as well as the kinetics with clavulanate [19]. The mutation at this position was shown to make the most difference with inhibitor susceptibility [17]. Bacterial cells expressing bla_{KPC-2} and mutation arginine to lysine at ambler position 220 were tested against ampicillin, piperacillin, as well as ampicillin and clavulanate or sulbactam combinations. As shown in table 4.2, SHV-1 is resistant to antibiotics with 16000 mg/L of ampicillin required for growth inhibition. On incubation with the inhibitor clavulanate, the susceptibility maintained indicating resistance (4 mg/L). Conversely, KPC-2 and mutation R220K were each susceptible to ampicillin at 256 mg/L and on the addition of clavulanate, showing decreased resistance (from 32 mg/L for WT to ≤1 for R220K). These results suggest that the mutation investigated has a direct impact on the susceptibility of the enzyme to antibiotics and inhibitors.

To further understand the impact of the mutation, the kinetics of inactivation were calculated. With wild type (WT) SHV-1, we see low-to-sub micromolar values for the dissociation (K_I) of the enzyme-inhibitor complex demonstrating that SHV-1 is less resistant to sulbactam inhibition (a higher concentration of sulbactam was needed to inhibit the enzyme) (table 4.3). A similar situation is seen in KPC-2 with respect to the R220K mutation. Although WT KPC-2 is somewhat resistant to sulbactam, the R220K mutation makes the enzyme more susceptible to inhibition. The binding (K_m) of clavulanate to KPC-2 is 25 μM, where the R220K mutation is 14 μM. Additionally, the R220K mutant loses the ability to hydrolyze clavulanate; the k_{cat} of WT KPC-2 is 18 s^{-1} and was undetectable for the R220K mutant.

	MIC (mg/L)			
	Ampicillin	Piperacillin	Ampicillin/ clavulanate[b]	Ampicillin/ sulbactam[c]
SHV-1[a]	16000	2000	4	
KPC-2	256	128	32[b]	512[b]
KPC-2 R220K	256	16	≤1	8

[a] From reference 17

[b] Inhibitor evaluated in the presence of 50 μg/mL of ampicillin

[c] Determined using the *K. pneumoniae* strain from which bla_{KPC-2} was cloned

Table 4.2. MICs of SHV-1 and KPC-2 and mutants

	Inhibitor Kinetics					
	Sulbactam			Clavulanate		
	K_m(μM)	k_{cat} (s^{-1})	k_{cat}/k_{iinact}	K_m(μM)	k_{cat} (s^{-1})	k_{cat}/k_{iinact}
KPC-2	184 ± 18	n/a	3000	25 ± 3	18 ± 2	9000
KPC-2 R220K	146 ± 15	n/a	250	14 ± 1	n/d	250
	K_I(μM)[a]	k_{cat} (s^{-1})	k_{cat}/k_{iinact}	K_I(μM)[b]	k_{cat} (s^{-1})	k_{cat}/k_{iinact}
SHV-1	8.6 ± 0.7	730 ± 40	13000 ± 100	0.14	1.2	40

[a] For details of K_I calculation, see reference 19

[b] For details of K_I calculation, see reference 17

n/a = not performed

n/d = not detectable

Table 4.3. Inhibitor kinetics of SHV-1 and KPC-2 and mutants

4.3.2 Mass Spectrometric studies of the inhibition of SHV-1

To understand the nature of the binding and intermediate formation involved in SHV-1 and KPC-2 inactivation, positive electrospray mass spectrometry was employed. Increasing inhibitor:enzyme ratios were investigated and the reactions stopped at specific timepoints for mass spectrometric analysis. Figures 4.7 and 4.8 show the reaction of 0.45 μM SHV-1 with 500x and 5000x (*mol/mol*) sulbactam (225 and 2250 μM) respectively. With the sulbactam concentration 500 times that of SHV-1, we see negligible adduct formation at room temperature over a 24 hour period. When the concentration of sulbactam is increased to 5000 times (2250 μM), multiple adducts are formed, +54, +72, +90, +106, +153 and +171 *m/z* (table 4.4). The adducts at +18 and +36 *m/z* likely correspond to [M + H + H2O] and [M + H + 2H2O] respectively. These results correspond to the MIC and kinetic analysis showing that SHV-1 β-lactamase does indeed bind with the inhibitor and allows the bacteria to become more susceptible to antibiotics. Sulbactam is a substrate that binds to the active site and turns over at a much slower rate, thus occupying the active site and allowing for a longer half-life of antibiotic in the bacterial system.

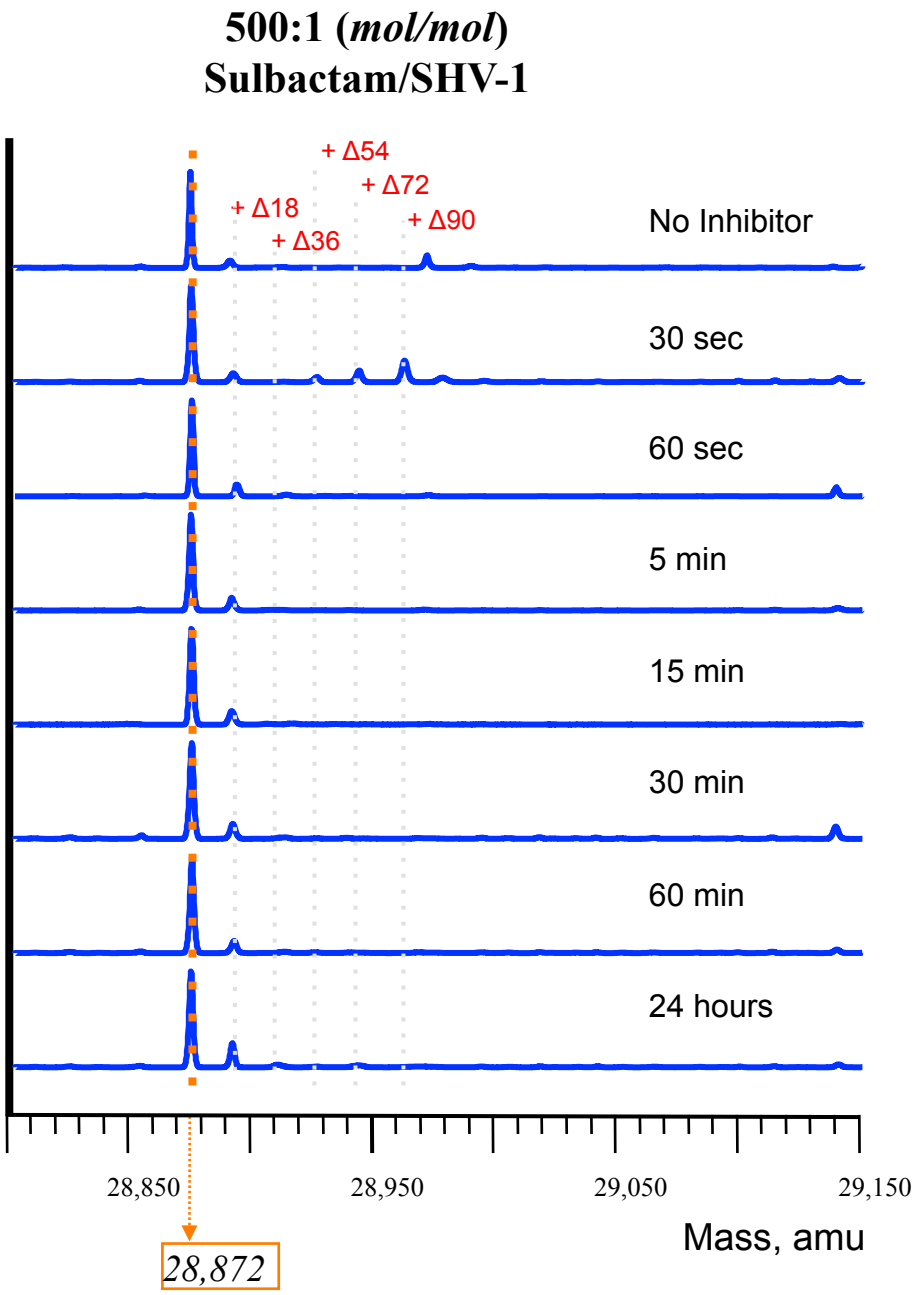

Figure 4.7. Timed mass spectrometric analysis of 500:1 sulbactam/SHV-1 incubation

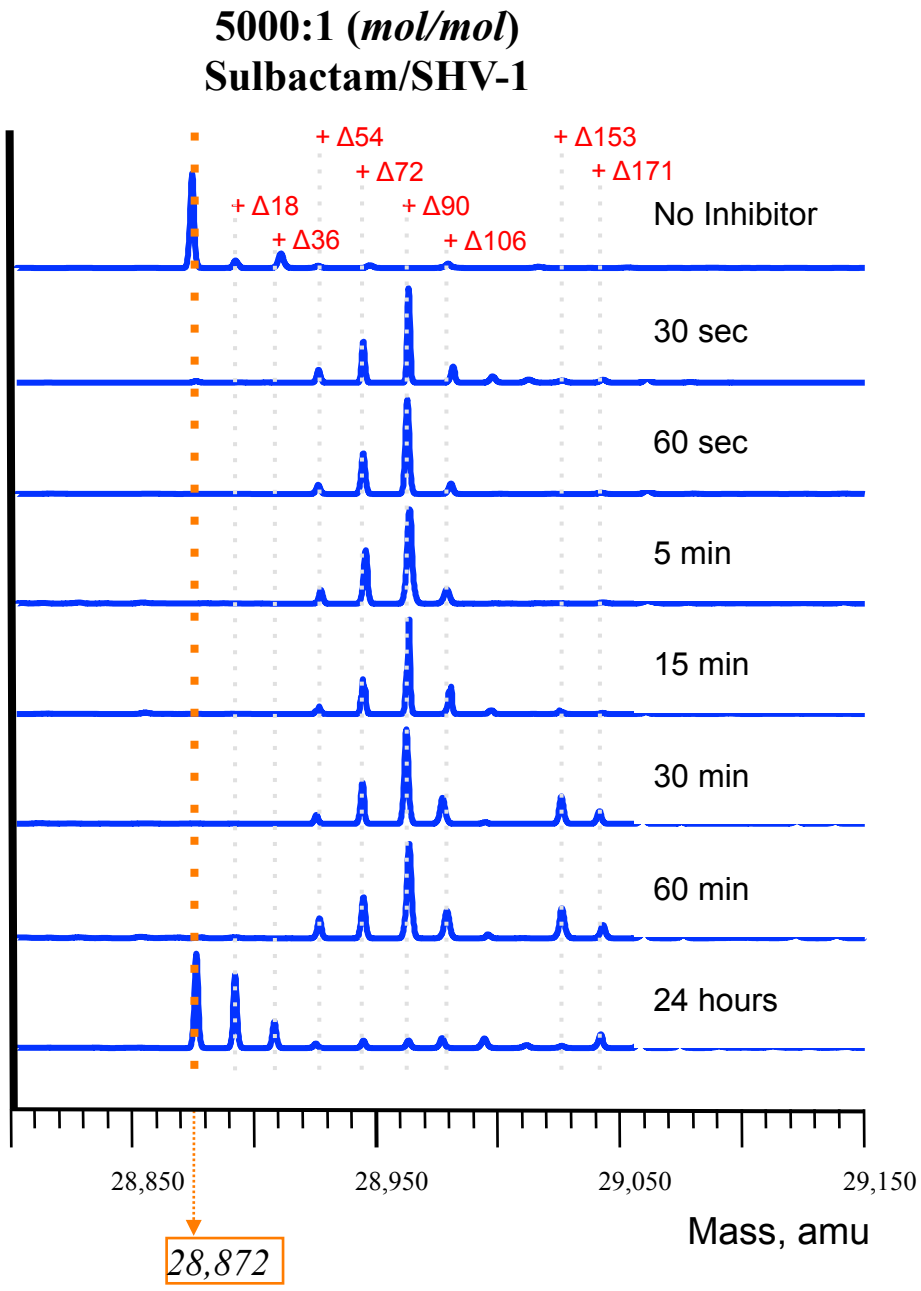

Figure 4.8. Timed mass spectrometric analysis of 5000:1 sulbactam/SHV-1 incubation

(A) 5000:1 (*mol/mol*) sulbactam/SHV-1

WT (amu)	Deconvoluted Mass (amu)	Δ mass (±3 amu)
28872		
	28926	54
	28944	72
	28962	90
	28978	106
	29025	153
	29043	171

Table 4.4. Adduct formation in 5000:1 (*mol/mol*) sulbactam/SHV-1

4.3.3 Mass Spectrometric studies of the inhibition of KPC-2 and KPC-2 R220K

Similar experiments were performed to elucidate binding information for KPC-2. Clavulanate at a ratio of 10,000 mM was incubated with 10 mM KPC-2 with the reaction stopped at specific timepoints for analysis by mass spectrometry. As shown in figure 4.9, WT KPC-2 formed negligible adducts with clavulanate, corresponding with the kinetic findings. The specificity, or tightness of binding, of KPC-2 was determined to be 25 μm but the turnover number (k_{cat}/k_{inact}) is large at 3000 (table 4.3). Comparing these data to the R220K mutation, the Km is only slightly smaller at 14 μm, but the turnover number is 12 times lower at 250 indicating the inhibitor potentially spends more time occupied inside the active site. Listed in table 4.3, the k_{cat} , measure of hydrolysis, of KPC-2 is calculated as 18 molecules per second, where R220K could not be determined. As illustrated by figure 4.10, incubating 100x (*mol/mol*) clavulanate with the mutation, R220K, adducts are visible through mass spectrometry. The inhibitor adducts at +51, +69, and +88 (table 4.5) appear at 1 minute, reach a maximum amount at 2.5 – 5 minutes, and decline thereafter. Figure 4.11 is a graph of the area of the deconvoluted mass found by mass spectrometry over time, showing the rise and fall of the occurrence of the various adducts. These results, together with the kinetic findings, including the loss of hydrolysis on mutation, suggest that the mechanism of inactivation of KPC-2 could indeed lie in the binding efficiency of the enzyme with clavulanate.

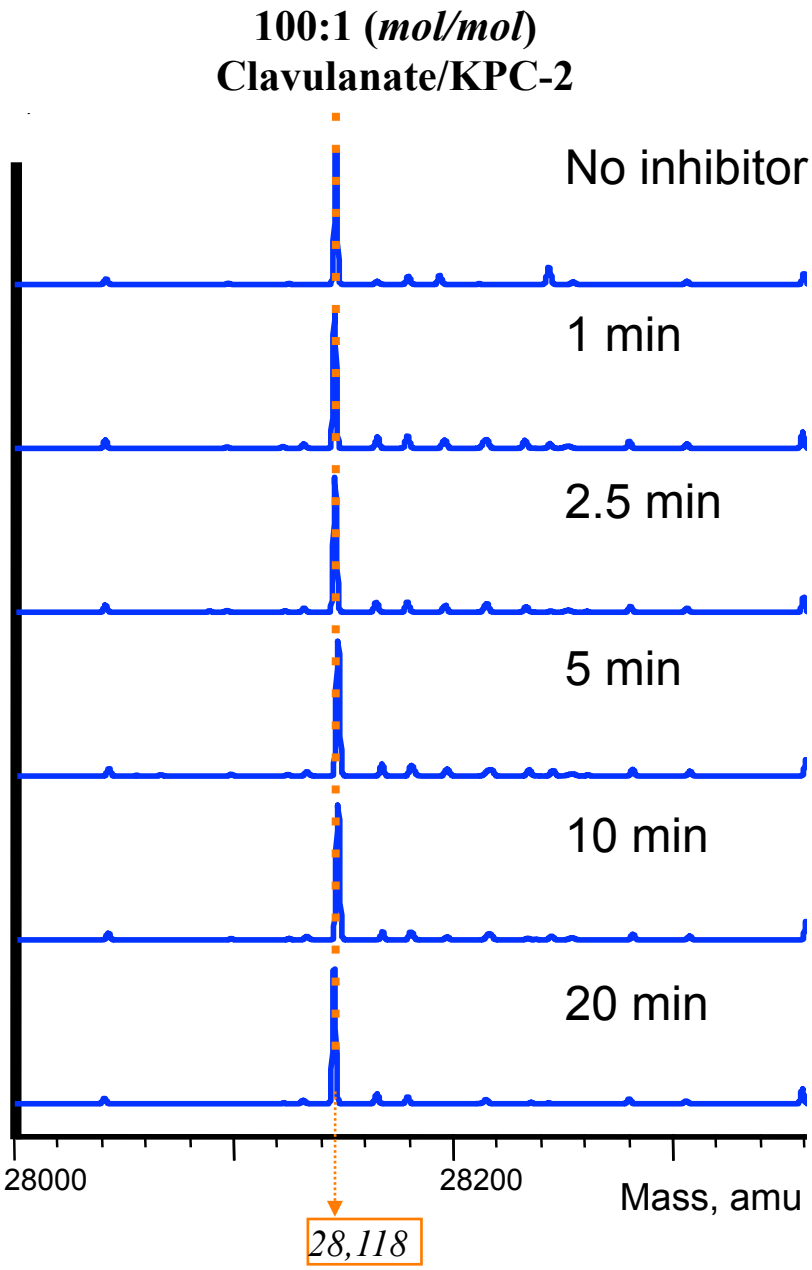

Figure 4.9. Timed mass spectrometric analysis of 100:1 clavulanate/KPC-2 incubation

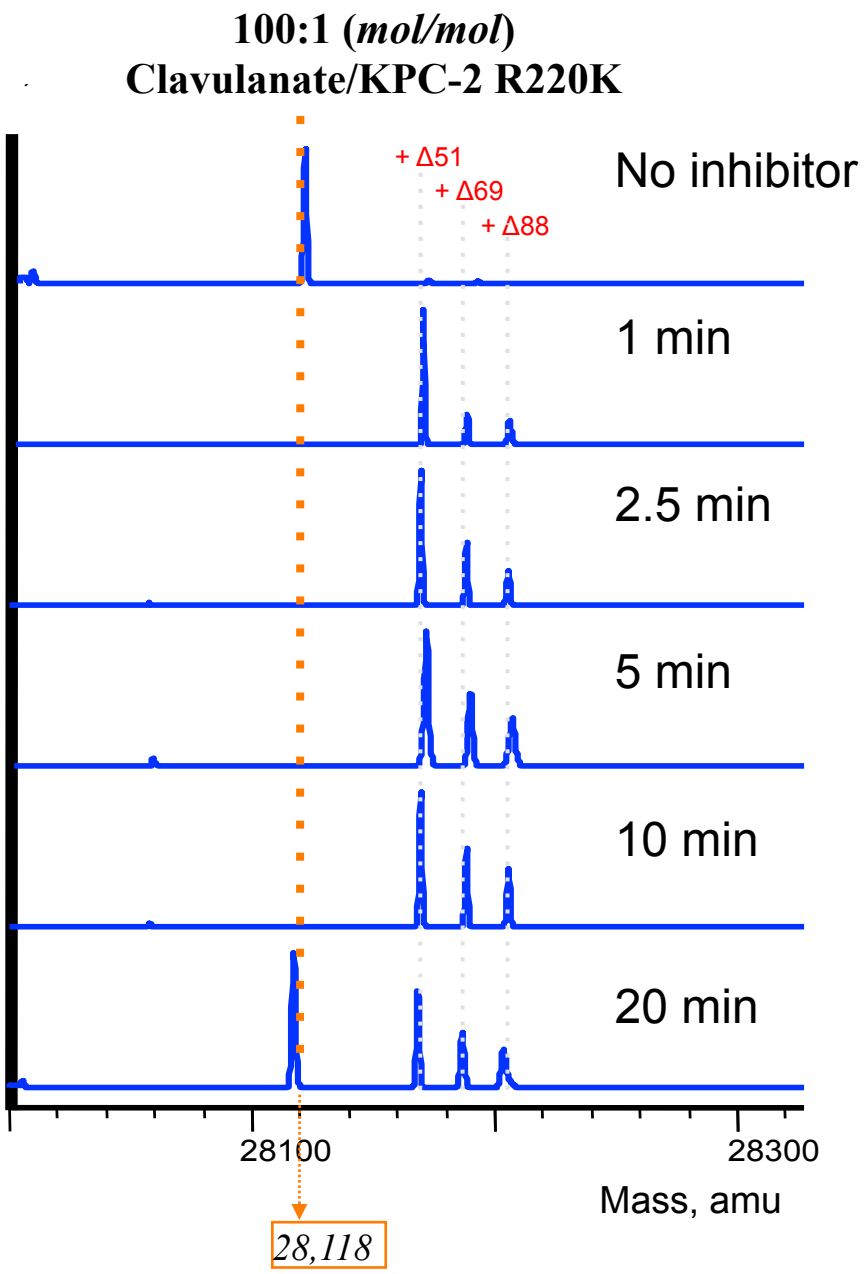

Figure 4.10. Timed mass spectrometric analysis of 100:1 clavulanate/KPC-2 R220K incubation

100:1 (*mol/mol*) clavulanate/KPC R220K		
WT (amu)	Deconvoluted Mass (amu)	Δ mass (±3 amu)
28147		
	28198	51
	28216	69
	28235	88

Table 4.5. Adduct formation in 100:1 (*mol/mol*) clavulanate/KPC R220K

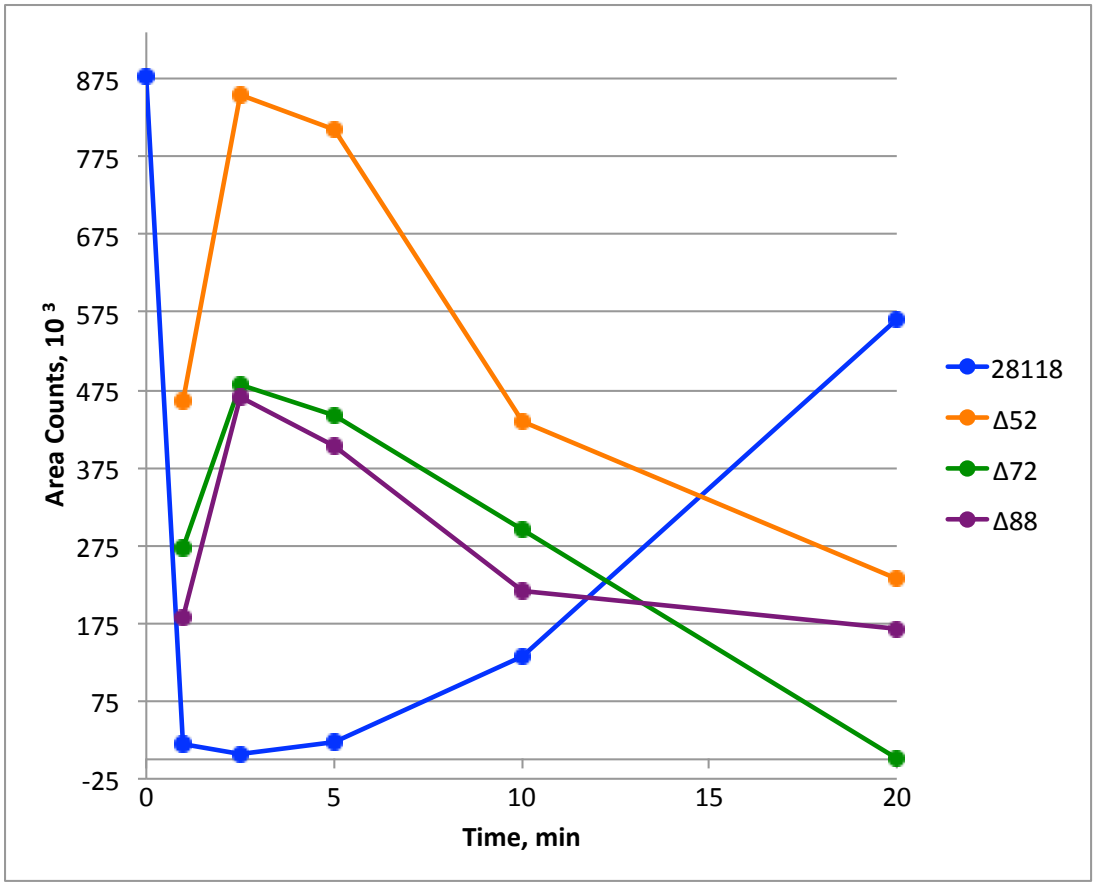

Figure 4.11. Timed mass spectrometric analysis of 100:1 clavulanate/KPC-2 R220K incubation; graph of the adduct mass areas

4.3.4 Proposed inactivation

Timed mass spectrometric analysis of the incubation of β-lactamase enzymes with inhibitors gives visual mass-adduct snapshots of the progression of inactivation. The analysis of the measured masses combined with UV as well as X-ray crystallographic and RAMAN spectroscopic techniques helps to build an understanding of the steps to inactivation.. Measurement of the enzyme adducts by mass spectrometry revealed three common predominant adducts in both SHV-1 and KPC-2: +Δ51 (±3), +Δ69 (±3), +Δ88 (±3), as well as +Δ106 (±3), +Δ153 (±3), and +Δ171 (±3) in SHV-1. Figure 4.12 depicts the proposed inactivation scheme for SHV-1 by sulbactam [20]. The serine at position 70 in the binding site attacks the β-lactam ring, opens, and finally forms the acyl-enzyme complex. The secondary ring opens and the reaction continues to an imine, cis- and/or trans-enamine, then finally to the inactivation products we visualize by mass spectrometry. The imine is converted to an aldehyde (+Δ70) and further to a hydrated aldehyde (+Δ88). Serine at position 130 helps to form a bridge and make an enol ether (+Δ52) that decomposes to a propynyl enzyme (+Δ52). Finally, the products are released and the enzyme regains activity. A very similar reaction scheme applies to the inactivation of KPC-2 by clavulanate and is depicted in figure 4.13.

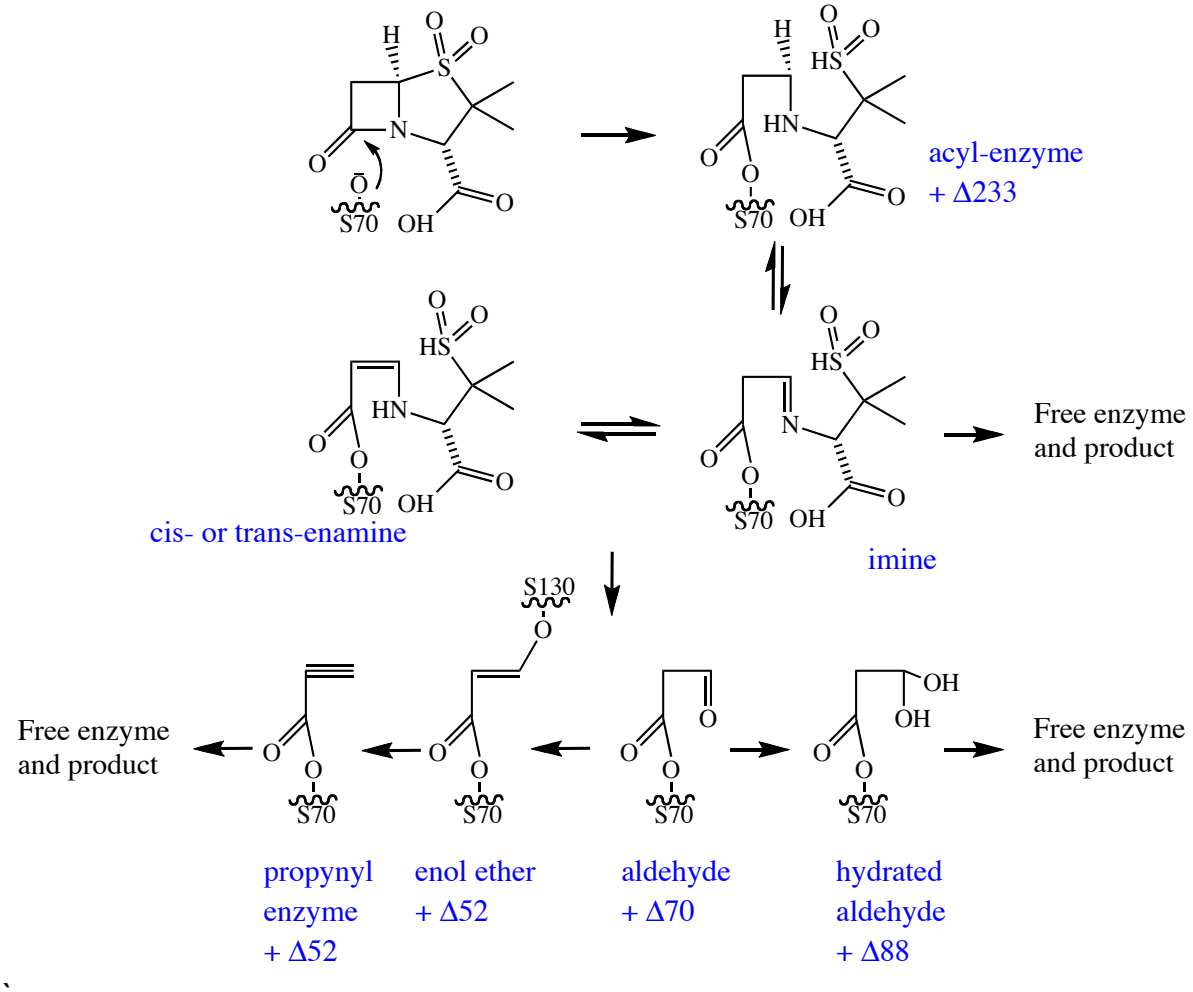

Figure 4.12. Proposed inactivation scheme for SHV-1 by sulbactam

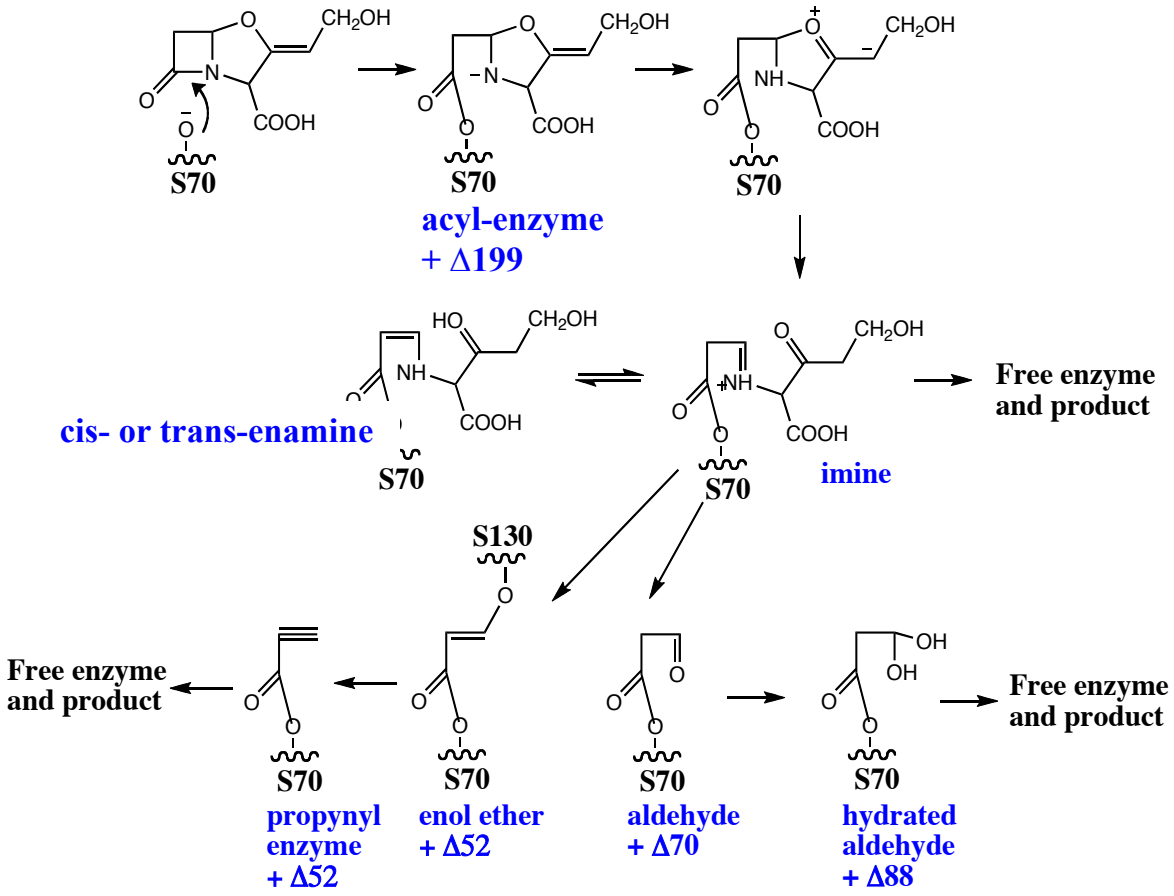

Figure 4.13. Proposed inactivation scheme for KPC-2 and KPC-2 R220K by clavulanate

4.4 Conclusion

SHV-1 has the preferred substrates of penicillins and some cephalosporins, where KPC-2 has a broad substrate profile that includes the penicillins, cephalosporins, and carbapenems [3]. In addition to the ability to hydrolyze a variety of antibiotics, these β-lactamases are (semi) resistant to commercially available inhibitors. Each β-lactamase can be found primarily in *Klebsiella pneumoniae* and represents a treatment threat to those infected. The work to understand how these enzymes can be inhibited will lead to the intelligent creation of new inhibitors. The use of mass spectrometry is a compliment to the enzyme kinetic work as it can give exact mass to the proposed enzyme-inhibitor complexes.

4.5 References

[1] D.J. Scheffers, M.G. Pinho, Microbiology and Molecular Biology Reviews, 69 (2005) 585.

[2] D.J. Waxman, J.L. Strominger, Annual Review of Biochemistry, 52 (1983) 825-869.

[3] S.M. Drawz, R.A. Bonomo, Clinical Microbiology Reviews, 23 (2010) 160-201.

[4] Y.J. Yang, B.A. Rasmussen, D.M. Shlaes, Pharmacology & Therapeutics, 83 (1999) 141-151.

[5] A. Zapun, C. Contreras-Martel, T. Vernet, Fems Microbiology Reviews, 32 (2008) 361-385.

[6] A. Matagne, J. Lamotte-Brasseur, J.M. Frere, Biochemical Journal, 330 (1998) 581-598.

[7] R.M. Klevens, M.A. Morrison, J. Nadle, S. Petit, K. Gershman, S. Ray, L.H. Harrison, R. Lynfield, G. Dumyati, J.M. Townes, A.S. Craig, E.R. Zell, G.E. Fosheim, L.K. McDougal, R.B. Carey, S.K. Fridkin, A.B.M. Investigators, JAMA-J. Am. Med. Assoc., 298 (2007) 1763-1771.

[8] H. Yigit, A.M. Queenan, G.J. Anderson, A. Domenech-Sanchez, J.W. Biddle, C.D. Steward, S. Alberti, K. Bush, F.C. Tenover, Antimicrobial Agents and Chemotherapy, 45 (2001) 1151-1161.

[9] G. Bou, A. Oliver, M. Ojeda, C. Monzon, J. Martinez-Beltran, Antimicrobial Agents and Chemotherapy, 44 (2000) 2549-2553.

[10] C. Heritier, L. Poirel, P.E. Fournier, J.M. Claverie, D. Raoult, P. Nordmann, Antimicrobial Agents and Chemotherapy, 49 (2005) 4174-4179.

[11] D. Yong, M.A. Toleman, C.G. Giske, H.S. Cho, K. Sundman, K. Lee, T.R. Walsh, Antimicrobial Agents and Chemotherapy, 53 (2009) 5046-5054.

[12] R. Labia, Andrillo.J, F. Legoffic, Febs Letters, 33 (1973) 42-44.

[13] K.M. Papp-Wallace, C.R. Bethel, A.M. Distler, C. Kasuboski, M. Taracila, R.A. Bonomo, Antimicrobial Agents and Chemotherapy, 54 (2010) 890-897.

[14] D. Sulton, D. Pagan-Rodriguez, X. Zhou, Y. Liu, A.M. Hujer, C.R. Bethel, M.S. Helfand, J.M. Thomson, V.E. Anderson, J.D. Buynak, L.M. Ng, R.A. Bonomo, Journal of Biological Chemistry, 280 (2005) 35528-35536.

[15] A. Galarneau, M. Primeau, L.E. Trudeau, S.W. Michnick, Nat. Biotechnol., 20 (2002) 619-622.

[16] A.M. Hujer, K.M. Hujer, R.A. Bonomo, Biochimica et Biophysica Acta, 1547 (2001) 37-50.

[17] M.S. Helfand, C.R. Bethel, A.M. Hujer, K.M. Hujer, V.E. Anderson, R.A. Bonomo, Journal of Biological Chemistry, 278 (2003) 52724-52729.

[18] K.M. Papp-Wallace, M.A. Taracila, K.M. Smith, Y. Xu, R.A. Bonomo, Antimicrobial Agents and Chemotherapy, *in press*, (2012).

[19] J.M. Thomson, A.M. Distler, R.A. Bonomo, Biochemistry, 46 (2007) 11361-11368.

[20] M. Kalp, M.A. Totir, J.D. Buynak, P.R. Carey, Journal of the American Chemical Society, 131 (2009) 2338-2347.